Microstructure optimization and structure-property relationships of thermoplastic nanocomposites

Dissertation

Michael Feuchter

Submitted to
Chair of Materials Science and Testing of Plastics
University of Leoben, Austria

Academic Advisor:

Univ.-Prof. Dr. Gerald Pinter
University of Leoben, Austria

Supervisor:

Dr. Günther A. Maier
Materials Center Leoben, Austria

Referees:

Univ.-Prof. Dr. Gerald Pinter
University of Leoben, Austria

Assoz. Prof. Dr. Jozef Keckes
University of Leoben, Austria

Leoben, 11.10.2011

Auch das kleinste Ding hat seine Wurzel in der Unendlichkeit,
ist also nicht völlig zu ergründen.

Wilhelm Busch

I declare in lieu of oath, that I wrote this dissertation and performed the associated research myself, using only the support indicated in the acknowledgements and literature cited.

Leoben, Oktober 11 *Dipl.-Ing. Michael Feuchter*

Acknowledgements

First, I would like to thank Prof. Gerald Pinter for his trust and patronage, which enabled me to develop a deeper understanding of polymers. He made his support available in a number of ways – offering feedback and review of my work, numerous discussions on scientific matters and possible interpretations of experimental results while further aiding me in honing my writing skills in regard to accurate scientific reporting.

This thesis would not have been possible without the encouragement and guidance of Dr. Günther Maier, who offered me the possibility to study in an interesting field of research and helped to keep the extensive nights at the numerous synchrotron locations short and entertaining. The various fruitful discussions and ideas contributed to the success of this work.

I owe a deep gratitude to Prof. Jozef Keckes, for his acceptance to act as the second referee of my doctoral committee. The critical questions and comments in our discussions allowed me to garner new insights and realize the great potential of this topic.

I am indebted to the Chair of Polymer Processing, especially Dr. Milan Kracalik and Dr. Stephan Laske, for acting as project partners and for supplying the materials investigated in this dissertation.

Special thanks go to my former colleague Ing. Alexander Lovas, who helped me with the thermo-mechanical measurements and was as an invaluable aid at the laboratory. Moreover, I am also grateful to my colleagues DI Gernot Pacher and Stefan Hinterdorfer, who invested a lot of time in the discussion of problems and in the improvement of my English.

Additionally, I would like to thank all my colleagues, who made my last five years at the chair and the PCCL comfortable and amusing.

Sincere thanks to Serafine Janisch and Ines Petek for helping me in all matters concerning administration.

I wish to thank my mother and my brother for their support during my studies. Last but not least, my deepest gratitude goes to my wife Isabella. She always kept me grounded and gave me the motivation to finish this work.

Kurzfassung

Füllstoffe in Polymeren besitzen seit jeher zwei unterschiedliche Aufgaben. Auf der einen Seite soll ihr Einsatz die Polymere billiger werden lassen, auf der anderen Seite besteht die Absicht das Eigenschaftsprofil der Kunststoffe zu verbessern. In den letzten 30 Jahren hat eine neue Art von Füllstoffen hohes Interesse hervorgerufen. Füllstoffe mit Dimensionen im Nanometerbereich besitzen eine große Oberfläche in Bezug auf ihr Volumen. Dadurch besitzen diese (im Gegensatz zu konventionellen Füllstoffen) mehr Anknüpfungspunkte an die Matrix und verbessern damit die Polymer/Füllstoff Interaktion. Schon bei geringen Mengen an Füllstoff werden Eigenschaftsverbesserungen erzielt, die bei herkömmlichen Füllstoffen nur mit hohen Füllgraden erreicht werden können. Strukturelle Eigenheiten und deren Auswirkung auf mechanische, optische und permeative Eigenschaften sind von hohem Interesse, da die meisten physikalischen Eigenschaften sehr stark von der Morphologie eines (gefüllten) Kunststoffes abhängen. Das Ziel dieser Arbeit ist es strukturelle Gegebenheiten von schichtsilikatverstärkten Kunststoffen mit den mechanischen Eigenschaften zu korrelieren.

Die Struktur von polymeren Nanokompositen kann anhand einer Vielzahl an Methoden charakterisiert werden: Röntgenstreutechniken, Transmissionselektronenmikroskopie, Rasterkraftmikroskopie, Infrarotspektroskopie und Kernspinresonanzspektroskopie sind die Methoden, die am häufigsten zur Anwendung kommen. Detaillierte Informationen der Nanostruktur wurden in der vorliegenden Arbeit mit Hilfe von Röntgenstreutechniken ermittelt. Strukturinformationen bis 100 Nanometer können mittels Kleinwinkelstreuung und Größenordnungen von 0.1 Nanometer können mit Hilfe der Weitwinkelstreuung detektiert werden. Zur Bestimmung der Verteilungsqualität des Füllstoffes wurden auch Nahinfrarotspektren aufgenommen, die mit den Röntgenergebnissen korreliert wurden. Die Veränderungen der strukturellen Gegebenheiten unter Krafteinwirkung wurde mit Hilfe von in-situ Röntgenstreumethoden charakterisiert. Diese Methode gibt Aufschluss über Änderungen des Deformationsverhaltens bei unterschiedlichen Nanostrukturen und des Verhaltens jener Strukturen. Die globalen mechanischen Kenndaten (bestimmt durch dynamisch mechanische Zugversuche, Zugversuche, Durchstoßversuche) wurden zur Ermittlung von Struktur-Eigenschaftsbeziehungen herangezogen.

Zwei verschiedene Typen von teilkristallinem, isotaktischem Polypropylen werden in dieser Arbeit als Matrixpolymer verwendet. Der Grund für die Wahl von zwei Typen (ein Extrusionstyp und ein Rohrtyp) war, die Anwendbarkeit und die Effizienz des Produktionsprozess darzustellen. Als Nanofüllstoff wurde ein smektisches Tonmineral Montmorillonit verwendet. Diese beiden Ausgangsmaterialien - Polypropylen und Montmorillonit - sind miteinander unverträglich, weswegen ein sogenannter Haftvermittler notwendig war. Die verwendete Produktionsmethode zur Herstellung von Polypropylen Nanokompositen war die Schmelzcompoundierung. Detailliertere Informationen und die theoretischen Grundlagen von polymeren Nanokompositen, vom verwendeten Produktionsprozess, sowie von den verwendeten Röntgenstreumethoden sind in Kapitel 2 ausführlicher dargestellt.

Im dritten Kapitel der vorliegenden Arbeit wird die Bestimmung der Verteilungsqualität des Füllstoffs mittels zweier unterschiedlicher Methoden erläutert. Die Bestimmung der Verteilungsqualität erfolgt einerseits während des Prozesses (Nahinfrarotspektroskopie und Dehnungsrheometrie) und andererseits nach dem Prozess (Röntgenstreumethoden). In diesem Teil werden der verwendete Prozess und die beiden Methoden zur Bestimmung der Verteilungsqualität näher dargestellt. Die Verwendung eines chemometrischen Modells erlaubt die Korrelation von Inline Nahinfrarotspektren mit den durch Röntgenstreumethoden ermittelten Strukturen (Schichtabstand, Exfolierungsgrad) der polymeren Nanokomposite. Auch eine Korrelation der dehnrheologischen Eigenschaften (Abzugskraft) mit jenen der mechanischen Eigenschaften (Elastizitätsmodul) war möglich. Mit den während des Prozesses gewonnenen Daten kann der Prozess schnell verändert werden, um die gewünschten Formulierungen (Struktur, mechanische Eigenschaften) zu erhalten.

Kapitel 4 beschreibt die Struktur und Strukturänderungen während des Produktionsprozesses. In mit Schichtsilikaten hergestellten Nanokompositen, kommt es meist zu einer Agglomeratbildung. Dies sind Gebiete in denen sich vermehrt die Schichtsilikate anhäufen. Die Struktur eines solchen Agglomerates wurde mit Hilfe eines sehr kleinen Röntgenstrahles untersucht. Das Matrixpolymer bildete unterschiedliche Formen (α und β-Polypropylen) aus. Die Strukturänderung des Füllstoffes (interkaliert bis exfoliert) konnte ebenfalls bestimmt werden. Während der Kern des Agglomerates selbst keine Veränderung des Schichtabstandes aufwies, zeigte sich am Rande des Agglomerates

eine zunehmend interkalierte Struktur. Diese wiederum war von einer exfolierten Schichtsilikat-Polypropylen Masse umgeben. Zusätzlich wurde die Struktur der Schichtsilikate und deren polymeren Kompositen unter prozessrelevanten Temperaturen untersucht. Der Schichtabstand des Schichtsilikates ist bei erhöhter Temperatur größer. Dies führt zu einer Vereinfachung des Interkalierungsprozesses mittels Schmelzcompoundierung.

Der fünfte Teil dieser Arbeit beschäftigt sich mit den Deformations- und Bruchmechanismen von schichtsilikatverstärktem Polypropylen. Reines Polypropylen zeigt unterschiedliche Deformationsmechanismen: Hohlraumbildung, Crazing und Mikrorissbildung begleitet von einem spröden Bruch einerseits und Scherfließen begleitet von einem duktilem Versagen andererseits. Bei Anwesenheit eines Füllstoffes muss (in der Regel) diese Liste um Ablöseerscheinungen und die sich somit ergebende schnellere Hohlraumbildung erweitert werden. In diesem Teil der Arbeit werden die prinzipiellen Deformationsmechanismen dargestellt. Die strukturellen Informationen rund um eine belastete Rissspitze wurden mit Hilfe von Röntgenstreumethoden ermittelt. Während bei schichtsilikatverstärktem Polypropylen die Ausbildung einer dünnen hochorientierten Zone zu einem spröden Versagen führt, ist bei reinem Polypropylen die Ausbildung einer ausgedehnten wenig orientierten Zone vorherrschend, die anschließend zu einem duktilen Versagen führt. Außerdem wurden in diesem Kapitel sogenannte röntgenelastische Konstanten bestimmt. Dazu wurden kristallographische Dehnungen mit der globalen Spannung zusammengeführt und daraus Konstanten ermittelt. Bei erneuter Messung der kristallographischen Dehnung des gleichen Materials (mit unbekanntem Querschnitt) ist es möglich, die vorherrschenden Spannungen (mit der Anwendung der vorher bestimmten Konstanten) zu ermitteln. Mit dieser Methode wurden strukturelle und mechanische Eigenschaften korreliert.

Im sechsten Kapitel wurden strukturelle Parameter mit mikro- und makromechanische Eigenschaften zueinander in Beziehung gesetzt. Die strukturelle Eigenschaft (Exfolierungsgrad) wurde mit den dynamisch-mechanischen Eigenschaften (Mobilität der Polymerketten) und den mechanischen Eigenschaften (Steifigkeit und Bruchdehnung) korreliert. Es konnte ein Zusammenhang zwischen der Beweglichkeit der Polymerketten und dem Exfolierungsgrad hergestellt werden: Je höher der Exfolierungsgrad, desto größer ist die Behinderung der Polymerketten. Dies führte zu einer Erhöhung der

Übergangstemperaturen, wie z.B.: der Glasübergangstemperatur und der α-Relaxaktionstemperatur. Weiter konnte eine Erhöhung der Steifigkeit durch die Anwesenheit von interkalierten Schichtsilikatstapeln gezeigt werden. Die Bruchdehnungen hingegen nahmen bei Anwesenheit von Schichtsilkatstapeln sehr stark ab. Die Erklärung für dieses Verhalten ist, dass die steifen Schichtsilikatstapeln einerseits den Materialverbund verstärken, andererseits sind diese auch Ausgangspunkte für Defekte. Bei einer Erhöhung des Exfolierungsgrades sinkt die Steifigkeit und die Bruchdehnung steigt. Somit kann gezeigt werden, dass die Struktur von schichtsilikatverstärkten Kunststoffen einen erheblichen Einfluss auf die mechanischen Eigenschaften besitzt.

Abstract

Polymeric nanocomposites have become increasingly popular in the scientific community, since the first publication 30 years ago. Due to the high surface to volume ratio of fillers with dimensions in the nanometres range, already a small amount of such fillers influences physical properties of polymers and often enhances multiple properties at once. Structural details and their relationships to the mechanical, optical and permeation properties of the nanocomposites are rather fascinating, because most physical parameters are triggered by an arrangement of the nanofiller in polymer matrix. Moreover, the low costs of clay-containing polymeric nanocomposites hold great appeal for the industrial community. The properties of a polymer nanocomposite basically depend on the behaviour of the matrix, the properties of the filler, the interactions between the filler and the polymer and finally on the arrangement of filler in matrix. Therefore, the structural details and their influence on the physical properties are very important for the system of this material. The main aim of this work was to correlate the structural details of clay-containing polymeric nanocomposites with mechanical properties.

Structural details can be determined via: X-ray scattering techniques, transmission electron microscopy, atomic force microscopy, infrared spectroscopy and nuclear magnetic resonance spectroscopy, which represent the most common applied techniques. For this work, X-ray scattering techniques, and near infrared spectroscopy, were conducted as structural investigations. Detailed nanostructure information was generated via application of different X-ray scattering techniques to cover structural information between 100 (small angle X-ray scattering) and 0.1 (wide angle X-ray scattering) nanometres. The behaviour of the structural details under external loads and under process conditions was determined by means of in-situ X-ray investigations. Thus, structure-property relationships were established. A correlation between structural details and global mechanical properties is presented in this work as well.

As matrix polymers, two different types of semi crystalline isotactic polypropylene were selected. Two different grades of polypropylene, one extrusion grade and one pipe grade, were chosen to demonstrate the functionality and efficiency of the production process. As a nanofiller, the commercial smectite clay mineral montmorillonite was used. These two materials were rather incompatible; hence, a compatibilizer (a polypropylene grafted with maleic acid anhydride) was needed. Detailed information on the structure of polymeric

nanocomposites and the production process of the investigated polymers is highlighted in the second chapter of this work. The selected production process was the melt compounding. Background information concerning X-ray scattering techniques is also presented in the second chapter of this work.

In the third chapter of this work, the distribution quality is characterised by the usage of two different techniques. For once, characterisation methods like inline near infrared or online extensional melt rheology help to determine the structural details during the production process. These methods were implemented by the Chair of Polymer Processing and can be used as a quick quality control for the individual processes. On the other hand, structural details were measured using X-ray scattering techniques. Chapter three delivers an overview on the employed production process and the two applied methods for characterisation of distribution quality. The use of a chemometric model allowed for a correlation of inline near infrared spectroscopy data with structural details (interlayer distance, degree of exfoliation) of the produced compound and correlation of online extensional melt rheology (tensile force at break) with mechanical properties (Young's Modulus). Therefore, a concurrent estimation of the structural and the mechanical properties of the produced compound is created. With that realtime knowledge, the production process can be altered fast enough to perform within desired specifications of the produced polymeric nanocomposites.

Chapter 4 of this thesis describes structural details of polymeric nanocomposites under process conditions. The results were used to demonstrate the compounding process and to optimize its conditions. In nanocomposites, often so called “agglomerates”, dense clusters of particles, are formed. The structure in and around an agglomerate was studied with nano-beam X-ray scattering microscopy at European Synchrotron Radiation Facility (ESRF) in Grenoble. The structural details around the filler in agglomerated form revealed various modifications of the polymer. Different structure formations of polypropylene (α- and β-form) around a layered silicate stack were observed. Accordingly, the understanding and analysis of mechanical behaviour of polymeric nanocomposites (with small amounts of agglomerates) was improved. Furthermore, structural details under process related temperatures were investigated. For example, the interlayer distance of the organic modified montmorillonite increased at higher temperatures. This information further

enhances the understanding and ultimate fine-tuning of the production process. Likewise, at higher filler concentration, the clay forms a super structure (card house).

The fifth chapter deals with in-service behaviour of polypropylene nanocomposites; more explicitly: the determination of deformation and fracture mechanisms in the polypropylene-nanoclay system. Virgin polypropylene showed different deformation mechanisms, void formation, crazing and micro cracking accompanied with brittle failure and shear yielding associated with ductile fracture. Due to the presence of a filler, the failure behaviour depends on the strength of the filler/matrix interaction; therefore the deformation mechanisms have to be extended by the debonding process and a faster void formation. Commonly known deformation mechanisms were analysed in regard to quality and described by means of structural properties. Due to the difference in virgin and clay-reinforced polypropylene, further investigations were performed. Structural details around crack tips, determined via scanning X-ray scattering techniques, were analysed to fully comprehend the change in the deformation mechanisms between polymer and polymer nanocomposites. The polypropylene nanocomposite displayed a thin zone with a high degree of orientation, which was related to brittle failure. However, virgin polypropylene formed a broad zone with a low degree of orientation, which was related to a ductile failure mechanism. Within this work, X-ray elastic constants were also observed. These constants can be exploited in the determination of stress in elusive positions. In consequence, micro-strains (strains in crystallographic planes) were correlated with the global applied stress. Wherefore structural details were correlated directly with mechanical properties.

In the sixth chapter of this work, structural parameters of clay-containing polypropylene nanocomposites, were correlated to micro- and macro-mechanical properties. The structural results (interlayer distance, degree of exfoliation) were correlated with the thermo-mechanical (mobility of polymer chains) and macro-mechanical (stiffness, elongation at break) results. This allowed for the conclusion that the mobility of polymer chains was influenced by the degree of exfoliation. The higher the degree of exfoliation, the more the mobility of the polymer chains was hindered and the transition temperatures (glass transition and α-relaxation temperatures) increased. Furthermore, due to the presence of intercalated stacks, the stiffness of the composite increased; however, the elongation at break decreased. This happened as the stiffly layered packages further strengthen, while simultaneously acting as a defect. Nevertheless, for composites with a

high degree of exfoliation, the mechanical properties change to a lower stiffness and a higher strain at break. Consequently, the degree of exfoliation influences the mechanical properties.

Table of content

Acknowledgements ..... **IV**
Kurzfassung ..... **V**
Abstract ..... **IX**
Table of content ..... **XIII**
Table of figures ..... **XIV**
1 Scope, content and structure **1**
2 Background **5**
2.1 Clay containing polymeric nanocomposites 5
2.2 X-ray and scattering of X-rays 9
2.3 References 29
3 Characterisation of distribution quality of layered silicates in polypropylene by X-ray scattering and near infrared techniques **32**
3.1 Major results 32
3.2 Paper 1 34
3.3 Paper 2 42
3.4 Paper 3 43
4 Morphology and structure of clay polypropylene nanocomposites **56**
4.1 Major results 56
4.2 Paper 4 58
4.3 Paper 5 70
5 Micromechanics of clay polypropylene nanocomposites **76**
5.1 Major results 76
5.2 References 78
5.3 Paper 6 79
5.4 Paper 7 88
5.5 Paper 8 89
6 Macromechanics of clay polypropylene nanocomposites **110**
6.1 Major results 110
6.2 Paper 9 112
7 Summary and outlook **124**
7.1 Summary of major results 124
7.2 Outlook 125

Table of figures

Figure 1 Structure of 2:1 phyllosilicates 5
Figure 2 Montmorrillonite with different organically modifications 6
Figure 3 Structures of layered silicates reinforced polymers 7
Figure 4 Schematic construction of single slit diffraction (left) and a typical diffraction pattern from single slit diffraction (right). 10
Figure 5 Schematic demonstration of two (or multi) slit diffraction. 10
Figure 6 Schematic presentation of the plane reflections 11
Figure 7 Radial integration 12
Figure 8 Azimuthal or χ - integration. 13
Figure 9 WAXS diffraction pattern with the (ab)-projection of the crystal lattice from the different forms of isotactic PP 14
Figure 10 Analysis of crystallographic strain. 15
Figure 11 Determination of the (mass) degree of crystallinity. 16
Figure 12 Determination of orientation by X-ray scattering techniques. 18
Figure 13 Determination of the degree of orientation 18
Figure 14 Electron density distribution η and the corresponding correlation function $\gamma(r)$ of a lamellar two phase system 19
Figure 15 Evaluation process for the usage of the one dimensional correlation function 20
Figure 16 Schematic representation of the scattering process 21
Figure 17 Distortions of first (a) and second (b) kind 27

1 Scope, content and structure

In the last decades, fillers, which improve polymer properties or give the polymer improved functionality, experienced an increase in demand. Especially fillers, which possess dimensions in the nanometers range, became highly popular in the industry and research centres concerning material sciences (Ray and Okamoto, 2003; Alexandre and Dubois, 2000; Coleman et al., 2006). Due to their high surface to volume ratio, the filler exhibit greater fusion potential with the polymer, duly enhancing the interaction between the polymer chains and the filler (Tjong, 2006; Pavlidou et al., 2008; Breuer and Uttandaraman Sundararaj, 2004). For that reason, polymeric nanocomposites offer similar performance with lower loading levels (2-3 wt.%), than conventional composites with 30-50 wt.% of reinforced material (Utracki, 2004). The main benefits of polymeric nanocomposites are increasing Modulus, strength, heat resistance, etc. and all simultaneously. Moreover, nano-fillers exhibit advanced functionality; for example carbon nanotubes increase the thermal conductivity dramatically (Gojny et al., 2006), layered silicates decrease the permeability (Ray and Okamoto, 2003), etc.

The properties of a polymer composite (and nanocomposite) basically depend on the behaviour of the matrix, the properties of the filler, the interactions between the filler and the polymer and on the spatial distribution and orientation of the filler (Utracki, 2004). The structure of heterogeneous systems is of high scientific and practical interest; particularly the behaviour of the filler (interactions with the matrix, distribution and orientation) is further important for understanding mechanical properties. For clay-containing polymeric composites, several superstructures of layered silicates are possible and depend on the distribution quality of the filler. These superstructures strongly influence the interaction between filler and matrix; consequently, the mechanical properties are affected.

Several strategies to adequately determine distribution quality were investigated in recent years. The most commonly used methods are transmission electron microscopy, atomic force microscopy, infrared spectroscopy, nuclear magnetic resonance spectroscopy and X-ray scattering techniques (Utracki, 2004). For this work, near infrared spectroscopy, transmission electron microscopy and X-ray scattering techniques were employed for structural characterisation of the produced polymeric nanocomposites. Micromechanic (mechanic of crystal lattice) and macromechanic (global mechanical properties) methods

were exploited to successfully characterise the influence of structural details on commonly known mechanical properties. Micromechanical investigations were performed, using in-situ X-ray scattering tensile tests. These were done utilizing the capabilities of several synchrotron radiation facilities (Berliner Elektronenspeicherring-Gesellschaft für Synchrotronstrahlung m.b.H. in Berlin and European Synchrotron Radiation Facility in Grenoble).

The aim of this thesis is to thoroughly investigate clay-containing polypropylene nanocomposites. There are several ways to produce intercalated (or exfoliated) polymeric nanocomposites (Ray and Okamoto, 2003). The selected production process was the melt compounding. Producing fully exfoliated layered silicates reinforced polymer produced by melt compounding is of high interest in the industrial community. To succeed, the production process has to be adapted. Here, the polypropylene nanocomposites were produced over a masterbatch process. In this way, a highly filled compound is produced, which is subsequently diluted to the final filler content. The amount of inserted shear energy and the mean residual time in the extruder are the two main principal process parameters, which are varied. The modification of those parameters influences the quality of distribution of the clay.

This dissertation consists of five main chapters, aiming to successfully answer its two principal goals: characterisation of the distribution quality and structure-property relationships of clay-containing polypropylene nanocomposites. The second chapter highlights the important basics of polymeric nanocomposites, especially layered silicate reinforced polypropylene, and the basics of structural investigations by X-ray scattering techniques. The third chapter deals with the distribution quality of silicate layers in the polymer, characterized by process inline near infrared and simple X-ray scattering methods. The fourth chapter focuses on the morphological structure of the produced polymeric nanocomposites. Accordingly, the structural changes of clay-containing polypropylene nanocomposites during the production process are illustrated by the means of in situ X-ray techniques. The structure of one residual agglomerate in the nanocomposite is investigated, resulting in improved understanding of the exfoliation process during melt compounding. Chapter five focuses on the micromechanics of clay-containing polypropylene nanocomposites and the structure-properties' relationships on a microscopic scale. Therefore, deformation mechanism and mechanics of crystallographic

lattice were investigated with the help of in situ X-ray scattering tensile tests. The sixth chapter concentrates on the structure-properties' relationships of polymeric nanocomposites on a macroscopic scale. Forasmuch, global mechanical properties (tensile test, puncture test, thermomechanical tensile test) were correlated with structural details (X-ray scattering techniques). The superstructures of layered silicate were correlated with the mobility of polymer chains and this was then related to global mechanical properties. The final chapter summarizes the major results and presents an outlook for future work.

1.1 References

Alexandre, M., Dubois, P. (2000). Materials Science and Engineering, **28**, 1.

Breuer, O., Uttandaraman Sundararaj (2004). Polymer Composites, **25**, 630.

Coleman, J.N., Khan, U., Blau, W.J., Gunko, Y.K. (2006). Carbon, **44**, 1624.

Gojny, F.H., Wichmann, M.H.G., Fiedler, B., Kinloch, I.A., Bauhofer, W., Windle, A.H., Schulte, K. (2006). Polymer, **47**, 2036.

Pavlidou S., Papaspyrides C.D. (2008). Progress in Polymer Science, **33**, 1119.

Ray S.S., Okamoto M. (2003). Prog. Polym. Sci., **28**, 1539.

Tjong S.C. (2006). Materials Science and Engineering R, **53**, 73.

Utracki, L.A. (2004). "Clay-Containing polymeric nanocomposites", Rapra Technology Limited, Shawbury, Shrewsbury, UK.

2 Background

2.1 Clay-containing polymeric nanocomposites

The clay-containing polymeric nanocomposites offers a couple of advantages related to matrix polymer or common composites. At loading levels from 2 to 3 wt. %, they are able to reach the same performance level as conventional composites with 30 to 50 wt. % (Utracki, 2004). Ergo, density of polymeric nanocomposites remains at the same level as the matrix polymer. Composites with filler dimensions in the nanometer range have a high surface to volume ratio. Due to their high surface to volume ratio, the filler exhibit greater fusion potential with the polymer, duly enhancing the interaction between the polymer chains and the filler (Tjong, 2006; Pavlidou et al., 2008; Breuer and Uttandaraman Sundararaj, 2004). The main advantages are improvements in Modulus, strength, heat resistance, flame resistance, barrier properties et cetera (Ray and Okamoto, 2003). The amount and size of the clay particles improve the useability and the transparency in opposition to highly filled, conventional composites (Pavlidou and Papaspyrides, 2008).

2.1.1 Montmorrillonite

Montmorillonite is a member of the smectite phyllosilicates family, a group of minerals that consists of two tetrahedral sheets, sandwiching a central octahedral sheet. Figure 1 demonstrates a typical structure of a phyllosilicate. Montmorillonite possess the chemical formula $M_x(Al_{4-x}Mg_x)Si_8O_{20}(OH)_4$, where M represents a monovalent cation and x the degree of isomorphous substitution (between 0.3 and 1.3). The particles are plate-shaped with dimensions in nanometres size (~ 1nm thickness and ~ 100 nm length).

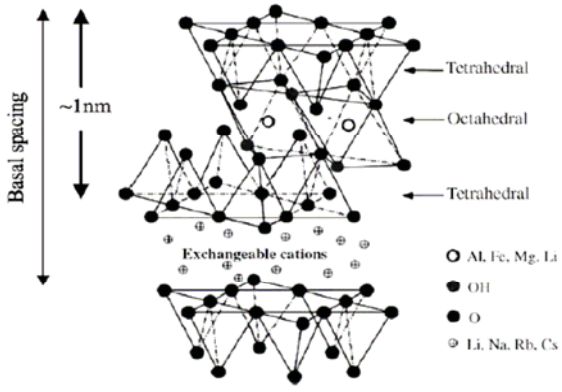

Fig. 1. Structure of 2:1 phyllosilicates.

Figure 1 Structure of 2:1 phyllosilicates (Giannelis et al., 1999).

Organic modification of the filler is necessary to improve the interaction between the hydrophilic surface of the nanoclay and the hydrophobic polymer. Surface modification of montmorrillonite is mainly performed by ion exchange reactions with cationic surfactants like alkylammonium or alkyl phosphonium cations. The alkyl can vary from very short chains (~ 2) to very long ones (~ 25). The length of the grafting chains influences the interactions between two clay platelets. Nevertheless, positive attraction between the individual layers exists. Different examples are sketched in Figure 2 (Heinz et al., 2007).

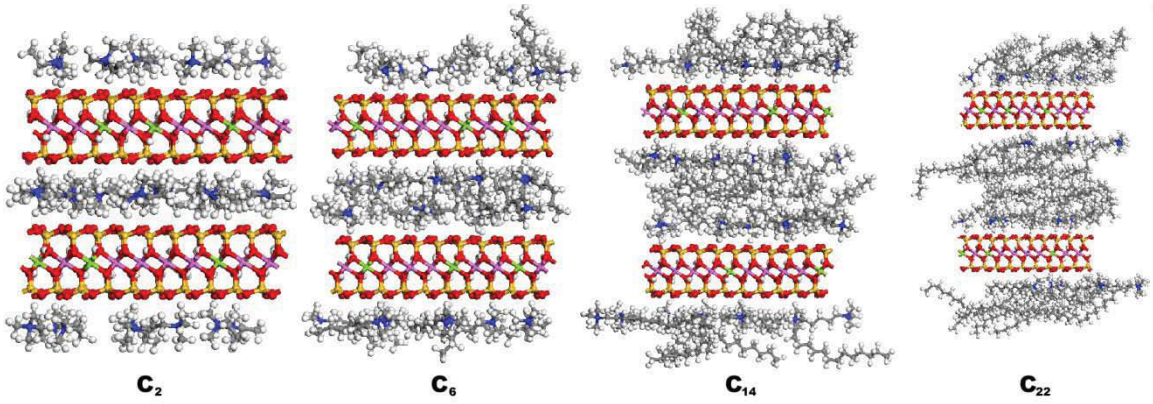

Figure 2 Montmorrillonite with different organically modifications. The captions intend to inform about the average length of the organic modifier (Heinz et al., 2007).

2.1.2 Structures of layered silicates reinforced polymers

For layered silicate-reinforced polymers, the structure of the filler can assume several modes of beings. The first one is the agglomerated condition. Here, the layered silicates have no interactions with the polymer and the agglomerates possess dimensions in the micrometer range (Alexandre and Dubois, 2000). The next state is the so-called “intercalated" one, where polymer chains are placed between the platelets. In this case, the silicate layers are interacting and the interlayer distance is higher, than in the agglomerated mode (Utracki, 2004; Tjong, 2006). The third state is called the “exfoliated” mode. This occurs, when more and more polymer chains gather between the platelets, causing the layered structure to break up. In that case, the platelets do not interact (Pavlidou and Papaspyrides, 2008). A fourth state is the so-called “flocculated” one. This is a special condition of the intercalated state, where the intercalated stacks possess an additional edge-to-edge interaction (Ray and Okamoto, 2003). In Figure 3, the different states of layered silicate reinforced polymers are illustrated.

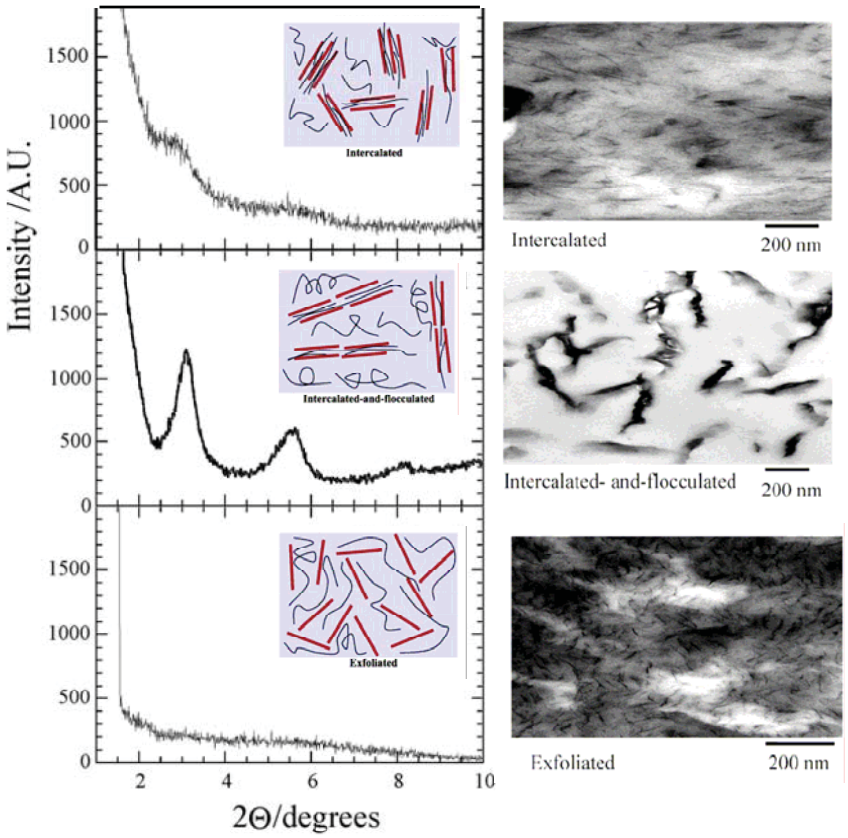

Figure 3 Structures of layered silicates reinforced polymers (Ray and Okamoto, 2003).

The different structures of clay-containing polymer nanocomposites result in various mechanical properties. In principle, the tensile strength and the Young's Modulus increase in clay-containing polypropylene; however, the elongation at break decreases (Ray and Okamoto, 2003). The intercalated form of layered silicates presents a distinct increase in stiffness, due to the stiffly layered package acting as strengtheners. The exfoliated form presents an increase as well; yet, the Young's Modulus is lower than in intercalated clay-reinforced polymeric nanocomposites (Tjong, 2006). The elongation at break dramatically decreases, if layered silicate is present in a polymer matrix. The decrease is more pronounced in the intercalated form, where the layered silicate package acts as a defect. The fracture behaviour dramatically improved in layered silicates, containing polymeric systems. High importance is placed upon the creation of a new surface through crack propagation, intended to toughen a clay-containing polymeric system (Zerda and Lesser, 2001).

2.1.3 Production of layered silicates reinforced polymers

Several strategies exist to produce exfoliated clay-containing polymers. The main methods are in-situ polymerization, polymer intercalation from solution and melt compounding (Utracki, 2004). All the measured samples in this work were produced via melt compounding.

The principle of melt compounding is to combine the polymer with clay. This can be done with an internal mixer for small amounts or with a twin screw extruder for throughputs on industrial scale dimensions (Utracki, 2004). The main difficulty of this production process is the incompatibility of the raw materials. The chosen raw materials were polypropylene and montmorrillonite. These materials are rather incompatible and melt compounding does not work without some modifications. Montmorrillonite possesses a polar and hydrophilic surface (Choy et al., 1997); however, polypropylene is hydrophobic and non-polar. In the case of melt compounding, both raw materials have (montmorrillonite and polypropylene) to be particularly prepared. Alkylammonium or alkyl phosphonium cations substitute the cations on the surface of the montmorillonite to increase the hydrophilicity and to pre-intercalate the layered structure of the silicate (Utracki, 2004). Otherwise, the polypropylene is partially grafted with maleic anhydride to make the polymer more polar. For the preparation of the mixture, a so-called “compatibilizer” (maleic anhydride grafted polypropylene) was used. The compatibilizer helps to improve the exfoliation process (Ke and Stroeve, 2005); albeit, the mechanical properties are negatively influenced. Therefore, the amount of compatibilizer plays an important role for the performance of the produced mixture.

Melt compounding works according to the following steps: (1) the clay is mixed with the polymer, both are not interacting (microcomposites); (2) the compatibilizer is getting between two silicate layers and the interlayer distance is increasing (intercalation); (3) virgin polymer is able to move between the dehisced structure of layered silicate stack until the layered structure is shattered (exfoliation) (Ray and Okamoto, 2003). During the process, two main properties are important to enhance the degree of exfoliation. On the one hand, the mean residual time can influence the exfoliation process. The longer the compound is exposed to heat and shear energy, the easier the mentioned steps can be performed. The mean residual time can be varied with the use of a string die behind the compounding process. On the other hand, the inserted shear energy can influence the

degree of exfoliation. The inserted shear energy can be changed by using different screw geometries and by varying the rotational speed of the screw.

2.2 X-ray and scattering of X-rays

The main structural investigations were completed by X-ray scattering techniques. Thus a detailed description of applied elastic scattering techniques and a review on the used evaluation techniques are included. There are many textbooks available, dealing with the interaction of X-rays with matter (Guinier, 1963; Alexander, 1969; Glatter, 1982; Balta-Calleja and Vonk, 1989). Henceforth, only a small introduction shall be provided here. X-radiation is electromagnetic radiation with a wavelength in the range of 0.01 to 10 nanometers. Basically, two different interactions between X-radiation and the electrons of matter exist: scattering and absorption. During the absorption processes, kinetic energy of the incoming rays is lost by means of the photoelectric effect (Auger effect) and inelastic scattering (Compton effect). (Guinier, 1963)

Elastic scattering is defined as follows: The incoming and the outgoing radiation possesses the same wavelength; consequently, no energy transfer between the radiation and the electron is observed. Inelastic (Compton) scattering, which includes an energy transfer between the incoming and outgoing waves, was not considered in this work. Elastic scattered waves are able to coherently interfere; that means that the outgoing scattering waves are superposing. As a result, it is possible that the summarized outgoing waves either congregate (= constructive interference) or are erased (= destructive interference) (Guinier, 1963).

The simplest explanation for diffraction concerns the single slit diffraction. An example of that is shown in Figure 4. If light irradiates a long infinitesimal slit, the light is diffracted into a series of circular waves; if, the slit is wider than the wavelength, interferences might still occur. These can be explained by assuming that the slit behaves as though it has a large number of point sources, spaced evenly across the width of the slit. If the light possesses a single wavelength, the minima and maxima of the diffracted light can be observed.

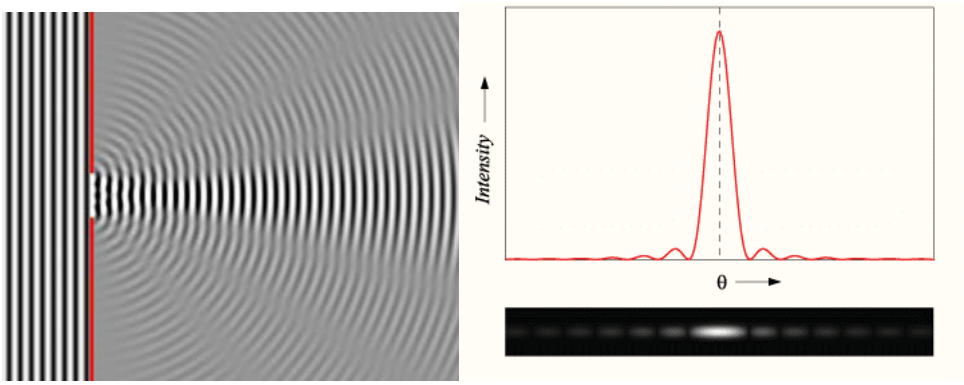

Figure 4 Schematic construction of single slit diffraction (left) and a typical diffraction pattern from single slit diffraction (right).

Multiple slit arrangements, which are narrow enough, can be described via the Fraunhofer approximation. In Figure 5, a simple two-slit example is illustrated and with the mentioned approximation, the maxima of the diffracted beam can be calculated by Eq. (1).

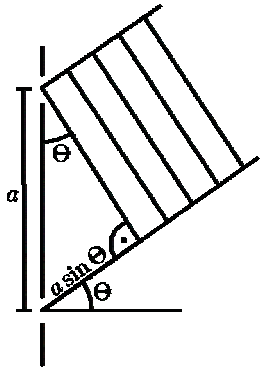

Figure 5 Schematic demonstration of two (or multi) slit diffraction.

Diffraction from a three-dimensional periodic structure (like atoms in crystals) is called "Bragg diffraction", which is a consequence of interfering waves, reflecting from crystal planes (see Figure 6).

$$a * \sin(\Theta) = n * \lambda \qquad \text{Eq. (1)}$$

n is an integer that labels the order of each maximum, l is the wavelength, a is the distance between the slits and Θ is the angle at which constructive interference occurs.

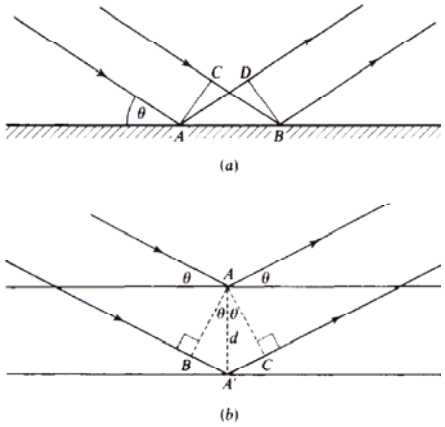

Figure 6 Schematic presentation of the plane reflections. (a) Parallel rays reflected from different points of one plane and (b) parallel rays reflected from points on neighbouring reflecting points. The reflected rays are in phase, when Bragg's law is obeyed. (Woolfson, 1970)

Bragg's law (Eq. (2)) defines the conditions of constructive interference (Bragg, 1913; Alexander, 1969).

$$n * \lambda = 2 * d * \sin(\Theta) \qquad \text{Eq. (2)}$$

In Eq. (2), n ($n = \sqrt{h^2 + k^2 + l^2}$) is an integer known as the order of the lattice plane (h,k,l), λ is the wavelength, d is the distance between crystal planes and Θ is the half scattering angle. With the knowledge of the scattering angle and the wavelength, the distance between the lattice planes d_{hkl} can be calculated. The indices h, k, l are representing the Miller indices, which are a notation system in crystallography for defining planes and directions in crystal lattices. The Bragg equation also provides insight to the reciprocal space coordination system, where diffraction occurs. For a diffraction pattern, large distances occur at small diffraction angles and vice-versa.

2.2.1 Data evaluation

Most of the measurements (Paper 1 to 3, Paper 5, Paper 9) were performed using a Bruker NanoStar (Bruker AXS, Karlsruhe, Germany) Small Angle X-ray scattering instrument. This system was equipped with a two-dimensional X-ray detector. A wavelength of 0.154 nm (CuKα) was used. The samples were measured in transmission and under vacuum conditions. In-situ and nano-beam measurements were performed, utilizing synchrotron radiation (Paper 4, Paper 6, Paper 7, Paper 8). The beamlines were also equipped with two-

dimensional X-ray detectors and the measurements were performed in transmission. In order to interpret the information, the two-dimensional diffraction pattern had to be reduced to a one-dimensional scattering curve. According to different structural information, the two-dimensional diffraction pattern can be integrated in different ways:

- Radial integration: the diffraction pattern is integrated from the beamcenter to the larger angle (Alexander, 1969).

$$I(q) = \int_0^{2\pi} I(q,\chi)d\chi \qquad \text{Eq. (3)}$$

This method is used to determine structural parameters like long period, interlayer distance, crystal structure, lattice parameter etc. In Figure 7, the radial integration is illustrated.

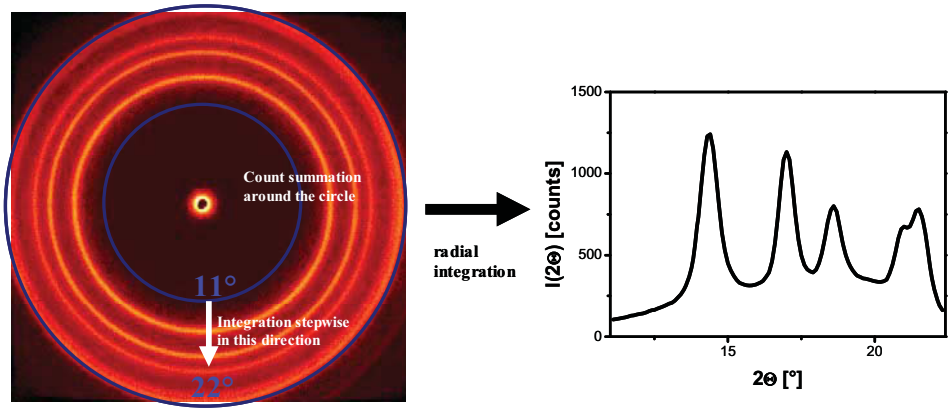

Figure 7 Radial integration

- Azimuthal or χ - integration: the diffraction pattern is integrated for each diffraction angle from the beamcenter to larger angles (Alexander, 1969).

$$I(\chi) = \int_{q_{\min}}^{q_{\max}} I(q,\chi)dq \qquad \text{Eq. (4)}$$

This method will be used for orientation quantification. The χ-integration is graphically explained in Figure 8.

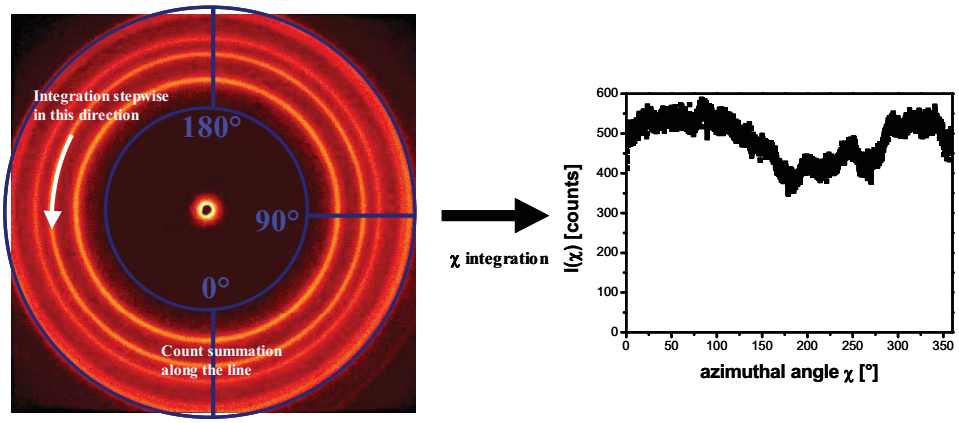

Figure 8 Azimuthal or χ - integration.

2.2.2 Wide Angle X-ray Scattering (WAXS)

For WAXS measurements, the generated diffraction pattern allows to determine the structural details with dimensions in the nanometres range or below, e.g.: phase composition of the polymer/filled polymer systems, the texture of the mentioned systems or degree of crystallinity (Alexander, 1969).

Phase composition

Semi-crystalline polymers consist of crystalline and amorphous domains. The crystalline part can be evaluated by the usage of WAXS measurements. Besides, the same polymer can exhibit a different crystal structure, so-called “polymorphs”. The exact crystal structure and the corresponding lattice parameters can be evaluated by the use of Miller Indices and the Bragg equation (see Eq. (2)).

Figure 9 shows three one-dimensional scattering curves of polypropylene. These are representing the three main types of crystal lattice, which can be observed in isotactic polypropylene (Brückner et al., 1991; Karger-Kocsics, 1995). The various types are the monoclinic form (called α-form), the hexagonal form (called β-form) and the orthorhombic form (called γ-form) (Wunderlich 1973). The corresponding unit cells of each type of PP are pictured additionally in Figure 9. With the knowledge concerning the different types of crystal lattice and with determined peak positions and their intensities, it is possible to calculate phase compositions of materials, which possess more than one crystalline lattice (Alexander, 1969).

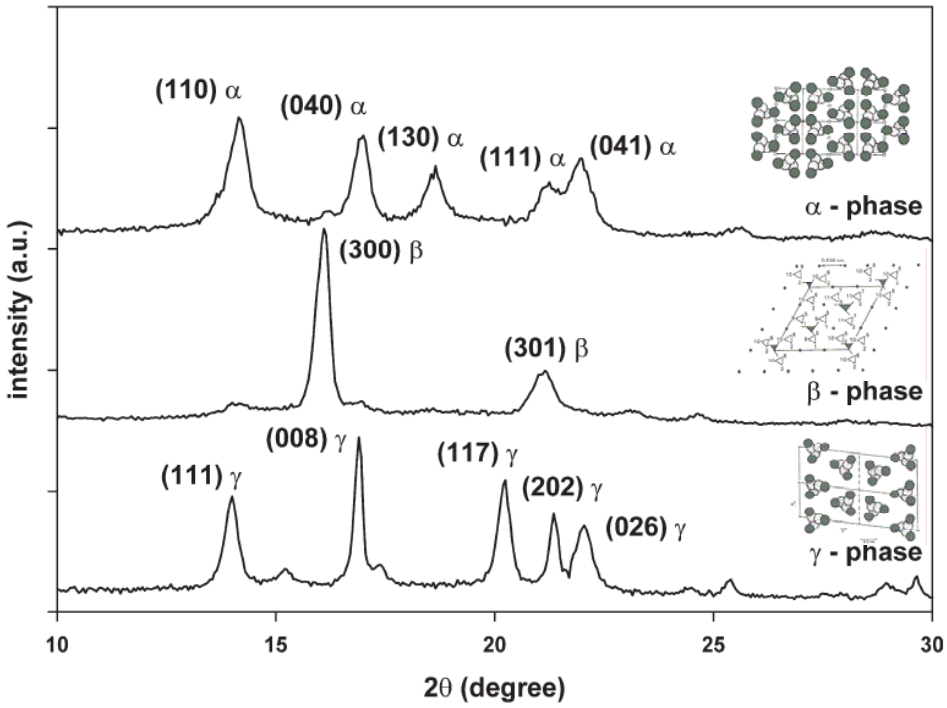

Figure 9 WAXS diffraction pattern with the (ab)-projection of the crystal lattice from the different forms of isotactic polypropylene (Karger-Kocsics, 1995; Lezak and Bartczak, 2005).

Peak shifting

The distance between two lattice planes can be determined by the use of Eq. (2). This distance can shift, due to residual stress, external loads or crystal imperfections. Figure 10 shows the possible changes of the peak positions during external load on a polypropylene sample. By knowing the initial plane distance d_0, micro strains can be determined using Eq. (5).

$$\varepsilon_{micro} = \ln\left(\frac{l}{l_0}\right) = \frac{d - d_0}{d_0} \qquad \text{Eq. (5)}$$

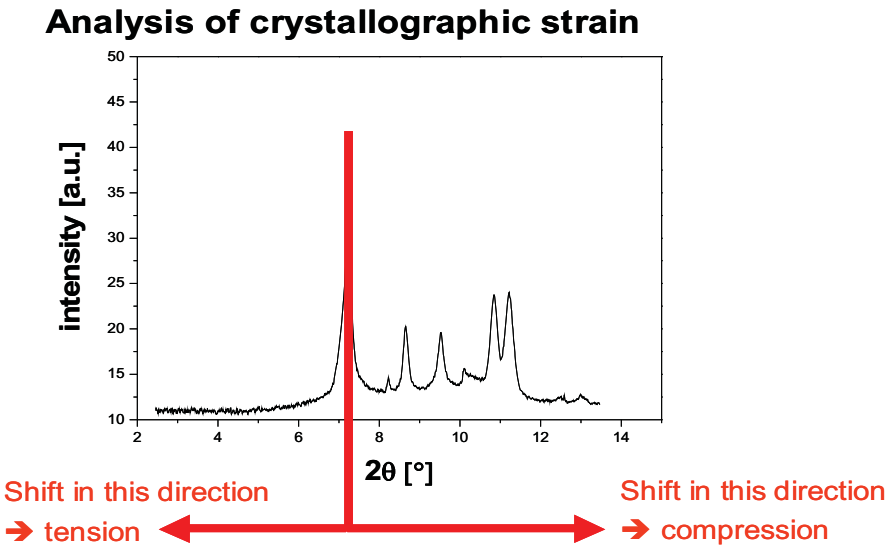

Figure 10 Analysis of crystallographic strain.

Degree of crystallinity

The weight degree of crystallinity can be evaluated by interpreting WAXS curves. Therefore, several methods were worked out during the last decades. One of them is to compare the areas under the WAXS curves. This method will be explained with the help of an example, presented in Figure 11. In Figure 11, a one-dimensional scattering curve of polypropylene is shown. The sharp peaks are representing the crystalline structure of an α-polypropylene. The amorphous halo is a very broad peak underneath the crystalline peaks (Debye 1915; Guinier 1963). The ratio of the sum of the areas of the amorphous content and the sum of the areas of the crystalline content characterise the degree of crystallinity (Ruland, 1964; Balta-Calleja and Vonk, 1989). In Figure 11, the basic procedure is graphically explained.

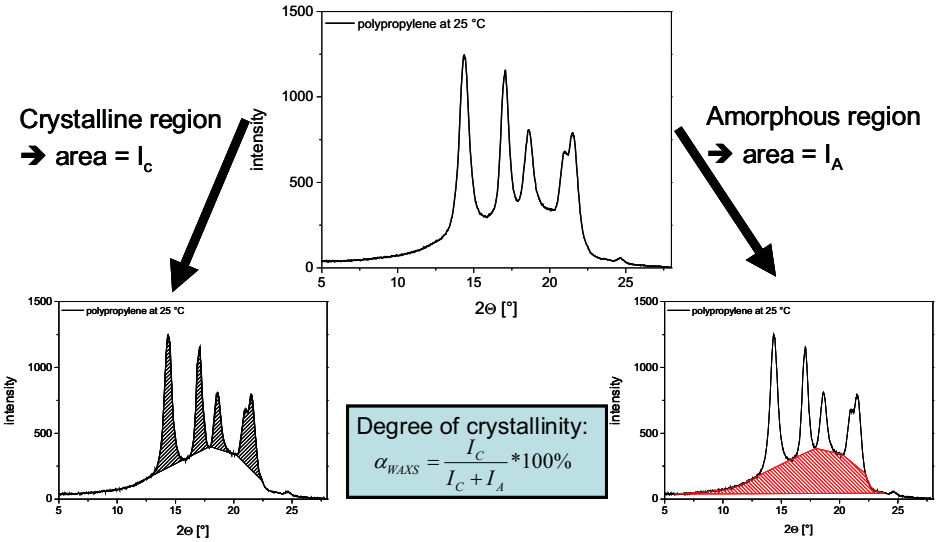

Figure 11 Determination of the (mass) degree of crystallinity.

2.2.3 Small Angle X-ray Scattering (SAXS)

Small angle X-ray scattering is applied for the determination of structural parameters, with dimensions larger than in the WAXS analysis. In contrast to WAXS, where a signal arises from regular arrangements of atoms in a crystal, SAXS signals rises from inhomogeneity in electron density fluctuations inside materials. It's common knowledge that the first applications of SAXS to elaborate structural information were performed by Gunier and Co-workers. These first advances into the work of small angle X-ray scattering are summarised in the famous book of Gunier (Guinier, 1963). In polymer science, SAXS measurements are used to determine e.g. the long period, the thickness of the crystalline and amorphous layer and the volume degree of crystallinity for one polymer analysis (Vonk and Kortleve, 1967; Strobl and Schneider, 1980). Furthermore, the dimensions of hard or soft segments e.g. for polyurethanes can be evaluated. Dimensions of air inclusion (naturally available or induced by external load) and fibril diameters can be determined by this powerful method. However, dimensions in the range of a few nanometers up to several decades of nanometers can be determined (Guinier, 1963). The application of 2D detectors also allows for characterization of texture.

Simple evaluation techniques

In a first step to determine structural parameters, the one-dimensional scattering data has to be corrected for background scattering (instrument, sample holder). Afterwards, a power

law function (according to Eq. (6)) can be subtracted from the scattering data to correct for multiple phase scattering, inelastic scattering, etc. The remaining intensity is multiplied with q^2; q being the magnitude of the scattering vector ($q = \frac{4\pi \sin(\Theta)}{\lambda}$, where Θ is half of the scattering angle and λ being the wavelength of the radiation). The peaks are fitted with a well-defined distribution function (Guinier, 1963; Alexander, 1969). As result, the peak can be described via the position, the width and the area.

$$I_{corr} = \frac{X_1}{q^{X_2}} + X_3 \qquad \text{Eq. (6)}$$

X_1, X_2 and X_3 are variables.

The peak position is a structural dimension (e.g. the long period in semi-crystalline polymers). The peak width can be interpreted as the crystal size (size of coherent scattering domains). The use of the Scherrer equation (see Eq. (7)) allows for a quantification of dimensions. This formula can be used for up to 100 nm crystal size (Guinier, 1963).

$$\tau = \frac{K\lambda}{\beta \cos(\theta)} \qquad \text{Eq. (7)}$$

K is the dimensionless shape factor (between 0.85 and 1; at polymers ~ 0.9), λ the X-ray wavelength, β the line broadening at the half maximum intensity in radians and θ is the Bragg angle. τ is the mean size of the crystalline domains (Guinier, 1963). The line broadening from the experimental setup (from the instrument such as beam size, detector smearing, etc.) can be determined by measuring a substance with sharply defined peaks e.g.: rat tail. The peak area represents the scattering quantities; the more scattering elements exist in the radiated volume, the larger the peak area (Guinier, 1963).

Determination of orientation

There are several strategies to interpret orientations in polymers. The determination of orientations by X-ray scattering methods is a very powerful tool. Figure 12 shows SAXS measurements of an orientated (left side) and a disorientated sample (right side). Additionally, the corresponding χ–integration curves can be found in this picture.

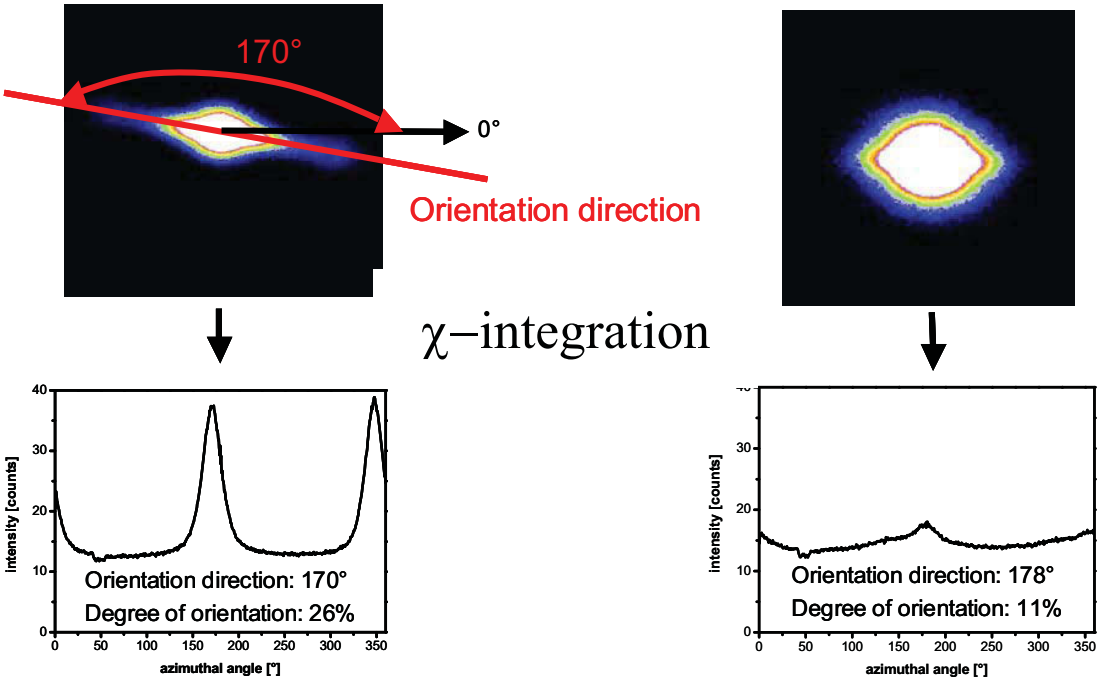

Figure 12 Determination of orientation by X-ray scattering techniques.

The degree of orientation and the orientation direction can be evaluated via the following steps: First, the χ–integration of the scattering data has to be completed and the data has to be corrected for background scattering. Afterwards, the direction of orientation can be evaluated by allocating the maxima of the curve, evident on the left side in Figure 13. The determination of the degree of orientation is pictured on the right side in Figure 13. There, the peak areas and the whole area had to be determined. The ratio of the peak areas and the whole area is the degree of orientation (Alexander, 1969).

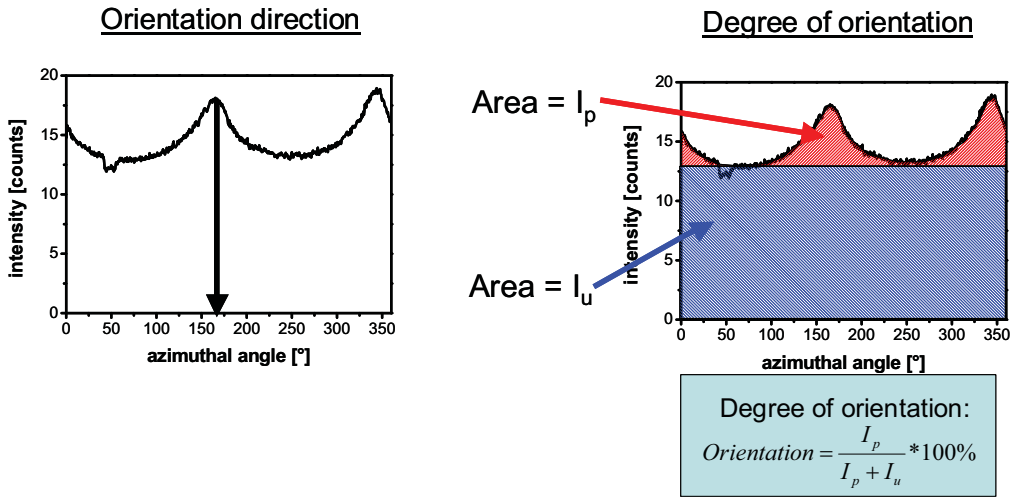

Figure 13 Determination of the degree of orientation.

One dimensional correlation function by Schröder/Vonk

In literature, many advanced techniques were published in the last decades. The most common one is the one-dimensional electron density correlation function by Vonk and Kortleve. This method for operating with polymers, is based on a model developed by Hosemann, where a semi-crystalline polymer is considered as a system of stacks of lamellar crystals, separated by amorphous layers (Hosemann, 1962). It is a powerful tool to examine structural parameters like long period, the thickness of the amorphous and crystalline layer and the degree of crystallinity of polymers (Vonk and Kortleve, 1967). In addition, layered structures with two different phases can be interpreted, for example as layered silicates.

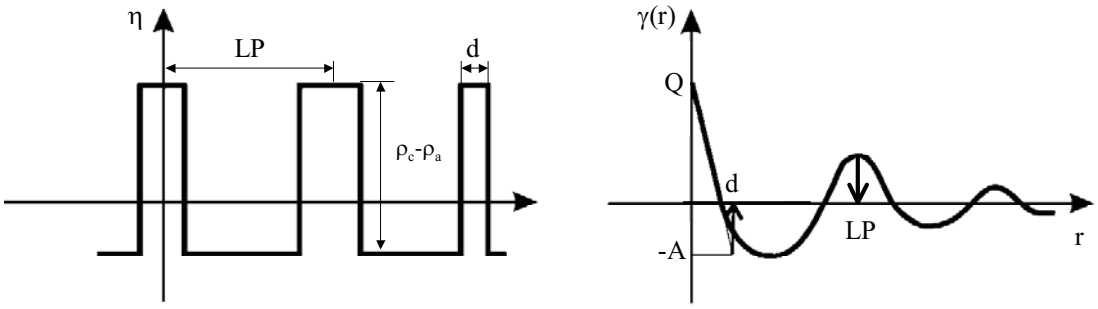

Figure 14 Electron density distribution η (right) and the corresponding correlation function γ(r) of a lamellar two-phase system. LP is the long period, d the thickness of the lamellar layer, Q is the invariant, ρ_c and ρ_a the electron density of the crystalline and the amorphous region (Strobl and Schneider, 1980).

On the left side in Figure 14, an electron density distribution of a lamellar two-phase system is illustrated. By way of the electron density distribution, it is possible to estimate the autocorrelation function γ, which is also called "one-dimensional correlation function". It might further be determined over a Fourier-transformation of the scattering intensity. The form of the one-dimensional correlation function is featured in Eq. (8) (Strobl and Schneider, 1980).

$$\gamma(r) = \frac{1}{2\pi^2} \int_0^\infty q^2 I(q) \cos(qr) dq \qquad \text{Eq. (8)}$$

On the right side in Figure 14, a one-dimensional correlation function is pictured. Likewise, the important parameters are graphically described in this figure. The maximum

of the curve is called invariant Q and can be found at r = 0. The first minimum of the curve (point A) is relevant for determination important parameters. The difference of Q and A is equal to the electron density difference of the two phases. The slope at the beginning of the curve ($d\gamma/dr$) is proportional to the inner surface (O_s) of the system and to the Porod constant. The intersection of $d\gamma/dr$ and A represents another important point - the thickness d. This thickness is either the mean thickness of the crystallites (for crystallinity $\phi_c<0.5$) or the mean thickness of the disordered (amorphous) region (for $\phi_c>0.5$). The second maximum of the curve is additional an important point, it is the mean thickness of one crystalline plus one amorphous layer. The crystallinity ϕ_c can be calculated as ratio of the thickness d and the long period (Strobl and Schneider, 1980). Figure 15 demonstrates the evaluation process by the use of the one-dimensional correlation function.

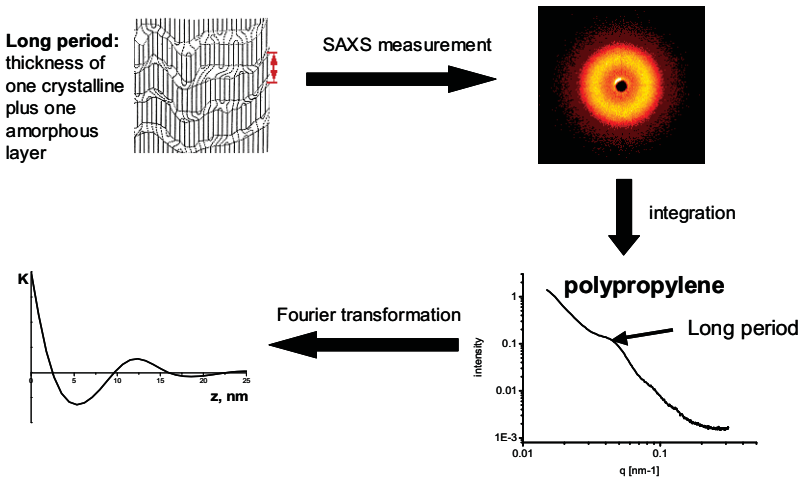

Figure 15 Evaluation process for the usage of the one dimensional correlation function.

2.2.4 Structure and form factor

The big disadvantage of the electron correlation function is that only "simple" two-phase systems (semi-crystalline polymers, layered silicates, etc.) can be effectively interpreted with this method. To interpret complex materials (for example layered silicate reinforced semi-crystalline polymers), other methods garnered the interest of researchers. These methods correlate directly the measured scattering intensity with the structural details of the material. They adapt the structure and form factor directly to the scattering intensity.

Fundamental definitions of the form and structure factor

There is a distinction between the form and the structure of a scattered element in small angle scattering analysis. Posthence, investigations on the structure and the form factor have to be completed. Detailed information on the different types of these factors can be found in literature (Roe, 2000).

In small angle scattering, the structural information is assembled by a structure factor, form factor and size distribution. To combine all the factors, the scattering cross section has to be explained (see Figure 16) (Roe, 2000).

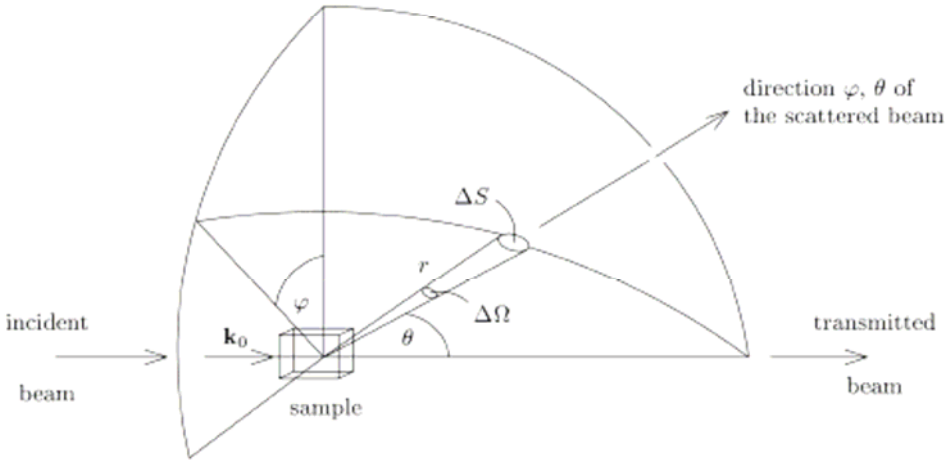

Figure 16 Schematic representation of the scattering process (Roe, 2000).

The radiation interacts with the sample; scattering occurs as well as a change of energy in the scattered beam. The result is described with the help of a cross section. Figure 16 schematically outlines the various important aspects of the cross section. The counting rate of the detector C is proportional to an incident beam, whereas the beam has a homogeneous, continuous flow density Φ_0 ([Φ_0] = photons per cm^2 and second) and contains the amount N of identical particles (Roe, 2000). The proportionality constant is called the "differential scattering cross section $\frac{d\sigma}{d\Omega}$" and $\frac{d\sigma}{d\Omega} = \frac{C}{\Phi_0 \in N\Delta\Omega}$, where $\in$ is the detector efficiency. In the case of inelastic scattering, the counting rate is proportional to δE as well. δE indicates a certain interval of transferred energy. The appropriate proportionality constant is the partial (or double) differential scattering cross section (Roe, 2000).

$$\frac{d^2\sigma}{d\Omega dE} = \frac{C}{\Phi_0 \in N\Delta\Omega\Delta E} = \frac{\text{Number of photons, which are scattered per second into the solid angle d}\Omega\text{ toward }\phi,\theta\text{ with an energy between E and E + dE}}{N\Phi_0 d\Omega dE} \quad \text{Eq. (9)}$$

The total differential cross section is defined as follows:

$$\sigma_{total} = \frac{\text{total number of scattered photons per second}}{\Phi_0} \quad \text{Eq. (10)}$$

The three different cross sections are related to each other by $\sigma_{total} = \int d\Omega \frac{d\sigma}{d\Omega}$ and $\frac{d\sigma}{d\Omega} = \int_0^\infty dE \frac{d^2\sigma}{d\Omega dE}$.

Small angle scattering normally does not resolve dimensions down to an atomic scale. Hencewith, the scattering cross section is defined in Eq. (11) as (Roe, 2000).

$$\frac{d\sigma}{d\Omega}(q) = \frac{1}{N}\left|\int_V dr\rho(r)e^{iqr_j}\right|^2 = \frac{1}{N}I(q) \quad \text{Eq. (11)}$$

whereby ρ(r) is the local scattering length density and I(q) the scattering amplitude. The differential scattering cross section is, mathematically speaking, the square of the Modulus of the Fourier transformation of the scattering length density, whereas the scattering length density ρ(r) is proportional to the locally averaged scattering potential (Roe, 2000).

General information about the structure factor

The structure factor is the Fourier-transformed electron dispersion inside a unit cell. Therefore, the structure factor is a mathematical description of how material scatters due to radiation. It is a useful tool in the interpretation of data from interference pattern of X-ray scattering in condensed matter physics and crystallography (Woolfson, 1970).

Diffraction definition of the structure factor

The intensity of a diffracted beam is defined as the wavefunction of a beam scattered a vector Δk (see Eq. (12)), and this is in the kinematical approximation proportional to the structure factor $F_{\Delta k}$ (Woolfson, 1970). The structure factor $F_{\Delta k}$ is defined by Eq. (13), where r_j is the position of an atom j in the unit cell, and f_j is the scattering power of the atom (also called the atomic form factor). The sum of all atoms in the unit cell is further used in these compuatations (Woolfson, 1970).

$$I_{diffracted} = |\psi_{\Delta k}|^2 \propto |F_{\Delta k}|^2 \qquad \text{Eq. (12)}$$

$\psi_{\Delta k}$ is the wavefunction of the scattered beam and $F_{\Delta k}$ the structure factor.

$$F_{\Delta k} = \sum_j f_j e^{-i\Delta k r_j} \qquad \text{Eq. (13)}$$

To compute structure factors for a specific lattice, the sum over the atoms in the unit cell is counted. This procedure can be easily done for simple lattices (Alexander, 1969).

In order to accurate define the small angle scattering structure factor, distortions (crystal imperfections) of first and second kind have to be considered too. The intensity is subsequently proportional to the single structure factor and the distortions factor (Vaia et al., 2003).

Form factor

The form factor describes the shape and electron density distribution inside an individual particle. Serving as the form factor, is the Fourier transformation of the electron dispersion of a particle. In SAXS, structure dimensions and their various shapes require consideration of factors from all kinds of SAXS evaluations (Alexander, 1969).

Size distribution

Under normal circumstances, natural products possess not one uniformly defined size; they all feature a size, which is naturally distributed. To describe natural distribution, several distribution functions are used in physics. They depend on the material, the production process, and which distribution function can be used to describe the size of a material. From very low-end functions (e.g.: uniform distribution function) to very complex functions (like Weibull distribution function) are commonly applied in scattering (diffraction) physics.

Scattering laws and structural parameter

Simple and useful tools have been developed based on Eq. (11). Guinier and Fournet have shown, that the radius of gyration (R_G) can be easily calculated by the use of the well-known Guinier approximation (Guinier and Fournet, 1955):

$$I(q) = I(0)e^{-q^2\frac{R_G^2}{3}} \qquad \text{Eq. (14)}$$

The Guinier law is valid for particles with a roughly isodiametric particle shape. For other structures, the Guinier law has to be modified slightly. Furthermore, this law is valid for the scattering vector interval $0 < q < \frac{1}{R_G}$ (Guinier and Fournet, 1955).

The Porod law describes the scattering behaviour at large q values. Utilizing this law, it is possible to garner more information on the specific surface of an illuminated sample volume (Porod, 1951; Porod 1952).

With the knowledge of the two laws, other structural parameters can be calculated. Porod volume (volume of a specific particle) and correlation length (average width of the correlation function) are two additional structural parameters, which can easily be calculated from the scattering information (Guinier and Fournet, 1955).

Methods to combine structure and form factor

Illuminated volumes during scattering experiments usually exhibit more than one scattering element. Each scattering object (possessing a size distribution N_i and a single structure factor S_i) can be included in data evaluation. Several ways were considered to include structure factors in mode calculations:

- The monodisperse approximation,
- Decoupling approach (Kotlarchyk and Chen, 1983),
- Local monodisperse approximation (Pedersen, 1994),
- Partial structure factor or scaling approximation of partial structure factors (Gazzillo et al., 1999).

In the case of Eq. (15), no interactions between different species of scattering objects were included, hence with, the total scattering is given by the sum of the scattering of the individual species i.

$$\frac{d\sigma}{d\Omega}(q) = \sum_{i=1}^{N} \frac{d\sigma_i}{d\Omega}(q) \qquad \text{Eq. (15)}$$

The easiest way to include a structure factor in the analysis is the monodisperse approach, which is calculated as follows:

$$\frac{d\sigma_i}{d\Omega}(q) = \left[\int_0^\infty N_i(x,l)F_i^2(q,a,x)dx\right] S_i(q,s) \qquad \text{Eq. (16)}$$

N_i is the distribution function of the species i with a corresponding parameter l, F_i^2 is the form factor of the species i with the corresponding parameter a and S_i is the structure factor of the species i with the corresponding parameter s. For this method, the interaction potential between particles assumes spherical symmetry and independent of particle size. Exact structure factors (partial structure factors approach) can further be used to describe polydisperse systems. The scattering cross section of the partial structure factor approach in combination with the monodisperse structure factor has the form of Eq. (17).

$$\frac{d\sigma_i}{d\Omega}(q) = \left[\int_0^\infty N_i(x,l)F_i^2(q,a,x)dx\right] + \frac{1}{n_i}\int_0^\infty\int_0^\infty N_i(x,l)N_i(x',l)F_i(q,a,x)F_i(q,a,x') \times \left[S_i(q,s,R_i(a,x),R_i(a,x')) - 1\right]dxdx' \qquad \text{Eq. (17)}$$

with

$$n_i = \int_0^\infty N_i(x,l)dx \,. \qquad \text{Eq. (18)}$$

The monodisperse structure factor is evaluated for the radius $\frac{R_i(a,x)+R_i(a,x')}{2}$, whereas the radius is defined as $R_i(a,x) = \sqrt[3]{\frac{3}{4\pi}V_i(a,x)}$.

Approaches

Layered silicate-reinforced polypropylene consists of two different components. In the small angle scattering pattern, both components are clearly visible. On the one hand, there exists information concerning the polymer; on the other hand, the structural details of the layered silicates provide further insight. The structural information of polypropylene, determined by SAXS, depends on a layered structure of amorphous and crystalline layers. Simultaneously, the filler montmorrillonite possess a layered structure in a stacked form. Knowing the structure of the two components, following structure and form factors are chosen for modelling (possibly to fit) small angle X-ray data.

Single layer scattering

For a thin disc, the form factor is defined as follows (Roe 2000; Vaia et al. 2003):

$$\left|F_P(q)\right|^2 = (\Delta\rho)^2 v_P^2 \int_0^{\frac{\pi}{2}} \left\{ \frac{\sin\left[qH\cos(\beta)\right]}{qH\cos(\beta)} \right\}^2 \left\{ \frac{2J_1\left[qR\sin(\beta)\right]}{qR\sin(\beta)} \right\}^2 \sin(\beta) d\beta \qquad \text{Eq. (19)}$$

β is the angle between the axis of the disc and the magnitude of the scattering vector q. J_1(....) is the first-order Bessel function. $\Delta\rho$ is the difference in coherent scattering length densities between the plate and the medium (it is normally expressed in cm^{-2}). v_P is the volume of one single particle. H is the thickness and R is the radius of one single platelet. This equation can be simplified for very thin discs (with an aspect ratio radius/thickness >> 1) and low q into following equation (Roe 2000; Glatter 1982):

$$\left|F_P(q)\right|^2 = (\Delta\rho)^2 v_P^2 \frac{2}{q^2R^2}\left[1 - \frac{J_1(2qR)}{qR}\right] \qquad \text{Eq. (20)}$$

Lattice or structure factor

Due to the short-range interference of the thin plates, the structure of a stack represents a one-dimensional lattice. The internal disorder of such a structure (crystal imperfections) can be divided into distortions of first and second kind (Alexander 1969; Vainshtein 1981). In Figure 17, the difference between distortions of first and second kind is illustrated. The distortions of first kind (see Figure 17 a) can be described as a net, representing the base of a lattice (a and b direction). The c-axis is perpendicular to the plane. If the c-axis intersects with the net plate at distance D, a lattice point is drawn on the lines . Displacements from regular arrangement in D are called (Figure 17 a) “distortions of first kind”. (Alexander 1969; Vainshtein 1981). Distortions of second kind can be described by non-ideal lattice structure, as in Figure 17 b (Alexander 1969; Vainshtein 1981).

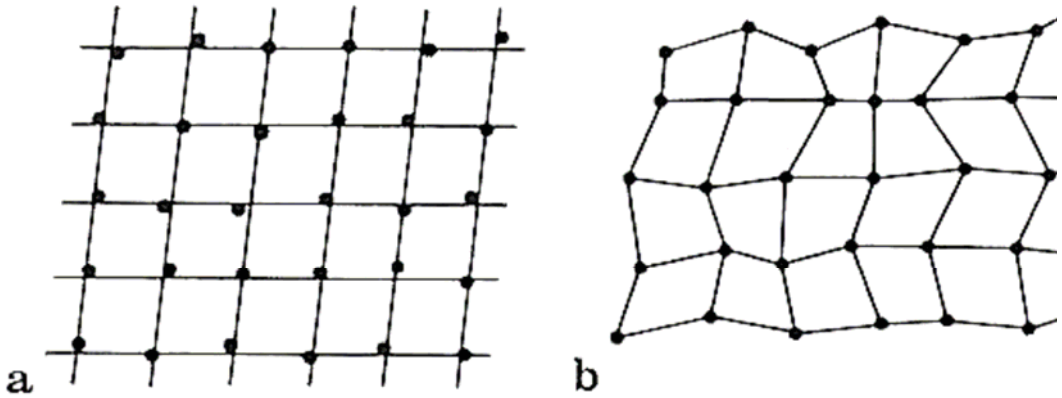

Figure 17 Distortions of first (a) and second (b) kind (Alexander 1969; Vainshtein 1981).

Distortions of the first kind can be described as the displacement of the scattering layers from an ideal lattice with spacing, D, given by a Gaussian probability with mean-square displacement, δD. Therefore, the interference function can be expressed as (Vainshtein 1966; Vaia et al. 2003):

$$Z_1(q) = \frac{1}{\langle N \rangle}\left[\langle N \rangle + 2\sum_{N=N1}^{N=N2} p(N) \sum_{n=1}^{n=N-1} (N-n) e^{-\frac{1}{2}q^2(\delta D)^2} \cos(qDn)\right] \qquad \text{Eq. (21)}$$

The summation $\sum_{n=1}^{n=N-1}(N-n)$ describes the finite stack size (dimension of coherent domain), whereas the term $e^{-\frac{1}{2}q^2(\delta D)^2}$ characterises the inhomogeneities in the structural order normal to the plates. The other summation $\sum_{N=N1}^{N=N2} p(N)$ describes the stack size's polydispersity, where $p(N)$ is the distribution of coherent layers per stack and N1 and N2 are representing the number of the smallest and the largest coherent stacks. $\langle N \rangle$ is the mean number of layers in a layer stack (crystallite) and can be defined as $\langle N \rangle = \sum p(N)N$.

For distortions of second kind, the nearest one-dimensional neighbouring correlations can be described with a Gaussian distribution of the distance between these. Distance D describes the mean spacing of neighbouring layers. For a finite stack size, the lattice factor can be described by Eq. (22) (Vainshtein 1966; Roe 2000).

$$Z_2(q) = \frac{1}{\langle N \rangle}\left\{\langle N \rangle + \sum_{N=N1}^{N=N2} p(N) \sum_{n=1}^{n=N-1} (N-n)\left[R^n(q) + R^{*n}(q)\right]\right\} \qquad \text{Eq. (22)}$$

$R(q)$ and $R^*(q)$ are the Fourier transform and complex conjugates of the probability function. This indicates the likelihood of finding the nearest neighbouring pair between a distance z and (z+dz). A good approximation of the probability function is given by a Gaussian distribution, described by Eq. (23).

$$R(q) = e^{\left[-\frac{1}{2}(\delta D)^2 q^2\right]} e^{(-iDq)} \qquad \text{Eq. (23)}$$

δD describes the standard deviation around the mean distance between plates.

Combinations of the equations Eq. (20)-Eq. (23) provide an expressions for the scattering intensity from independently scattering stacks of layers. The scattering intensity per unit volume is given by Eq. (24) (Vaia et al. 2003).

$$i(q) = \frac{I(q)}{V} = \phi \nu_P (\Delta\rho)^2 \left[\frac{\left|F_P(q)\right|^2}{\nu_P^2 (\Delta\rho)^2}\right]\left[\chi + (1-\chi) Z(q)\right] \qquad \text{Eq. (24)}$$

ν_P is the layer volume, $\Delta\rho$ the scattering length density and ϕ the volume fraction of silicates. χ represents the degree of exfoliation, where $\chi = 1$ for complete exfoliation.

Polypropylene

The lamellar structure of semi-crystalline polymers can be represented as a one-dimensional structure as well. For this reason, the same structure and form factor as mentioned for the filler montmorrillonite can be adapted to analyse SAXS data.

Status

All of the above mentioned methods were used during this thesis. We were able to describe basic structural parameters as well as advanced structure-mechanical dependencies. One goal - to establish advanced fitting routines for a standard analysis of polymer nanocomposites - failed due to the following reason: the developed Matlab script requires too much computing power. An optimization of the developed code, based on Vaia 2003, was not possible during the span of this work.

2.3 References

Alexander, L.E. (1969). "X-ray Diffraction Methods in Polymer Science", John Wiley & Sons Inc., New York.

Alexandre, M., Dubois, P. (2000). Materials Science and Engineering, **28**, 1.

Balta-Calleja, F.J., Vonk, C.G. (1989). "X-ray scattering of synthetic polymers", Elsevier, Amsterdam.

Bragg, W.L. (1913). Proc. Cambridge Phil. Soc., **17**, 43.

Breuer, O., Uttandaraman Sundararaj (2004). Polymer Composites, **25**, 630.

Brückner, S., Meille, S.V., Petraccone, V., Pirozzi, B. (1991). Progress in Polymer Science, **16**, 361.

Choy, J.H., Kwak,S.Y., Han, Y.S., Kim, B.W. (1997). Materials Letters, **33**, 143.

Coleman, J.N., Khan, U., Blau, W.J., Gunko, Y.K. (2006). Carbon, **44**, 1624.

Debye, P. (1915). Ann. Physik, **46**, 809.

Friedrich, K. (1983). Advances in Polymer Science, **52**, 225.

Gazzillo, D., Giacometti, A., Valle, R.G.D., Venuti, E., Carsughi, F. (1999). Journal of Chemical Physics, **111**, 7636.

Giannelis, E.P., Krishnamoorti, R., Manias E. (1999). Advances in Polymer Science, **138**, 107.

Glatter, O., Kratky, O. (1982). "Small Angle X-ray Scattering", Academic Press, London - New York - Paris - San Diego - San Francisco - Sao Paulo - Sydney - Tokyo - Toronto.

Gojny, F.H., Wichmann, M.H.G., Fiedler, B., Kinloch, I.A., Bauhofer, W., Windle, A.H., Schulte, K. (2006). Polymer, **47**, 2036.

Guinier, A., Fournet, G. (1955). "Small-Angle Scattering of X-rays", John Wiley & Sons Inc., New York.

Guinier, A. (1963). "X-ray Diffraction", Freeman, San Francico.

Heinz, H., Vaia, R.A., Krishnamoorti, R., Farmer, B.L. (2007). Chemistry of Materials, **19**, 59.

Hosemann, R. (1962). "Direct analysis of diffraction by matter", North-Holland Pub. Co., Amsterdam and New York.

Karger-Kocsics, J. (1995). "Polypropylene - Structure, blends and composites", Chapmann & Hall, London.

Ke, Y.C., Stroeve, P. (2005). "Polymer-Layered Silicate and Silica Nanocomposites", Elsevier B.V., Amsterdam.

Klug, H.P., Alexander, L.E. (1974). "X-ray Diffraction Procedures for Polycrystalline and Amorphous Materials", 2nd ed., Wiley-Interscience, New York.

Kotlarchyk, M., Chen, S.-H. (1983). Journal of Chemical Physics, **79**, 2489.

Lezak, E., Bartczak, Z. (2005). Fibres & textiles in Eastern Europe, **13**, 53.

Narisawa, I., Ishikawa, M. (1990). Advances in Polymer Science, **91**, 354.

Pavlidou S., Papaspyrides C.D. (2008). Progress in Polymer Science, **33**, 1119.

Pedersen, J.S. (1994). Journal of Applied Crystallography, **27**, 595.

Porod, G. (1951). Kolloid Zeitschrift, **124**, 83.

Porod, G. (1952). Kolloid Zeitschrift, **125**, 51 and 109.

Ray S.S., Okamoto M. (2003). Prog. Polym. Sci., **28**, 1539.

Roe, R.J. (2000). "Methods of X-ray and neutron scattering in polymer science", Oxford University Press, New York.

Ruland, W. (1964). Polymer, **5**, 89.

Strobl, G.R., Schneider, M. (1980). Journal of polymer science: Polymer physics edition, **18**, 1343.

Tjong S.C. (2006). Materials Science and Engineering R, **53**, 73.

Utracki, L.A. (2004). "Clay-Containing polymeric nanocomposites", Rapra Technology Limited, Shawbury, Shrewsbury, UK.

Vaia, R.A., Weidong, L., Koerner, H. (2003). Journal of Polymer Science: Part B: Polymer Physics, **41**, 3214.

Vainshtein, B.K. (1966). "Diffraction of X-rays by Chain Molecules", Elsevier, New York.

Vainshtein, B.K. (1981). "Fundamentals of Crystals", Springer Verlag, Berlin - Heidelberg - New York.

Vonk, C.G., Kortleve, G. (1967). Kolloid Zeitschrift, **220**, 19.

Woolfson, M.M. (1970). "An introduction to X-ray crystallography", Cambridge University Press, UK.

Wunderlich, B. (1973). "Macromolecular Physics - Volume 1", Academic Press, New York.

Zerda, A.S., Lesser, A.J. (2001). Journal of Polymer Science: Part B: Polymer Physics, **39**, 1137.

3 Characterisation of distribution quality of layered silicates in polypropylene by X-ray scattering and near infrared techniques

In order to efficiently determine the distribution quality of clay-containing polypropylene nanocomposites, many methods are available. The main structural investigations in this work were completed with the help of X-ray scattering methods. This part serves to demonstrate simple X-ray analysis methods.

A new way to determine material homogeneity is the use of near infrared spectroscopy. One of the advantages of this method lies in its allowance for quick measurement procedures. Albeit, it can be used for the characterisation of polymer melts during a compounding process. In this part of the work, the structural properties of the produced compounds (determined by X-ray scattering methods) are correlated with inline near spectroscopy results. This chapter provides an additional overview, concerning the production processes, which were used to produce the polymeric nanocomposites for this thesis.

3.1 Major results

Paper 1 demonstrates in great detail, the applied production process melt compounding. Using this process, a compatibilizer to strengthen the interaction between polypropylene and silicate layers is necessary. However, optimal compatibilizer content has to be detected, due to the negative effect of the compatibilizer on certain properties. A high amount of compatibilizer results in a higher interlayer distance, including a lower Young's Modulus. The optimum amount of compatibilizer was discerned by balancing the intercalation grade and the mechanical properties. Likewise, a correlation between extensional rheometry and tensile tests was discovered. In that case, an easy online process measurement of extensional rheological properties was suggested to control the process and thus improve final mechanical properties.

Paper 2 deals with inline near infrared spectroscopy and a correlation with structural and mechanical properties. For inline measurements, the production process was equipped with a spectroscopic measuringement system behind the string die. The collected data was

correlated with mechanical (Young's Modulus) and structural properties (interlayer distance of the silicate stacks). Applying a chemometric model made it possible to directly describe the structural and mechanical properties during processing. It is suggested to use this method for fast process optimization and process control.

Paper 3 deals with inline near infrared spectroscopy and the correlation with mechanical properties (Young's Modulus). Unlike Paper 2, the compared structural property is the quantity of scattering elements (represented by the peak area of the silicate layer peak, see paper 9). This quantity of scattering elements can be explained as the degree of exfoliation. Hence, it is possible to describe the degree of exfoliation during the process via the utilization of a chemometric model.

Extensional rheology and near infrared spectroscopy are useful methods for process controlling. This chapter shows that a correlation of near infrared spectrogram with structural properties (interlayer distance, degree of exfoliation) and mechanical properties (Young's Modulus) is possible. Extensional rheology (tensile force at break) can be correlated with mechanical properties (Young's Modulus) as well. Therefore, the methods near infrared spectroscopy and extensional rheology can be bestowed for fast process optimization and process control.

3.2 Paper 1

S. Laske, M. Kracalik, M. Gschweitl, M. Feuchter, G. Maier, G. Pinter, R. Thomann, W. Friesenbichler, G. R. Langecker

Estimation of Reinforcement in Compatibilized Polypropylene Nanocomposites by Extensional Rheology

Journal of Applied Polymer Science (2009), 111 (5), pp. 2253-2259

Estimation of Reinforcement in Compatibilized Polypropylene Nanocomposites by Extensional Rheology

Stephan Laske,[1] Milan Kracalik,[1] Michael Gschweitl,[1] Michael Feuchter,[2] Günther Maier,[3] Gerald Pinter,[2] Ralf Thomann,[4] Walter Friesenbichler,[1] Günter Rüdiger Langecker[1]

[1]*Institute of Plastics Processing, University of Leoben, Leoben 8700, Austria*
[2]*Institute of Materials Science and Testing of Plastics, University of Leoben, Leoben 8700, Austria*
[3]*Materials Center Leoben Forschung GmbH, Roseggerstrasse 12, Leoben 8700, Austria*
[4]*Freiburg Materials Research Center, University of Freiburg, Freiburg 79104, Germany*

Received 23 April 2008; accepted 9 August 2008
DOI 10.1002/app.29163
Published online 13 November 2008 in Wiley InterScience (www.interscience.wiley.com).

ABSTRACT: Structural characterization in polymer nanocomposites is usually performed using X-ray scattering and microscopic techniques, whereas the improvements in processing and mechanical properties are commonly investigated by rotational rheometry and tensile testing. However, all of these techniques are time consuming and require quite expensive scientific equipment. It has been shown that a fast and efficient way of estimating the level of reinforcement in polymer nanocomposites can be performed by melt extensional rheology, because it is possible to correlate the level of melt strength with mechanical properties, which reflect both the 3D network formed by the clay platelets/polymer chains as well as final molecular structure in the filled system. The physical network made of silicate filler and polymer matrix has been evaluated by X-ray diffraction and transmission electron microscopy. Extensional rheometry and tensile testing have been used to measure efficiency of the compatibilizer amount in a polypropylene-nanoclay system. © 2008 Wiley Periodicals, Inc. J Appl Polym Sci 111: 2253–2259, 2009

Key words: nanocomposites; melt compounding; melt strength

INTRODUCTION

Nanocomposites using different polymer matrices and layered silicates have been intensively investigated because of the improvements in their processing and use properties. Consequently, it is possible to prepare new, tailored, materials[1] or to use nanofillers in polymer recycling.[2–4] The improvement in material properties due to nanoclay addition has usually been evaluated using a combination of transmission electron microscopy (TEM) and morphological (X-ray diffraction (XRD), mechanical (tensile testing), and sometimes also rheological (rotational rheometry) analyses. However, these conventional methods require quite expensive scientific equipment and long sample preparation and characterization times. Generally, intercalated and delaminated (partially exfoliated) polymer nanocomposites reveal significant enhancements in their properties: higher elastic modulus, tensile strength, thermal resistivity, lower gas and liquid permeability, reduced flammability,[5] and improved rheological properties (e.g., higher melt strength) compared with the unfilled polymer matrix.[1] The high level of possible reinforcement due to the addition of the layered silicates results from their large active surface area (in the case of montmorillonite 700–800 m^2/g).[6] In the case of highly dispersed systems, a 3D physical network is achieved, formed by the silicate platelets and the polymer chains. This phenomenon can be investigated by analyzing the melt elasticity using rotational rheometry.[1–4,6–22] A fast way to evaluate this network effect is using elongational rheometry,[23–26] which provides information about the melt strength.

To disperse the clay in hydrophobic polypropylene (PP), a compatibilizer (mostly PP grafted with maleic acid anhydride (MA)) must be admixed. However, the molecular weight of the compatibilizer is usually lower than that of the PP matrix due to the grafting reaction and the presence of free MA molecules.[27]

We have already presented[23,24] that the effective level of reinforcement in PP nanocomposites cannot be based solely on an evaluation of the delamination level (increase in interlayer distance) determined by X-ray scattering. In the PP-PPMA-nanoclay system, the simple rule "higher delamination leads to an improvement in material properties" is not always

Correspondence to: M. Kracalik (Milan.Kracalik@mu-leoben.at).
Contract grant sponsor: PlaComp1 Project (NanoComp research project cluster founded by the Austrian Nanoinitiative).

Journal of Applied Polymer Science, Vol. 111, 2253–2259 (2009)

TABLE I
Temperature profile in different extruder sections

Section	1	2	3	4	5	6	7	8	9	10
Temperature (°C)	cool	160	180	190	200	200	200	200	200	200

valid because of the influences of the grafted PP on the material properties. With a higher compatibilizer addition, the final delamination increases but the average molecular weight decreases. This means that there is an optimal compatibilizer admixture at which physical reinforcement caused by silicate delamination is still higher than the deterioration in mechanical properties due to decreasing molecular weight and combination of the interfacial area able to be generated.

A fast and accurate method to find this optimal compatibilizer admixture in different PP nanocomposites is to compare the material reinforcement in the systems using extensional rheometry. A further advantage of elongational experiments is the use of primary granulates: no preparation of samples is necessary. To date, a few articles have dealt with the possibility of using extensional rheometry for the characterization of elongational viscosity in polymer nanocomposites.[28,29] However, no correlation between the melt strength and the mechanical properties with respect to nano-structural details has yet been published. The goal of this article is to present a fast, qualitative method of reinforcement evaluation based on extensional rheology in polymer nanocomposites with a view to speed up the industrial application of the systems investigated.

EXPERIMENTAL

Materials

The isotactic PP homopolymer HC600TF (MFI 2.8 g/10 min; 230°C/2.16 kg) was supplied by Borealis, Inc., Linz, Austria. Used nanofiller (montmorillonite intercalated with dimethyl distearyl ammonium chloride) with commercial indication Nanofil 5 was supplied by Süd-Chemie Inc., Munich, Germany. The compatibilizer (Scona TPPP 2112 FA, MFI 14.8 g/10 min) was supplied by Kometra, Ltd., Schkopau, Germany.

TABLE II
Press profile

Temperature (°C)	200	200	200	200	50
Pressure (bar)	1	20	1	100	150
Time (min)	20	5	5	7	7

Preparation of nanocomposites

For the compounding process, an intermeshing, corotating twin screw extruder Theysohn TSK30/40D (Theysohn Holding Ltd, Vienna, Austria) with a string die was used. The feed rate was set at 20 and 7 kg/h, with a screw speed of 200 rpm. The temperature profile is described in Table I. The compatibilizer admixture content relative to the organoclay content (5 wt %) was chosen at ratios (clay : compatibilizer) from 1 : 0 to 1 : 3.

For the Rheotens measurements, the primary granulate obtained from the extrusion process was used. For structural (X-ray diffraction, transmission electron microscopy) and mechanical characterization, plates with a thickness of 2 mm and standard dog-bone shaped specimens (150 mm length, 20 mm width, 4 mm thickness), respectively, were prepared using the hydraulic vacuum press machine (Collin 200 PV, Dr. Collin Ltd., Ebersberg, Germany). The press profile is given in Table II.

Extensional melt rheology

As stated in the introduction, two methods of reinforcement assessment can be used in the molten state in polymer nanocomposites: analysis of the melt elasticity using rotational rheometry or melt strength evaluation, e.g., using Rheotens equipment. The advantage of Rheotens measurements consists in their simplicity without the need for expensive scientific equipment and additional time for sample preparation. The principle of Rheotens measurements can be seen in Figure 1. It is based on the

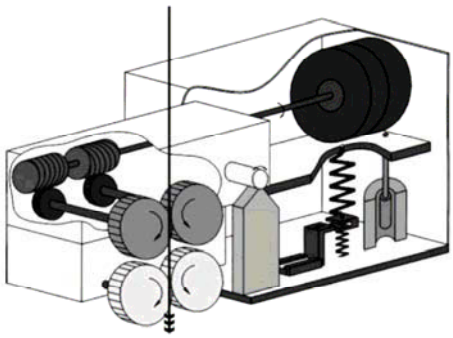

Figure 1 Principle of Rheotens measurement.[30]

TABLE III
Capillary rheometer testing specification

Cylinder diameter	12 mm
Die (length/diameter)	30/2 mm
Temperature	210°C
Piston speed	1.9 mm/s
Shear rate	273.6 s^{-1}

elongation of an extruded string by two or four rotating wheels connected with a force transducer. The rotation speed is linearly increased until the molten string breaks. The tensile force applied to the wheels and the draw rate at break allows the calculation of the melt strength (stress at break)[31]:

$$\sigma_b = F_b v_b / A_0 v_0,$$

σ_b—stress at break (Pa),
F_b—tensile force at break (N),
v_b—draw rate at break (mm s^{-1}),
A_0—initial cross section of molten string (at the die outlet) (m^2),
v_0—extrusion speed of molten string (piston speed) (mm s^{-1}).

We used the Rheotens 71.97 (Göttfert Ltd., Buchen, Germany) in a combination with a capillary rheometer. The measuring conditions for capillary rheometer are listed in Table III. The rheotens equipment has been set applying wheel acceleration of 60 mm/s^2 and gap between wheels of 0.6 mm. To compare the melt strength level of different nanocomposite systems (revealing different magnitudes of v_b), the tensile force at a draw rate of 320 mm/s was chosen for comparison (Fig. 2).

The silicate platelets form different levels of 3D physical network in the polymer matrix depending on their level of delamination.[1–4] Higher delamination results in a higher extent of physical network (higher material reinforcement) and, therefore, in an increase in melt strength. Different particle–particle and polymer–particle physical interactions result in variations in viscoelastic response. Therefore, Rheotens measurements are used to identify changes in the melt elongational behavior. Individual silicate platelets form nanoscale network (cardhouse structure)[21] and raise the melt strength of the composite. Depending on the degree of delamination, this transformation is obvious compared with the unfilled polymer.

Small angle X-ray scattering

X-ray measurements were performed using Bruker NanoSTAR (Bruker AXS, Karlsruhe, Germany) small angle X-ray scattering (SAXS) equipment. This system was equipped with a two-dimensional X-ray detector. A wavelength of 0.154 nm (CuKα) was used. The samples were measured in transmission.

To avoid the influence of texture, all scattering measurements were performed on plate samples. The gallery period[1] of the nanofiller was determined on a powder sample. To avoid statistical effects, the scattering curves recorded at three different positions on the samples were averaged. To determine the gallery period, scattering curves were corrected for background scatter and the Lorenz correction was applied.[32] The Lorenz correction was performed by multiplying the scattered intensity ($I(q)$) by q^2, q being the magnitude of the scattering vector. The position of the gallery peak was then determined by fitting with a Lorenz function.

Transmission electron microscopy

The TEM experiments were performed using a Zeiss LEO 912 Omega transmission electron microscope (Carl Zeiss Inc., Jena, Germany) using an acceleration voltage of 120 kV. The samples were prepared using a Leica Ultracut UCT ultramicrotome (Leica Microsystems Ltd, Wetzlar, Germany) equipped with a cryo chamber. Thin sections of about 50 nm were cut with a Diatome diamond knife at −120°C.

Mechanical properties

A universal tensile testing machine (Type: Z010, Zwick Ltd and Co. KG, Ulm, Germany) was used to carry out the tensile tests according to ISO 527-1. All tests were carried out under standardized conditions (23 ± 2°C/50 ± 5% r.H.). The data was evaluated using the testXpert II software (ZWICK, Ulm, Germany).

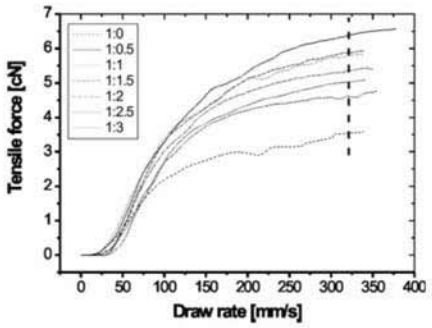

Figure 2 Melt strength level comparison.

RESULTS AND DISCUSSION

Extensional melt rheology

The elongational behavior of nanocomposite masterbatches prepared using different compatibilizer admixtures at two throughput rates is shown in Figure 3. It is obvious that the compatibilizer content as well as the effect of the feed rate on material properties can be analyzed by evaluating the melt strength. As stated in the Introduction section, determination of the optimum compatibilizer admixture in polyolefine nanocomposites is essential to reach the maximal reinforcement using layered silicates. We have shown[23,24] that the MFI difference in PP matrices results in different optimum compatibilizer admixtures. The lower the MFI, the lower the compatibilizer content needed. The high molecular weight of the HC600TF matrix leads to high shear forces in the compounder and, therefore, facilitates delamination of silicate platelets. A lower quantity of compatibilizer is, therefore, required. Using the HC600TF matrix led to higher level of material reinforcement due to requiring two to four times less compatibilizer compared with other lower molecular weight PP matrices.[23,24] It is obvious that the exact determination of the optimum compatibilizer admixture is a key factor in both maximizing the level of polymer reinforcement and minimizing compatibilizer costs. For the effect of the feed rate (at a constant screw speed) on the optimum compatibilizer content, an opposite trend was found to that for MFI. A lower throughput rate leads to a higher need for compatibilizer, which is explained by the lower fill factor in the screw segments. A higher feed rate leads to a higher fill factor and, subsequently, to higher shear forces applied on silicate tactoids to be delaminated. Therefore, it is necessary to evaluate the optimum compatibilizer admixture for PP matrices with different molecular structures or by varying the processing conditions such as throughput rate. To our knowledge, this important aspect in the preparation of PP-organoclay nanocomposites has not been discussed in depth so far.

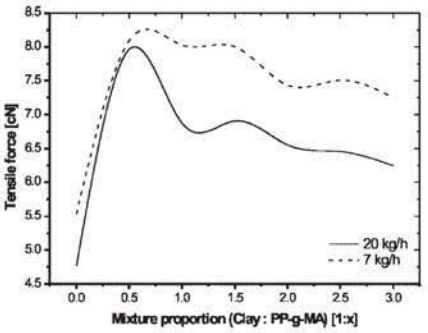

Figure 3 Melt strength level of nanocomposites.

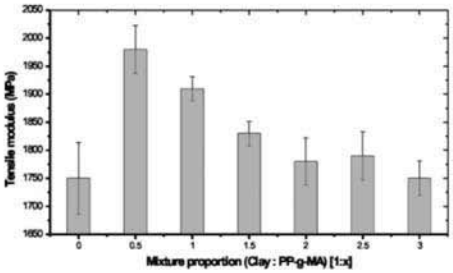

Figure 4 Tensile modulus in nanocomposites with different compatibilizer admixture.

Mechanical properties

The results of mechanical testing in the solid state reflect those in the melt state. In Figure 4, the Young's modulus is plotted for the nanocomposites with differing compatibilizer admixtures. The same trend can be observed as for the extensional behavior. The highest increase in stiffness was found in the system filled with 2.5 wt % of compatibilizer. A further increase in the compatibilizer admixture leads to a decline in the tensile modulus. At 15 wt % compatibilizer the mean value of modulus reaches approximately the same value as for the mixture without compatibilizer. This result is in agreement with that published by Paul et al.,[33] where the mechanical properties of PP nanocomposites with different compatibilizer admixtures (1 : 0 to 1 : 2 PP-g-MA to organoclay ratio) were investigated. However, supposedly due to the high melt flow index of the matrix used (37 g/10 min, 230°C), an increase in

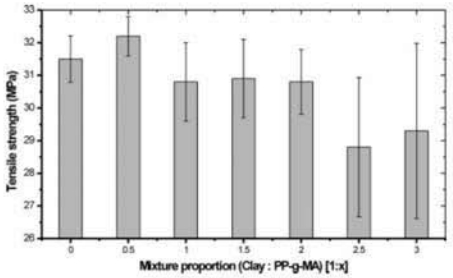

Figure 5 Tensile strength in nanocomposites with different compatibilizer admixture.

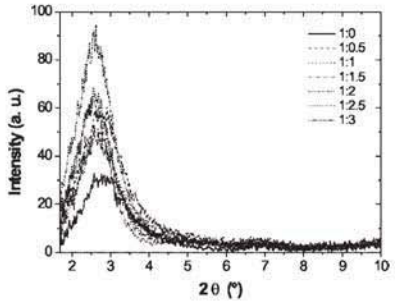

Figure 6 X-ray diffraction patterns of nanocomposites.

the compatibilizer content (1 : 0.5 up to 1 : 2 PP-g-MA to organoclay ratio) reported by Paul et al. did not result in a significant decrease in tensile modulus. As we already reported,[23,24] molecular structure (in particular molecular weight) of PP matrix has significant influence on the optimum compatibilizer admixture and compatibilizing efficiency. The polymer matrix with the highest molecular weight possible to process with other composite components is favored to ensure maximal shear forces during compounding. Results for tensile strength (Fig. 5) reveal a similar trend as for melt strength and tensile modulus. The highest mean value of tensile strength was reached at a compatibilizer admixture of 2.5 wt %, while higher amounts resulted in a decline in tensile strength. The highest level of polymer-filler interfacial shear strength in the system, using 2.5 wt % of compatibilizer, is reflected in the high magnitudes of both melt and tensile strength. Therefore, it is possible to correlate the reinforcement level in the melt state with that in the solid state. In this way, extensional rheology can be used in terms of estimating the prior routes in the development of nanocomposites and, presumably, any other filled systems based on polymer matrix.

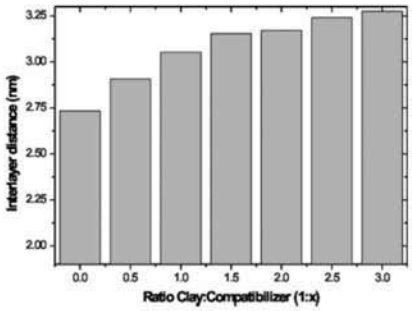

Figure 7 Gallery periodicity as a function of compatibilizer content.

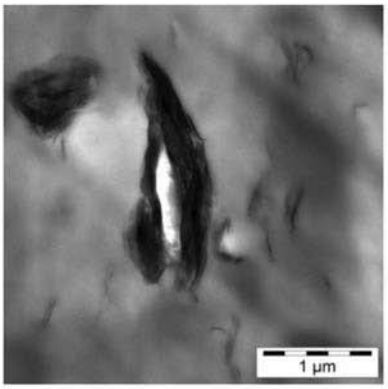

Figure 8 TEM of nanocomposite with 1 : 0 compatibilizer ratio.

Delamination of organoclay in polypropylene

The morphological analysis revealed a clear trend in delamination and homogeneity of silicate platelets in PP nanocomposites. In Figure 6, X-ray diffraction patterns of all investigated systems can be observed. The highest intensity peak was revealed in the system filled with 10 wt % of compatibilizer. On the other hand, the lowest peak can be seen in nanocomposite without compatibilizer. Calculated interlayer distance of organoclay is plotted in Figure 7 (relative to pure organoclay). It is obvious that the increase in

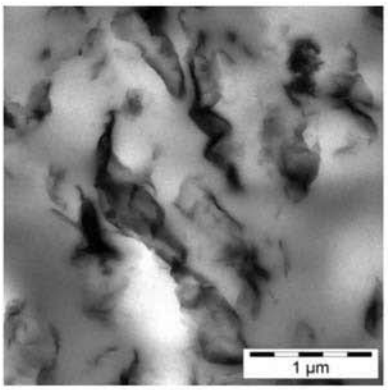

Figure 9 TEM of nanocomposite with 1 : 0.5 compatibilizer ratio.

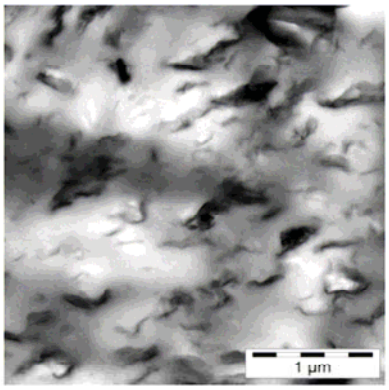

Figure 10 TEM of nanocomposite with 1 : 1 compatibilizer ratio.

compatibilizer admixture leads to a higher interlayer distance of montmorillonite in the nanocomposite system. The same trend was observed concerning the homogeneity of the prepared systems, as can be seen in Figure 8–12. The nanocomposite without compatibilizer revealed a stacking of silicate platelets rather than delamination behavior. On the other hand, a significantly higher level of homogeneity occurs in the 2.5 wt % compatibilizer admixture (Fig. 9), with a maximum at 15 wt % compatibilizer (Fig. 12). It can be clearly seen that results of structural measurements revealed completely other trend when compared with the mechanical and rheological testing. Therefore, grade of delamination in compatibilized PP nanocomposites cannot possess information on the level of polymer reinforcement, as in the case of systems without compatibilizers.[2–4] Nevertheless, extensional rheology cannot replace conventional measuring techniques and is introduced in this paper only as a possibility of fast reinforcement estimation in the filled polymer systems.

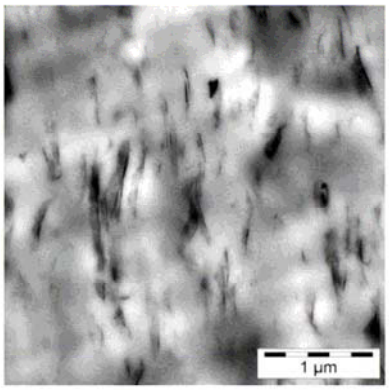

Figure 11 TEM of nanocomposite with 1 : 2.5 compatibilizer ratio.

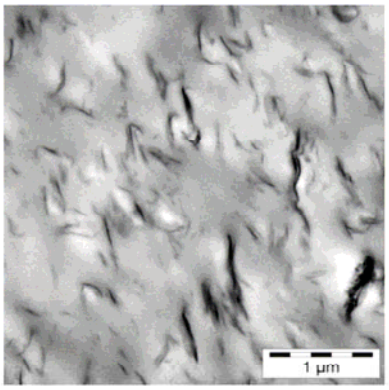

Figure 12 TEM of nanocomposite with 1 : 3 compatibilizer ratio.

CONCLUSIONS

The PP-PPMA-nanoclay system was investigated to find the omptimum amount of compatibilizer. Although X-ray scattering and TEM revealed an increase in silicate dispersion with an increase in compatibilizer content, the mechanical and rheological properties of the material reached an optimum at significantly lower amounts of compatibilizer. Therefore, the effective reinforcement in PP-layered silicate nanocomposites cannot be evaluated successfully using only structural characterization methods. It was shown that the results of melt extensional rheometry can be correlated with those of tensile tests in a solid state. In this context, the method could be used as a fast, accurate, and cheap way to estimate the reinforcement in polymer nanocomposites. From industrial point of view, extensional rheometry could be employed on-line in the processing line and, subsequently, control and dose composite components in the adequate proportion directly during compounding. In the case of PP nanocomposites, an optimum compatibilizer content can also be assessed by this technique. However, it is necessary to measure this optimum each time by variation in PP, compatibilizer or filler type.

The authors thank Dr. Tung Pham, Borealis, Inc., Linz, for cooperation within the Nanocomp cluster.

References

1. Ray, S. S.; Okamoto, M. Prog Polym Sci 2003, 28, 1539.
2. Kracalik, M.; Mikesova, J.; Puffr, R.; Baldrian, J.; Thomann, R.; Friedrich, C. Polym Bull 2007, 58, 313.
3. Kracalik, M.; Studenovsky, M.; Mikesova, J.; Sikora, A.; Thomann, R.; Friedrich, C.; Fortelny, I.; Simonik J. J. Appl Polym Sci 2007, 106, 926.
4. Kracalik, M.; Studenovsky, M.; Mikesova, J.; Kovarova, J.; Sikora, A.; Thomann, R.; Friedrich, C. J Appl Polym Sci 2007, 106, 2092.
5. Gilman, J. W.; Kashiwagi, T.; Lichtenhan, J. D. SAMPE J 1997, 33, 40.
6. Lee, K. M.; Han, C. D. Macromolecules 2003, 36, 7165.
7. Hoffmann, B.; Dietrich, C.; Thomann, R.; Friedrich, C.; Mülhaupt, R. Macromol Rapid Commun 2000, 21, 57.
8. Hoffmann, B.; Kressler, J.; Stöppelmann, G.; Friedrich, C.; Kim, G. M. Colloid Polym Sci 2000, 278, 629.
9. Sanchez-Solis, A.; Garcia-Rejon, A.; Manero, O. Macromol Symp 2003, 192, 281.
10. Sanchez-Solis, A.; Romero-Ibarra, I.; Estrada, M. R.; Calderas, F.; Manero, O. Polym Eng Sci 2004, 44, 1094.
11. Solomon, M. J.; Almusallam, A. S.; Seefeldt, K. F.; Somwangthanaroj, A.; Varadan, P. Macromolecules 2001, 34, 1864.
12. Hyun, Y. H.; Lim, S. T.; Choi, H. J.; Jhon, M. S. Macromolecules 2001, 34, 8084.
13. Ray, S. S.; Yamada, K.; Okamoto, M.; Ueda, K. Polymer 2003, 44, 857.
14. Incarnato, L.; Scarfato, P.; Scatteia, L.; Acierno, D. Polymer 2004, 45, 3487.
15. Lepoittevin, B.; Devalckenaere, M.; Pantoustier, N.; Alexandre, M.; Kubies, D.; Calberg, C.; Jérôme, R.; Dubois, P. Polymer 2002, 43, 4017.
16. Lee, K. M.; Han, C. D. Polymer 2003, 44, 4573.
17. Kotsilkova, R. Mechanics Time-Dependent Mater 2002, 6, 283.
18. Krishnamoorti, R.; Giannelis, E. P. Macromolecules 1997, 30, 1097.
19. Kim, T. H.; Jang, L. W.; Lee, D. C.; Choi, H. J.; Jhon, M. W. Macromol Rapid Commun 2002, 23, 191.
20. Gelfer, M.; Song, H. H.; Liu, L.; Avila-Orta, C.; Yang, L.; Si, M.; Hsiao, B. S.; Chu, B.; Rafailovich, M.; Tsou, A. H. Polym Eng Sci 2002, 42, 1841.
21. Wagener, R.; Reisinger, T. J. G. Polymer 2003, 44, 7513.
22. Lim, S. T.; Hyun, Y. H.; Choi, H. J.; Jhon, M. S. Polym Prepr 2001, 42, 640.
23. Laske, S.; Kracalik, M.; Gschweitl, M.; Langecker, G. R. International Conference Polymermischungen 2007, March 28–29, Bad Lauchstädt, Germany, 2007, Proceed; p 20.
24. Kracalik, M.; Laske, S.; Gschweitl, M.; Feuchter, M.; Maier, G.; Pinter, G.; Friesenbichler, W.; Langecker, G. R. International Conference NanoEurope 2007, September 11–13, 2007, St. Gallen, Switzerland, Proceed; p 13–14.
25. Laske, S. Improvement of the Rheological Properties of Unbranched Polypropylene with Nano-Particles with Regard to Foam Extrusion, M.Sc. Thesis, University of Leoben, 2005.
26. Gschweitl, M. Assembling and Implementing a Line for Producing Exfoliated Nanocomposites, M.Sc. Thesis, University of Leoben, 2007.
27. Tong, G. S.; Liu, T.; Hu, G. H.; Hoppe, S.; Zhao, L.; Yuan, W. K. Chem Eng Sci 2007, 62, 5290.
28. Koo, C. M.; Kim, J. H.; Wang, K. H.; Chung, I. J. J Polym Sci Part B: Polym Phys 2005, 43, 158.
29. Wang, K. H.; Xu, M.; Choi, Y. S.; Chung, I. J. Polym Bull 2001, 46, 499.
30. Göttfert Ltd. Buchen, Germany. Available at: http://www.goettfert.com.
31. Rheotens 71.97. Technical Documentation; Göttfert Ltd.: Germany, 1998.
32. Balta-Calleja, F. J.; Vonk, C. G. X-ray Cattering of Synthetic Polymers; Elsevier: Amsterdam, 1989.
33. Kim, D. H.; Fasulo, P. D.; Rodgers, W. R.; Paul, D. R. Polymer 2007, 48, 5308.

3.3 Paper 2

A. Witschnigg, S. Laske, M. Kracalik, M. Feuchter, G. Pinter, G. Maier, W. Märzinger, M. Haberkorn, G. R. Langecker, C. Holzer

In-Line Characterization of Polypropylene Nanocomposites Using FT-NIR

Journal of Applied Polymer Science (2010), 117 (5), pp. 3047-3053

In-Line Characterization of Polypropylene Nanocomposites Using FT-NIR

Andreas Witschnigg,[1] Stephan Laske,[1] Milan Kracalik,[1] Michael Feuchter,[2] Gerald Pinter,[2] Günther Maier,[3] Wolfgang Märzinger,[4] Michael Haberkorn,[5] Günter Rüdiger Langecker,[1] Clemens Holzer[1]

[1]*Institute of Plastics Processing, University of Leoben, Leoben 8700, Austria*
[2]*Institute of Materials Science and Testing of Plastics, University of Leoben, Leoben 8700, Austria*
[3]*Material Center Leoben, Leoben 8700, Austria*
[4]*i-RED Infrarot Systeme GmbH, Hafenstrasse 47-51, Linz 4020, Austria*
[5]*RECENDT GmbH, Hafenstrasse 47-51, Linz 4020, Austria*

Received 22 October 2009; accepted 27 December 2009
DOI 10.1002/app.32024
Published online 29 April 2010 in Wiley InterScience (www.interscience.wiley.com).

ABSTRACT: The morphology of polymer nanocomposites is usually characterized by various methods like X-ray diffraction (XRD) or transmission electron microscopy (TEM). In this work, a new approach for characterizing nanocomposites is developed: the results of small angle x-ray scattering, on-line extensional rheometry (level of melt strength) and Young's modulus out of tensile test are correlated with those of near infrared (NIR) spectroscopy. The disadvantages of the common characterization methods are high costs and very time consuming sample preparation and testing. In contrast, NIR spectroscopy has the advantage to be measured in-line and in real time directly in the melt. The results were obtained for different aggregate states (NIR spectroscopy and on-line rheotens test in melt state, tensile test, and XRD in solid state). Therefore, important factors like crystallization could not be considered. Nevertheless, this work demonstrates that the NIR-technology is perfectly suitable for quantitative in-line characterization. The results show that, by the installation of a NIR spectrometer on a nanocomposite-processing compounder, a powerful instrument for quality control and optimization of compounding process, in terms of increased and constant quality, is available. © 2010 Wiley Periodicals, Inc. J Appl Polym Sci 117: 3047–3053, 2010

Key words: nanoparticles; polymer composite materials; FTNIR spectroscopy

INTRODUCTION

The use of nanocomposites has developed rapidly over the last years. One reason is their great potential for improving material properties with only a small amount of filler. Nanocomposites are polymers filled with particles where at least one dimension is in the order of nanometers. There are several types of nanofillers, which are classified in three structures (spherical, laminar, or fibrous particles). Because of the high aspect ratio, which is linked with the ability to improve polymers, fibrous, and laminar particles are commonly used.

There are two reasons for the improvement of material properties by the application of nanofillers. The first reason is the enforcement of the polymer matrix by means of the particles (like it is the case for other fillers). The second effect is the movement-restrictive effect on the polymer chains caused by the layered anorganic nanofillers. Therefore mainly layered silicates (most common montmorillonite) with an aspect ratio up to 1000 are used.

To reach best interactions between polymer matrix and nanofiller (especially layered silicates) a homogeneous dispersion is essential. Because of the technological simplicity, nanocomposites are preferably produced by using a twin screw extruder operating at high temperatures and pressures.[1,2] Shearing forces, induced by the rotation of the screw and thermodynamical interactions between polymer chain and layered silicate clay are delaminating the layered silicate. During the process, the structures which are responsible for the level of reinforcement are formed by physical bonding between the hydrophilic clay, the hydrophobic polymer matrix and a compatibilizer.[3]

According to the dispersion and the homogeneity of the nanofiller conventional composites, intercalated nanocomposites and exfoliated nanocomposites can be formed. To determine the homogeneity of the material a variety of methods are commonly used. These include optical [scanning (SEM) and transmission (TEM) electron microscopy], mechanical (tensile

Correspondence to: S. Laske (stephan.laske@unileoben.ac.at).
Contract grant sponsor: Austrian Nano Initiative (project Nanocomp – 0901 PlaComp1).

strength, extensional rheology) and light scattering methods (small angle (SAXS) and wide angle (WAXS) X-ray scattering). A new way to determine material homogeneity is the use of near infrared (NIR) spectroscopy. NIR spectroscopy is a nondestructive, optical method to obtain information about the composition of samples and interactions within the sample. Near- and mid-infrared methods (NIR, MIR) measure the absorbance of light due to excitation of molecular vibrations of the substance under investigation. Mid-infrared measurements (often referred to only as IR) are exploiting radiation in a spectral range between 2500 and 25,000 nm, detecting fundamental molecular vibrations, while NIR is operating in the spectral range between 780 and 2500 nm. Therefore NIR detects the overtones and combinations of the molecular vibrations. Although NIR signals are 100–1000 times weaker than IR signals, only the NIR technique is suitable for in-line implementation due to the use of quartz based optics and optical fibers for signal transfer from the measuring probe to the NIR spectrometer.

If light is transmitted through a sample, vibrations of the molecular bondings are excited, resulting in an energy absorbance at specific wavelengths depending on the type of molecule and molecular bondings, which can be detected by NIR spectroscopy. The wavelength position of the absorbance bands in the NIR spectrum provides the information for identification of substances and chemical functionalities. The prevailing conditions in the sample (chemical state, number, and type of interactions) are narrowly linked with the mechanical properties, which can therefore be determined by NIR spectroscopy.[4]

NIR measurements have a variety of successful applications in polymer science, such as the analysis of polymerization or copolymerization (mostly done by detecting the characteristically absorption caused by chemical groups as e.g., OH groups or vinyl acetate groups in ethylene vinyl acetate), crystallinity, molecular weight, anisotropy, intermolecular interactions, molar mass, porosity, specific surface area, tacticity, orientation, concentrations of flame retardants (e.g., melamine cyanurate), density measurements, and other chemical processes that appear during polymer processing.[5–16]

In other studies, nanocomposites[6,15–17] are analyzed regarding crystallization properties and particle size[16] using NIR measurements.

The near infrared technique combined with stress–strain curves to evaluate filled rubbers (using SiO_2, TiO_2, layered silicate, and Nanotubes) with regard to changes in crystallization and degree of exfoliation under strain has also been investigated. A coherence between crystallization under strain and a shift in NIR spectra has been found.[17]

In addition, NIR spectroscopy has successfully been used to monitor the processing of pharmaceutical nanoparticles and to classify them by their particle size in a high solids dispersion.[18]

The analysis of the melt strength of a polypropylene (PP) nanocomposite with off-line NIR spectroscopy (correlated with off-line rheotens measurement) has already been achieved.[4]

EXPERIMENTAL

Materials

The isotactic PP homopolymer HC600TF (melt flow index (MFI) 2.8 g/10 min; 230°C/2.16 kg) was supplied by Borealis, Linz, Austria. The used nanofiller (montmorillonite intercalated with dimethyl distearyl ammonium chloride) with commercial indication Nanofil 5 was supplied by Sud-Chemie, Munich, Germany. The compatibilizer (Scona TPPP 2112 FA, MFI 14.8 g/10 min) was supplied by Kometra, Schkopau, Germany.

Preparation of polypropylene nanocomposites

For the compounding process, an intermeshing, corotating twin screw extruder Theysohn TSK30/40D (Theysohn Holding, Vienna, Austria) with a string die was used. The feed rate was set at 10 kg/h, with a screw speed from 100 to 300 rpm. The formulation of the nanocomposite was constant at 5 wt % organoclay, 5 wt % compatibilizer and 90 wt % polypropylene. A melt pump was used ($\Delta p \sim -100$ bar) to increase the residence time and shear rate and therefore improve the dispersion of the nanofiller. A bypass system was used to create a melt string for on-line rheotens measurement. Two different screw geometries, in the following referred to as geometry 1 and geometry 2, were used to produce nanocomposites with varying layer distance and mechanical properties. The main difference between these screw geometries is the number and position of kneading elements resulting in different values of induced shear energy and residence time. As can be seen in Figure 1, both geometries are identical until the side feeder. From this point, geometry 1 consists of a kneading block right after the side feeder followed by a short kneading block at the end of the screw for additional induced shear energy in the backpressure zone caused by the melt pump. In opposite to that, geometry 2 consists only of conveying blocks.

For structural and mechanical characterization, plates with a thickness of 2 mm and standard dog bone shaped specimens (150 mm length, 20 mm width, 4 mm thickness), respectively, were prepared using the hydraulic vacuum press machine (Collin

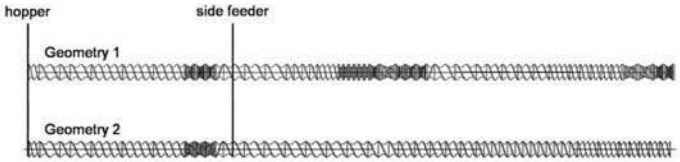

Figure 1 Schematically illustration of screw geometry 1 and 2.

200 PV, Dr. Collin, Ebersberg, Germany) and the injection molding machine (Engel ES330/80H, 800 KN closing force, Schwertberg, Austria).

Small angle x-ray scattering

X-ray measurements were performed using Bruker NanoSTAR (Bruker AXS, Karlsruhe, Germany) small angle X-ray scattering (SAXS) equipment. This system was equipped with a two dimensional X-ray detector. A wavelength of 0.154 nm (Cu-Kα) was used. The samples were measured in transmission at a temperature of 23°C. To avoid the influence of texture, all scattering measurements were performed on plate samples. The gallery period 1 of the nanofiller was determined on a powder sample. To avoid statistical effects, the scattering curves recorded at three different positions on the samples were averaged. To determine the gallery period, scattering curves were corrected for background scatter and a Lorenz correction was applied. The Lorenz correction was performed by multiplying the scattered intensity (I(q)) by q^2, q being the magnitude of the scattering vector. For the determination of the peak position the data were fitted with a Pseudo-Voigt function.[19] The interlayer distance is then calculated with the Bragg's law. The modulus of scattering vector q is defined as $q = (4\pi \sin\theta)/\lambda$ where λ is the wavelength of the used radiation and θ is the half of the scattering angle 2θ. The SAXS data evaluation was basically performed by applying a correlation function method according to Strobl and Schneider.[20]

Mechanical properties - tensile test

A universal tensile testing machine (Type: Z010, Zwick and Co. KG, Ulm, Germany) was used to carry out the tensile tests according to ISO 527–1. All tests were carried out under standardized conditions (23 ± 2°C/50 ± 5% r.H.). The data was evaluated using the testXpert II software (ZWICK, Ulm, Germany).

Rheotens measurements

The different physical crosslinking and bonding between polymer chains and organoclay results in a diversity of viscoelastic response. Therefore rheotens measurements are used to identify changes of the elongational viscosity. Individual nanoparticles act as entanglement or crosslinking sites and raise the extensional stiffness of the composite.[21]

The Rheotens 71.97 equipment (Göttfert, Buchen, Germany) was used. The melt string was applied through a bypass system directly from the extruder to achieve on-line measurement. Two or four rotating wheels (linearly accelerated) are connected to a force transducer while drawing off the extruded string until it breaks. The drawing force applied to the wheels at a specific draw rate is the reference value for the melt strength level. To compare the draw force level of different nanocomposite systems, the drawing force at a draw rate of 150 mm/s has been chosen as a comparative value. The data of at least three measurements for each sample were evaluated.

In-line FTNIR measurements

For in-line measurement a Fourier transform near infrared (FTNIR) spectrometer of i-Red Infrared Systems (Linz, Austria) with a probe installed right before the die was used. The spectrometer is working at a spectral range of 12,000 – 3800 cm^{-1} (900–2600 nm) with a spectral resolution of 1.5 cm^{-1}. The probe was connected to the spectrometer using fiber optics. The spectral data was collected with near infrared process spectrometer software (NIPS). The chemometric evaluation of the measured spectra was done with the software package Thermo GRAMS/AI from Thermo Fisher Scientific.

For a single spectrum 50 scans (10 scans per second) were averaged. For each setting 100 spectra were used to create a chemometrical model. To avoid drift effects caused by environmental or other parasitic effects, the measurement settings were chosen randomly.

Evaluation of NIR data

For the realization of an adequate process monitoring it is essential to find relations between composition of the sample, particle size or mechanical properties. This procedure is extensive, because NIR

measurements detect combinations of vibrations and overlapping bands. Therefore statistics provides various algorithms that establish a relationship between spectral data and a chemometric model. The intricacy for building a chemometric model is the problem of finding the right algorithm, the right preprocessing method and the right wavelength range. NIR measurements are in need of reference investigations (for linking them with mechanical properties), which are providing the values used for correlation with the spectral data. It is of immense importance for the accurateness of the chemometric model that these values are as precise as possible.

The multivariate data applied by NIR spectra are more dimensional (n-dimensional space). Therefore it is necessary to project the data on a two dimensional plane. The emerging picture is changing if the data points are rotated in the n-dimensional space. The possibilities of such projections are infinitive so it is essential to find the direction where the scatter along the axis reaches its maximum (maximum of information). If such a direction is found an axis orthogonal on the first axis is rotated until the scattering of data is reaching the maximum again. This approach is continued as all n-dimensions are considered. This procedure is defined mathematically as eigenvalue problem.

All performable evaluation methods, such as principal component analysis (PCA), principal component regression (PCR) or partial least squares (PLS 1 and PLS 2) are working basically on this approach.

It is of great advantage to exclude some regions with irrelevant spectral information. This can be done by calculating an absorption spectra out of two different spectra. This absorption spectra shows those wavelength regions with the highest difference and preferably low signal noise. This region can then be chosen to achieve good correlating chemometrical models.

Before the spectra are used for further calculation a preprocessing is often beneficial to get rid of parasitic effects like light straying caused by irregularities in the melt. One of the methods used is mean centering, which is calculating an average spectrum out of all used spectra and subtracts it from every single spectrum to get rid of offset effects. A way to achieve path length correction is to normalize the spectra to correct simple nonlinearities or to use algorithms such as standard normal variate transformation (SNV) or multiplicative scatter correction (MSC).

Experimentally NIR spectra of samples with varying but known responses were measured, pretreated and then the PLS 1 algorithm was used to generate a linear calibration model for calculating the responses from the measured NIR data using reference values. Then a cross validation was performed on the calculated chemometrical model. The principle of a cross validation is always the same. The model data are separated in two excluding sets (one experimental adjustment is sequentially left out). The bigger set is called training set and is used to calculate the model. The second set (test-set) is used to affirm the model. This procedure is repeated for all experimental adjustments. The bigger the training set gets the better cross validation works, especially when extrapolation is needed. The quality and the predictive ability of the model is rated basically with the coefficient of determination R^2 and the root mean square error of cross validation RMSECV. R^2 (values between 0 and 100%) shows the correlation of the NIR data with the reference values of the response parameter. The coefficient of determination R^2 should lie above 90 for quantitative calculation and above 70 for qualitative calculation. All models with values below 70 can not be used reasonably. Additionally, a precise model has a RMSECV as low as possible. A good and stable model should also not consist of many eigenvectors (referred to as "factors"), because the more factors are used the more unsteady the chemometric model becomes. So it is clear that the number of factors used should always stay in relation to the problem investigated. In the case of the investigation of nanocomposites the number of factors should preferably not be higher than 8.

RMSECV and R^2 are calculated the following:

$$\mathrm{RMSECV} = \sqrt{\frac{\sum_{i=1}^{n}(Y_{ki} - Y_{pi})^2}{n}}$$

$$R^2 = 1 - \frac{\sum_{i=1}^{n}(Y_{pi} - \overline{Y}_j)^2}{\sum_{i=1}^{n}(Y_{ki} - \overline{\overline{Y}}_j)^2}$$

Y_k. . .actual measurement value

Y_p. . .predicted value

$\overline{Y}, \overline{\overline{Y}}$. . . mean value

RESULTS AND DISCUSSION

Near infrared spectroscopy with Young's modulus as reference value

For this measurement, the response of interest is the Young's Modulus. The gained chemometric model should be close to the best model for the evaluation of the Young's Modulus values from NIR measurements. Very good correlation of tensile test and NIR measurements can be achieved by designing an optimized chemometric model. The chosen spectral pretreatment methods were mean centering and SNV. A coefficient of determination R^2 = 97.70% (factors = 5) with an RMSECV of 30 MPa for screw geometry 1 and R^2 = 90.55% (factors = 4) with an RMSECV of 94 MPa

TABLE I
Sample Description, Actual Values and Values Predicted by NIR for the Young's Modulus

Geometry	Clay/PP-MA content (wt %)	Screw speed (rpm)	Young's modulus (MPa)	NIR (MPa)
G1	5/5	100	2220	2230
		150	2190	2195
		200	2220	2214
		250	2200	2197
		300	2010	2074
G2	5/5	100	2340	2199
		150	2280	2275
		200	2260	2295
		250	2280	2237
		300	2210	2356

TABLE II
Sample Description, Actual Values, and Values Predicted by NIR for the Layer Distance

Geometry	Clay/PP-MA content (wt %)	Screw speed (rpm)	Layer distance (mN)	NIR (nm)
G1	5/5	100	42.35	2.708
		150	37.42	2.637
		200	31.56	2.599
		250	23.77	2.621
		300	17.23	2.716
G2	5/5	100	50.35	2.765
		150	45.32	2.677
		200	40.88	2.658
		250	36.53	2.602
		300	28.66	2.554

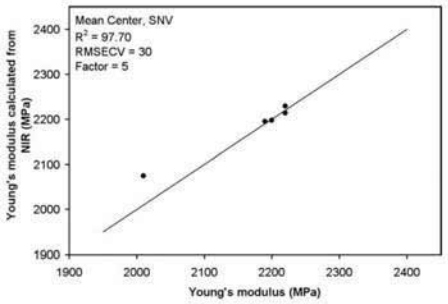

Figure 2 Young's modulus values calculated versus measured for geometry 1.

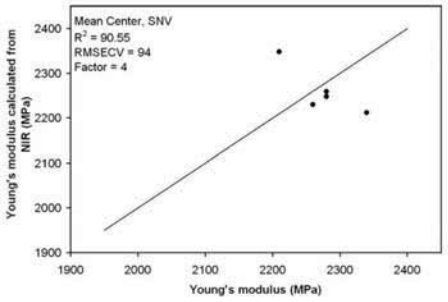

Figure 3 Young's modulus values calculated versus measured for geometry 2.

for screw geometry 2 could be achieved. Table I, Figures 2 and 3 show the results for both geometries.

The calculated Young's Moduli for geometry 1 are very close to the real values regarding that the performed tensile test has a mean standard deviation of 67 MPa.

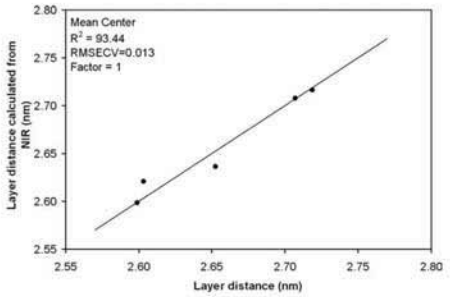

Figure 4 Layer distance calculated versus measured for geometry 1.

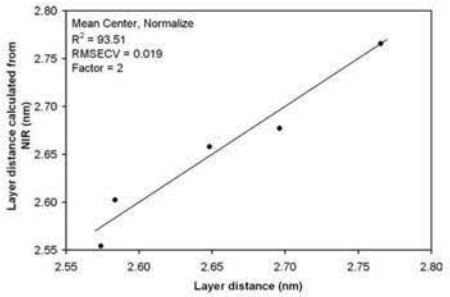

Figure 5 Layer distance calculated versus measured for geometry 2.

The values for geometry 2 at screw speed 100 and 300 show greater deviations, which can be explained with the fact that cross validation is not always that efficient with extrapolation. Nevertheless, the values are quite precise regarding that the tensile test has a mean standard deviation of 166 MPa for geometry 2.

TABLE III
Sample Description, Actual Values, and Values Predicted by NIR for the Drawing Force

Geometry	Clay/PP-MA content (wt %)	Screw speed (rpm)	Drawing force (mN)	NIR (mN)
G1	5/5	100	42.35	40.30
		150	37.42	36.93
		200	31.56	29.39
		250	23.77	26.04
		300	17.23	12.83
G2	5/5	100	50.35	49.66
		150	45.32	43.39
		200	40.88	41.94
		250	36.53	37.68
		300	28.66	32.13

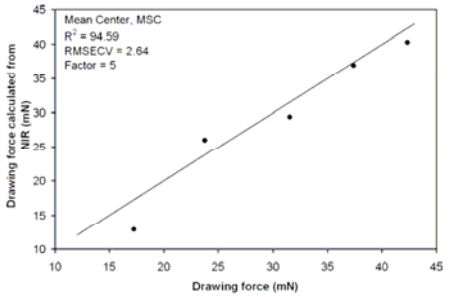

Figure 6 Drawing force calculated versus measured for geometry 1.

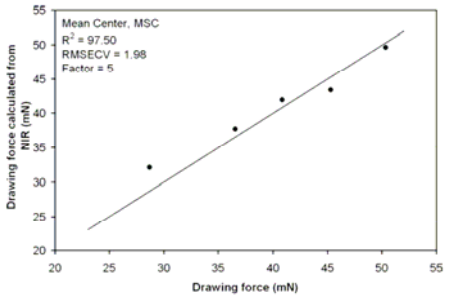

Figure 7 Drawing force calculated versus measured for geometry 2.

Near infrared spectroscopy with layer distance as reference value

The second response of interest is the interlayer distance gained by SAXS measurements. The interlayer distance is the spacing of one particle including the distance to the next particle. A very good correlation is achieved when the chemometric model is optimized with mean centering and normalization (Fig. 5). The coefficient of determination R^2 calculated for screw geometry 1 was 93.44% (factors = 1) with an RMSECV of 0.013 and R^2 = 93.51% (factors = 2) with an RMSECV of 0.019 nm for screw geometry 2. Table II, Figures 4 and 5 show the values for the layer distance calculated with the chemometrical model.

Near infrared spectroscopy with drawing force as reference value

The third response of interest is the on-line measured drawing force. To gain good correlation the chemometric model is optimized with mean centering and Multiplicative Scatter Correction (MSC). A coefficient of determination R^2 = 94.59% (factors = 5) with an RMSECV of 2.64 mN for screw geometry 1 and R^2 = 97.50% (factors = 5) with an RMSECV of 1.98 mN for screw geometry 2 could be achieved. Table III, Figures 6 and 7 show the results measured and calculated for both geometries.

CONCLUSIONS

As shown in this work the Young's Modulus, the layer distance and the drawing force exhibit good correlation with NIR data analyzed by PLS 1 algorithm. It can bee seen that near infrared spectroscopy is a quantitative method for monitoring nanocomposite quality although the measurements were done at different aggregate states and samples with different processing history caused by sample preparation. Therefore important parameters like crystallization could not be considered by the NIR measurements. It is evident that the different aggregate states (melt state vs. semicrystalline solid state) and the postprocessing procedures (cooling down, heating up, molding, and cooling down again) causing for example preferential orientations, are affecting the chemometric models negatively. Nevertheless this work shows that it is possible to determine the Young's modulus, the layer distance and the drawing force with sufficient precision for quantitative evaluation with near infrared spectroscopy. Therefore NIR spectroscopy is perfectly suitable for in-line quality control and characterization of nanocomposites in real time and directly in the melt during production, leading to a faster composite optimization process with reduced rejections and costs.

Parts of the FTNIR research work were done within the FH Plus - Project AMiESP (Advanced Methods in Embedded Signal Processing).

References

1. Vaia, R. A.; Jandt, K. D.; Kramer, E. J.; Giannelis, E. P. Chem Mater 1996, 8, 2628.
2. Davis, C. H.; Mathias, L. J.; Gilman, J. W.; Schiraldi, D. A.; Shields, J. R.; Trulove, P.; Sutto, T. E.; Delong, H. C. J Polym Sci Part B: Polym Phys 2002, 40, 2661.
3. Pinnavaia, T. J.; Beall, G. W. Polymer-Clay Nanocomposites; John Wiley & Sons: New York, 2000.
4. Laske, S.; Kracalik, M.; Feuchter, M.; Pinter, G.; Maier, G.; Märzinger, W.; Haberkorn, M.; Langecker, G. R. J Appl Polym Sci 2009, 114, 2488.
5. Heigl, N.; Petter, C. H.; Rainer, M.; Najam-Ul-Haq, M.; Vallant, R.; Bakry, R.; Bonn, G.; Huck, C. J Near Infrared Spectrosc 2007, 15, 269.
6. D. Fischer, I. Alig, J. Hutschenreuter, Presented at the 21st Annual Meeting of the Polymer Processing Society (PPS21), Leipzig, 2005.
7. Fischer, D.; Kirschner, U. GIT 2002, 11, 1267.
8. Barnes, S.; Sibley, M.; Brown, E.; Edwards, H.; Scowen, I.; Coates, P. Annu Tech Conference 2003, 3, 3311.
9. Fischer, D.; Sahre, K.; Abdelrhim, M.; Voit, B.; Sadhu, V.; Pionteck, J.; Komber, H.; Hutschenreuter, J. CR Chimie 2006, 9, 1419.
10. Barrès, C.; Bounor-Legaré, V.; Melis, F.; Michel, A. Polym Eng Sci 2006, 46, 1613.
11. Watari, M.; Ozaki, Y. Appl Spectrosc 2006, 60, 529.
12. Nagata, T.; Ohshima, M.; Tanigaki, M. Polym Eng Sci 2000, 40, 1107.
13. Barnes, S.; Brown, E.; Sibley, M.; Edwards, H.; Scowen, I.; Coates, P. Appl Spectrosc 2005, 59, 611.
14. Barnes, S.; Brown, E.; Sibley, M.; Edwards, H.; Coates, P. Analyst 2005, 130, 286.
15. Steinhoff, B.; Lellinger, D.; Pötschke, P.; Alig, I. Presented at the 21st Annual Meeting of the Polymer Processing Society (PPS21), Leipzig, 2005.
16. Asai, K.; Okamoto, M.; Tashiro, K. Polymer 2008, 49, 5186.
17. Bokobza, L.; Diop, A.; Fournier, V.; Minne, J.; Brunell, J. Macromol Symp 2005, 230, 87.
18. Higgins, J.; Arrivo, S.; Thurau, G.; Green, R.; Bowen, W.; Lange, A.; Templeton, A.; Thomas, D.; Reed, R. Anal Chem 2003, 75, 1777.
19. Balta-Calleja, F. J.; Vonk, C. G. X-Ray Scattering of Synthetic Polymers; Elsevier: New York, 1989.
20. Strobl, G. R.; Schneider, M. J Polym Sci 1980, 18, 1343.
21. Laske, S.; Kracalik, M.; Gschweitl, M.; Feuchter, M.; Maier, G.; Pinter, G.; Thomann, R.; Friesenbichler, W.; Langecker, G. R. J Appl Polym Sci 2009, 111, 2253.

3.4 Paper 3

S. Laske, A. Witschnigg, M. Kracalik, G. R. Langecker, Clemens Holzer, M. Feuchter, G. Pinter, G. Maier

Real-time characterization of polypropylene nanocomposites in a corotating twin screw extruder

Annual Technical Conference - ANTEC, Conference Proceedings 2 (2010), pp. 1167-1171

Real-time characterization of polypropylene nanocomposites in a corotating twin screw extruder

Stephan Laske, Andreas Witschnigg, Milan Kracalik, Günter R. Langecker and Clemens Holzer,
IKV – Institute of Plastics Processing, University of Leoben, Leoben, AT
Michael Feuchter, and Gerald Pinter,
Institute of Materials Science and Testing of Plastics, University of Leoben, Leoben, AT
Günther Maier, Materials Center Leoben Research Ltd., Leoben, AT

Abstract

Using layered silicates in polymer processing developed rapidly over the last decade. Depending on the particle structure in the polymer a significantly higher level of reinforcement can be achieved. Characterization of nanocomposites is usually done with optical, mechanical and light scattering methods, which are off-line and require very time consuming sample preparation and tests. In contrast, implementing in-line near infrared spectroscopy in a twin screw compounder enables real-time material characterization during compounding and provides a powerful instrument for quality control and optimization of the compounding process in terms of increased and constant quality.

Introduction

Nanocomposites are modified polymers with particles, where at least one dimension is in the order of nanometers. Polymer material reinforced by nanoscale particles exhibit significantly higher performance, for example higher elastic modulus, tensile strength, thermal resistance, lower gas and liquid permeability, reduced flammability and enhanced rheological properties already for small amounts of fillers [1, 2]. For preparation of polymer nanocomposites, layered silicates (clay, especially montmorillonite, MMT) have been the most commonly used nanofillers due to the possibility to achieve aspect ratios ideally up to 1000.
According to the dispersion and the homogeneity of the nanofillers, conventional composites, intercalated nanocomposites and exfoliated nanocomposites can be formed. To determine the homogeneity of the material a variety of methods are commonly used. These include optical (scanning (SEM) and transmission (TEM) electron microscopy), mechanical (tensile strength, extensional rheology) and light scattering methods (x-ray diffraction (XRD)). A new way to determine material homogeneity is the use of near infrared spectroscopy (NIR). NIR-spectroscopy is a non-destructive, optical method to obtain information about the composition of samples and interactions within the sample. Near- and mid-infrared methods measure the absorbance of light due to excitation of molecular vibrations of the substance under investigation. Mid-infrared measurements (often referred to only as IR) are exploiting radiation in a spectral range between 2500 and 25000 nm, detecting fundamental molecular vibrations, while NIR is operating in the spectral range between 780 and 2500 nm. Therefore NIR detects the overtones and combinations of the molecular vibrations (Figure 1). Although NIR signals are 100-1000 times weaker than IR signals, only NIR technique is suitable for in-line implementation due to the use of quartz based optics and optical fibers for signal transfer from the measuring probe to the NIR spectrometer.

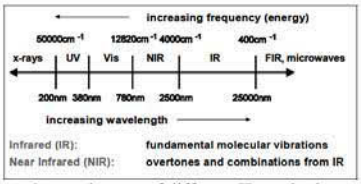

Figure 1: Spectral range of different IR methods

If light is transmitted through a sample, vibrations of the molecular bondings are excited, resulting in an energy absorbance at specific wavelengths, depending on the type of molecule and molecular bondings, which can be detected by NIR spectroscopy (Figure 2). The wavelength position of the absorbance bands in the NIR spectrum provides the information for identification of substances and chemical functionalities.

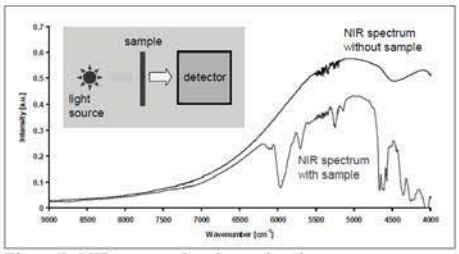

Figure 2: NIR energy absorbance bands

NIR measurements have a variety of successful applications in polymer science, such as the analysis of polymerization or copolymerization, crystallinity, molecular weight, anisotropy, intermolecular interactions, molar mass, porosity, specific surface area, tacticty, orientation, concentrations of flame retardants (e.g., melamine cyanurate), density measurements and other chemical processes that appear during polymer processing [3-11]. The prevailing conditions in the sample (chemical state, number and type of interactions) are narrowly linked with the mechanical properties which can therefore be determined by NIR spectroscopy [12].

Experimental

Materials: The isotactic PP homopolymer HC600TF (melt flow rate (MFR) 2.8 g/10 min; 230°C/2.16 kg) was supplied by Borealis, Inc., Linz, Austria. The used nanofiller (montmorillonite intercalated with dimethyl distearyl ammonium chloride) with commercial indication Nanofil 5 was supplied by Sud-Chemie Inc., Munich, Germany. The compatibilizer (Scona TPPP 2112 FA, MFR 14.8 g/10 min) was supplied by Kometra, Ltd., Schkopau, Germany.

Preparation of polypropylene nanocomposites: For the compounding process, an intermeshing, co-rotating twin screw extruder Theysohn TSK30/40D (Theysohn Holding Ltd, Vienna, Austria) with a string die was used. The feed rate was set at 10 kg/h, with a screw speed from 100 to 300 rpm. The formulation of the nanocomposite was constant at 5 wt% organoclay, 5 wt% compatibilizer (PP-MA) and 90 wt% polypropylene. A melt pump was implemented as a throttle to increase the residence time and shear rate and therefore improve the dispersion of the nanofiller. Two different screw geometries, in the following referred to as geometry 1 and geometry 2, were used to produce nanocomposites with varying layer distance and mechanical properties. The main difference between these screw geometries is the number and position of kneading elements resulting in different values of induced shear energy and residence time (Table 1).

Table 1: Process settings

Geometry	Screw speed (rpm)
G1	100 150 200 250 300
G2	100 150 200 250 300

For structural and mechanical characterization, plates with a thickness of 2 mm were prepared using a hydraulic vacuum press (Collin 200 PV, Dr. Collin Ltd., Ebersberg, Germany).

Small angle x-ray scattering: X-ray measurements were performed using Bruker NanoSTAR (Bruker AXS, Karlsruhe, Germany) small angle X-ray scattering (SAXS) equipment. This system was equipped with a two-dimensional X-ray detector. A wavelength of 0.154 nm (Cu-Kα) was used. The samples were measured in transmission. To avoid the influence of texture, all scattering measurements were performed on plate samples. To obviate statistical effects, the scattering curves recorded at three different positions on the samples were averaged. To determine the gallery period, scattering curves were corrected for background scatter and a Lorenz correction was applied. For evaluating the degree of exfoliation, the area under the silicate layer peak was calculated (see Figure 3). This area is proportional to the number of particles hit by the x-ray beam. The better the nanocomposite is exfoliated, the lower the number of particles and therefore the smaller the area is.

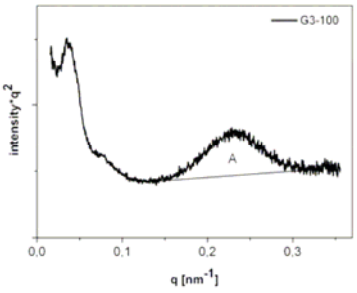

Figure 3: Calculation of degree of exfoliation

Mechanical properties - tensile test: A universal tensile testing machine (Type: Z010, Zwick Ltd and Co. KG, Ulm, Germany) was used to carry out the tensile tests according to ISO 527-1. All tests were carried out under standardized conditions (23 ± 2°C / 50 ± 5% r.H.). The data was evaluated using the testXpert II software (ZWICK, Ulm, Germany).

In-line FT-NIR measurements: For in-line measurement a Fourier-transformed near infrared (FT-NIR) spectrometer of i-Red Infrared Systems Inc. (Linz, Austria) with a probe installed right before the die was used. The spectrometer is working at a spectral range of 12000 – 3800 cm^{-1} (900-2600 nm) with a spectral resolution of 1.5 cm^{-1}. The spectral data was collected with near infrared process spectrometer software (NIPS). The chemometric evaluation of the measured spectra was done with the software package Thermo GRAMS/AI (Thermo Fisher Scientific Inc., Waltham, USA). For a single spectrum 50 scans (10 scans per second) were averaged. For each setting 100 spectra were used to create

a chemometrical model. To avoid drift effects caused by environmental or other parasitic effects, the measurement settings were chosen randomly.

For the realization of an adequate process monitoring, it is essential to find relations between composition of the sample, particle size or mechanical properties. This procedure is extensive, because NIR measurements detect combinations of vibrations and overlapping bands. The intricacy for building a chemometric model is the problem of finding the right algorithm, the right pre-processing method and the right wavelength range. NIR measurements are in need of reference investigations, which are providing the values used for correlation. It is of immense importance for the accurateness of the chemometric model, that these values are as precise as possible.

NIR spectra of samples processed with geometry 1 using the according process settings with known responses (Young's modulus and degree of exfoliation) were measured. After pre-treating the spectra, the partial least squares (PLS) 1 algorithm was used to generate a linear calibration model for calculating the responses from the measured NIR data using the reference values. Then a cross validation was performed on the calculated chemometrical model. The quality and predictive ability of the model is rated basically with the coefficient of determination R^2 and the root mean square error of cross validation RMSECV. R^2 (values between 0 and 100 %) shows the correlation of the NIR data with the reference values of the response parameter. The coefficient of determination R^2 should lie above 90 for quantitative calculation and above 70 for qualitative calculation. All models with values below 70 can not be used reasonably. Additionally, a precise model has a RMSECV as low as possible. A good and stable model should also not consist of many eigenvectors (referred to as "factors"), because the more factors are used the more unsteady the chemometric model becomes. So it is clear that the number of factors used should always stay in relation to the problem investigated. In the case of the investigation of nanocomposites the number of factors should preferably not be higher than 8.

After establishing the chemometric model, samples were processed using geometry 2 and the same process settings. The NIR spectra of geometry 2 samples were obtained during processing and analyzed by the chemometric model resulting in predicted values. The results from tensile test and x-ray diffraction of this sample set were used to verify the predicted values and therefore approve the model.

Results and Discussion

Figure 4 shows the results of the XRD measurements. It can be seen that with increasing screw speed (increasing shear rate, decreasing residence time) the peak area decreases. Therefore, a higher shear rate means smaller particle size and consequently a higher exfoliation, which is covered by literature. As well as the fact, that a high shear screw geometry is also advantageous for the exfoliation of the layers.

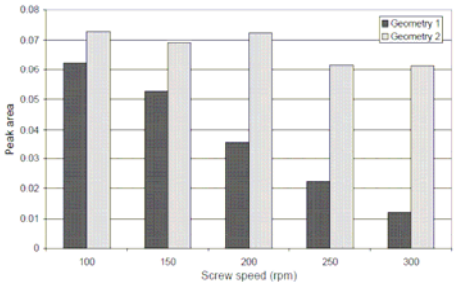

Figure 4: XRD results of geometries 1 and 2

In opposite to the XRD results, Figure 5 shows the results of the tensile tests. It is clearly shown that with increasing screw speed the mechanical properties are more or less decreasing. This can be explained by the reduced time for the diffusion of the polymer chains into the clay. The clay platelets work as cross-linking points, when polymer chains are bounded in-between, causing a seeming increase in chain length respectively molecular weight. Furthermore a physical network is established, enhancing the mechanical properties significantly. When the time for diffusion is too short, the chains can not penetrate into the clay gallery. The same effect can be seen with exfoliated layers.

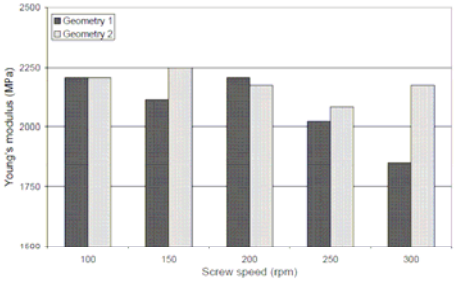

Figure 5: Tensile test results of geometries 1 and 2

According to this, for a good exfoliation high shear rate and for good mechanical reinforcement a high residence time is needed. So, for processing polyolefin nanocomposites, the correct process settings have to be found for both high exfoliation and mechanical properties. NIR spectroscopy possesses the ability to find these settings in real-time during compounding.

Figure 6 and Figure 7 show the results of the chemometric modeling for geometry 1 with Young's modulus and peak area as reference values. The gained chemometric models should be close to the best model for the evaluation of the Young's modulus and peak area values from NIR measurements. Very good correlation of tensile test, XRD and NIR measurements can be achieved by designing an optimized chemometric model. The chosen spectral pre-treatment methods were mean centering and SNV.

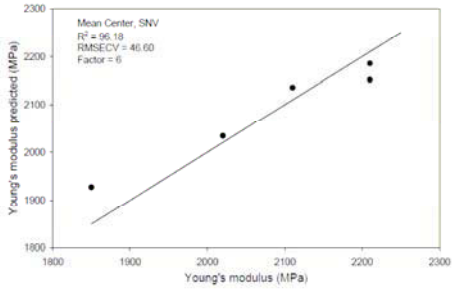

Figure 6: Chemometric model for the Young's modulus from geometry 1

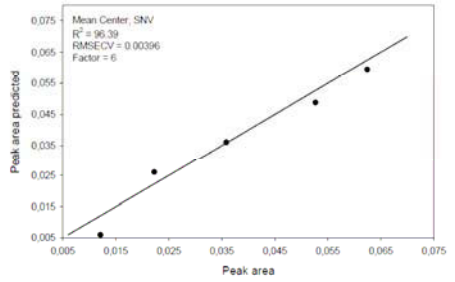

Figure 7: Chemometric model for the degree of exfoliation from geometry 1

The coefficient of determination R^2 = 96.18 % (factors = 6) with an RMSECV of 47 MPa for the Young's modulus and R^2 = 96.39 % (factors = 6) with an RMSECV of 0,004 for the peak area could be achieved. These results show, how powerful NIR can be for characterizing the material properties of polymer nanocomposites. With this model and the gained R^2 and RMSECV values, a quantitative evaluation of the material properties is possible. Hence prospective material properties are available already during processing.

Figure 8 and Figure 9 show the results of the predicted values obtained for geometry 2. The chemometric model, established with the values from geometry 1, is used for evaluating the spectra gained during processing with geometry 2.

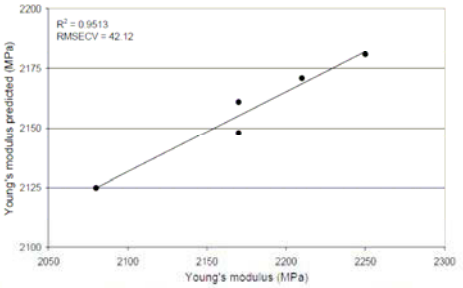

Figure 8: Predicted values for the Young's modulus from geometry 2

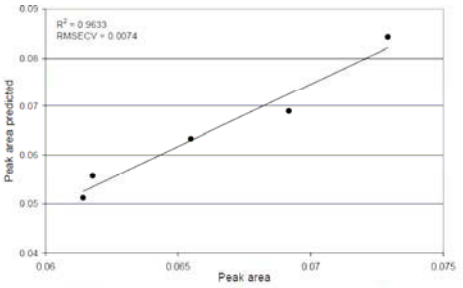

Figure 9: Predicted values for the degree of exfoliation for geometry 2

The calculated coefficient of determination R^2 is 95.13 % with an RMSECV of 42.12 MPa for the Young's modulus and 96.33 % with an RMSECV of 0.0074 for the peak area. These results show that NIR spectroscopy is capable of predicting material properties during processing quantitatively. The models created with reference values from geometry 1 are correlating very well and can be used for predicting the values obtained with geometry 2.

Conclusions

As shown in this work, the Young's modulus and the peak area exhibit very good correlation with NIR data analyzed by PLS 1 algorithm with reference values from geometry 1. Using the obtained model for spectra from different process settings predicts the material property values quantitatively. It can bee seen, that near infrared spectroscopy is a quantitative method for monitoring nanocomposite quality although the measurements were

done at different aggregate states (fluid in case of NIR and solid in case of XRD and tensile test) and samples with different processing history caused by sample preparation for the off-line measurements. Therefore important parameters like crystallization are not considered by the NIR measurements. It is evident, that the different aggregate states (melt vs. semi-crystalline solid state) and the post-processing procedures (cooling down, heating up, molding and cooling down again), causing for example unequal crystallinities or preferential orientations, are affecting the chemometric models negatively. Nevertheless, this work shows, that it is possible to determine the Young's modulus and peak area respectively the degree of exfoliation with sufficient precision for quantitative evaluation with near infrared spectroscopy. Therefore NIR spectroscopy is perfectly suitable for in-line quality control and characterization of nanocomposites in real-time and directly in the melt during production, leading to a faster composite optimization process with reduced rejections and costs.

References

1. J. W. Gilman et al. *J. D. Sampe J.*, **33**, 40 (1997)
2. S. S. Ray et al. *Progr. Polym. Sci.*, **28**, 1539 (2003)
3. N. Heigl et al. *J. Near Infrared Spectr.*, **15**, 269-282 (2007)
4. D. Fischer et al. *GIT*, **11**,1267, (2002)
5. D. Fischer et al. *C.R. Chemie*, **9**, 1419-1426, (2006)
6. C. Barrès et al. *Polym. Eng. and Sci.*, **46**, 1613-1624, (2006)
7. M. Watari et al. *Appl. Spectr.*, **60**, 529-538, (2006)
8. T. Nagata et al. *Polym. Eng. and Sci.*, **40**, 1107-1113, (2000)
9. S. Barnes et al. *Appl. Spectr.*, **59**, 611-619, (2005)
10. K. Asai et al. *Polymer*, **49**, 5186-5190, (2008)
11. J. Higgins et al. *Anal. Chem.*, **75**, 1777-1785, (2003)
12. S. Laske et al. *Journ. App. Polym. Sci.*, **114**, 2488-2496 (2009)

Acknowledgement

This work was done within the project Nanocomp – 0901 PlaComp1 funded by the Austrian Nano Initiative.

Key Words: Near infrared spectroscopy, polymer nanocomposites, compounding.

4 Morphology and structure of clay polypropylene nanocomposites

This chapter deals with the principal structure and morphology of clay polymeric nanocomposites. The arrangement of clay in polymeric nanocomposites (intercalated or exfoliated structure) is often used to describe the structure of such mixtures. Notwithstanding, this simple description of the structure of clay-containing polymer nanocomposites seems to be insufficient. There remains a lack of understanding as to where the filler is interacting with the polymer (amorphous or crystalline phase) and which interactions take place (how does the filler influence the polymeric structure). Accordingly, specific research work was completed and published in Paper 4 and Paper 5.

4.1 Major results

Paper 4 pertains to the nanomorphology of clay-containing polymer nanocomposites; particularly to the local structure of one agglomerate of stacks. This was determined by the use of a sub micrometer X-ray beam at the ESRF, which is located in Grenoble (France). This publication points out the formation of different polypropylene-structures around an agglomerate. The dominant structure of the polymer in the nanocomposite is α-polypropylene; however; there was a formation of β- polypropylene in the surrounding area of the agglomerate. Besides, the structure of the clay can be described very well. It was shown that all clay superstructures existed in the compound. The core of the agglomerate exhibited the agglomerated form, which was surrounded by a strongly intercalated structure. Exfoliated particles can be detected surrounding the agglomerate. The exfoliated particles indicated no influence on the polymeric structure (pure α-polypropylene and no change in degree of crystallinity). Yet, the degree of crystallinity is lowered due to the presence of a layered silicate stack.

Paper 5 highlights the morphology of clay-containing polymeric nanocomposites under processing conditions. The structure of one of the raw materials - an organic modified montmorrillonite - was strongly influenced by the exposion to higher temperatures. At process-related temperatures, the gap distance of this montmorillonite was higher than at room temperature. Therefore, the layered silicates were more easily exfoliated with the use of a melt compounding strategy. Furthermore, a super structure (card house) was

discovered in the high filled sample and the differences in structure between low and high filled samples at process related temperatures should be highlighted. Knowledge on the structure of clay polymeric nanocomposites under process related temperature is rather helpful for the production of layered silicate reinforced polypropylene and should alleviate the understanding of the exfoliation process during the melt compounding route.

4.2 Paper 4

G. A. Maier, M. Feuchter, M. Burghammer, M. Kracalik, S. Laske, J. Keckes

Local structure around nano-clay agglomerates in PP composites – a scanning X-ray diffraction study with sub micron resolution

Journal of Polymer Science Part B: Polymer Physics, *to be submitted*

Local structure around nano-clay agglomerates in PP composites – a scanning X-Ray diffraction study with sub micron resolution.

G. A. Maier[1], M. Feuchter[2], M. Burghammer[3], M. Kracalik[4], S. Laske[4] and J. Keckes[5]

[1] Materials Center Leoben Forschung, Roseggerstrasse 12, 8700 Leoben, Austria

[2] Dep. Testing and Material Science of Polymers and Polymer Competence Center Leoben, Roseggerstrasse 12, 8700 Leoben Austria

[3] European Synchrotron Radiation Facility, 38043 Grenoble, Cedex 9, France

[4] Institute of Plastics Processing, University of Leoben, Franz Josef Strasse 18, 8700 Leoben, Austria

[5] Dep. Materialphysics, University of Leoben and Erich Schmid Institute, Austrian Academy of Science, Jahnstrasse 12, 8700 Leoben

Abstract

Agglomerates influence most of the physical properties in polymer nanocomposites. Unfortunately, in many nanocomposites, agglomerates exist. We prepared polypropylene-nanoclay composites with high level of agglomeration. With the aid of X-Ray nano-beam diffraction, we were able to characterize structural details in and around an agglomerate with a dimension of about 10µm. The results showed strong gradients in crystallographic phases around and at the border of agglomerate, which indicates that β-PP formed at high local concentrations of nanofiller. The agglomerate was found not to be homogenous. At the border, where the agglomerate was located, slightly higher interlayer distances were allocated. Fuerthermore, gradients in interlayer distance and regions, where integral extents of clay were exfoliated, were also found in the sample.

Introduction

Polymeric nanocomposites, especially with the filler montmorrillonite, have become of predominant interest to the scientific community and industry in recent years [1-4];

particularly structural details and their connection to the mechanical, rheological, optical and permeation properties of the nano-composites are of high interest.

There are different methods to produce polymer nanocomposites [1-4]. In this study, melt compounding has been applied in order to produce intercalated polypropylene silicate nanocomposites. The intercalated structure is the first step towards reaching the exfoliation state by means of a melt intercalation; therefore, this structure is of special interest. It is usual for polymer nanocomposites, prepared by melt mixing, that a certain amount of tactoids (silicate agglomerates) persists. On the one hand, the stiff agglomerates increase the Young's modulus, but on the other hand they serve as sources of defects and stress concentrations, where cracks can be initiated, leading to premature failure, thus enacting a strong influence on the strain at break [4]. Further, Polymer-clay nanocomposites show a reduction in flammability [5] and permeability [6].

The structure of layered silicates, the arrangement of the silicate platelets, the influence of fillers on spherolithic growth and the changes in polypropylene phase content have been observed by numerous researchers [7-11]. All of these properties are influenced by the distribution of particles in polymeric matrix.

Isotactic polypropylene exhibits polymorphic behavior, which was be distinguished in various modifications. Monoclinic α-form is the most common for melt crystallized specimen, whereas the trigonal β-form can be produced only under special crystallization conditions or in the presence of nucleating agents [12].

Though much is known about bulk morphology and structure, only very little is known about local structure around an agglomerate in PP composite. In this paper, the authors present a position resolved X-Ray diffraction study with sub micron position resolution. The study was performed via application of a 250nm “wide” X-Ray beam at ID13 beamline at ESRF, Grenoble. The domain scanned in the thin sample, was restricted to a section where predominantly an agglomerate was presumed. From the data, phase composition, local composition and interlayer distances were evaluated.

Experimental

Material and preparation

The isotactic polypropylene (PP) HC600TF (Borealis Inc., Linz, Austria), an organically modified montmorillonite with the commercial indication Nanofil 5 (Süd-Chemie Inc., Munich, Germany) and a maleic anhydride acid grafted polypropylene (Kometra Ltd., Schkopau, Germany) were used in this work to produce polymeric nanocomposites with the aid of melt intercalation.

For the compounding process, an intermeshing, co-rotating twin screw extruder Theyson TSK30/40D (Theyson Ltd., Vienna, Austria) with a string die was used. The feed rate was set at 20 kg/h with a screw speed of 150 rpm. A masterbatch with 20 wt. % nanofiller and 20 wt. % compatibilizer was produced and analyzed [13,14].

For the detailed structural characterization of one silicate layered agglomerate the sample had to be prepared by carrying out the following steps: first, the granulated materials were pressed to plates with a thickness of 4 mm using a hydraulic vacuum press machine (Collin 200 PV, Dr. Collin Ltd., Ebersberg, Germany). Then rectangular pieces (50 x 10 mm^2) were cut out of these plates. The final step of sample preparation was to trim the thickness of the sample by using a microtom (Histocom, Wiener Neudorf, Austria); therefore the final sample thickness was 10 µm.

Measurements and data evaluation

The samples were measured in transmission mode at ID13 beamline at ESRF [11]. The dimension of X-Ray beam was 250nm (full width half maximum). Energy of 13.8 keV was used, which corresponds to a wavelength of 0.09 nm. A FRELON 2000 CCD Detector [15] with 2048x2048 pixel was used. A Beamstop with 300µm diameter allowed for further simultaneous mid range SAXS and WAXD measurements .

The samples were placed on a piezo driven scanning stage with a positional resolution of 10nm. Measurement position was ascertained with a high-resolution drop-down microscope. This microscope was calibrated to the beam position. This allowed high-magnification

sample visualization and provided a means of selecting specific areas on the sample for detailed study.

2D XRD patterns were radially averaged using FIT2D software [16] as exemplified in Figure 1. An average of 100 dark current measurements were used to correct for detector readout noise and an average of 50 frames recorded with sample in beam path were utilized for background correction. It was not possible to determine sample transmission due to sample degradation caused by X-Rays. Therefore we used an integral value for sample transmission, provided by a Laboratory instrument for instrumental background subtraction.

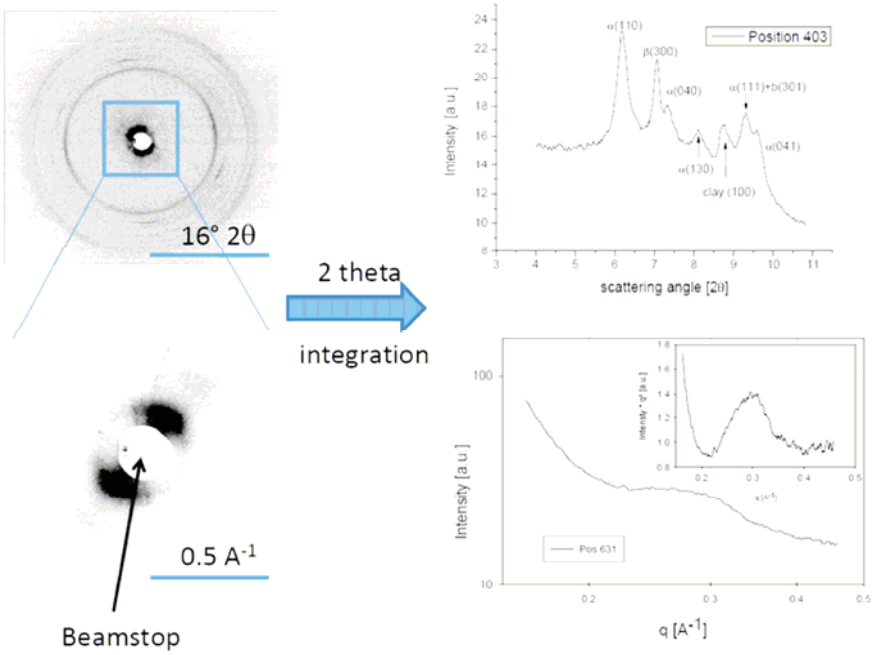

Figure 1: Scattering pattern (left side) and corresponding 1D scattering curves (right side). Wide-angle pattern were indexed according to [17, 2]. In the SAXS scattering curve (right bottom) the "Lorenz" corrected scattering curve is drawn conjointly.

The high flux density at ID13 led to a degradation of crystalline lattice in PP matrix. We tested the possible measuring times at one point and observed that the sample resisted 10s

of irradiation per measuring position. A measuring time of 5s per frame and a step size of 900nm were chosen for this study.

Interlayer (gap) distance was determined by fitting the background, Lorenz corrected and smoothed scattering curves using Gauss functions in SigmaPlot software. Lorenz correction was performed by multiplying scattering curves with the second order of magnitude of the scattering vector q. Integral SAXS intensity was calculated by integration of Lorenz corrected scattering curves between q_{min}=0.5 and q_{max}=4.5nm^{-1}.

All peaks of crystallographic lattices from clay, α-PP and β-PP were fitted together simultaneously with an amorphous background using MATLAB software. Functions with a Gaussian shape were chosen.

The degree of crystallinity (Xc) was calculated [18] using Equation 1:

$$Xc = \frac{Icry}{Icry + Iamo}$$

$$Icry = \sum I\alpha PP\,(110{,}040{,}130{,}111{,}041) + I\beta PP(300)$$

Iamo was the scattered intensity concentrated in the background.

The β-PP to α-PP ratio, xβ, was estimated with Equation 2:

$$x\beta = \frac{I\beta PP(300)}{I\alpha PP(040 + 130) + I\beta PP(300)}$$

Results

In Figure 2, a light microscopy image of the investigated area and a composite image, including all 1024 recorded scattering patterns, are presented. In visible light, the agglomerate looks homogeneous. In terms of diffraction patterns, it appeared that the agglomerate was split into two individual parts. In the composite image, each individual scattering pattern represents an area of 0.9x0.9µm² on the sample. Differences in scattering intensity and structure were already visible in this image. This indicated major inhomogenites in the composition of the analyzed area. Outside of agglomerate, the overall scattering intensity, especially in the SAXS regime, is much lower than inside of the agglomerate.

Moreover in the WAXS regime, structural inhomogenities can be deduced in the diffraction pattern.

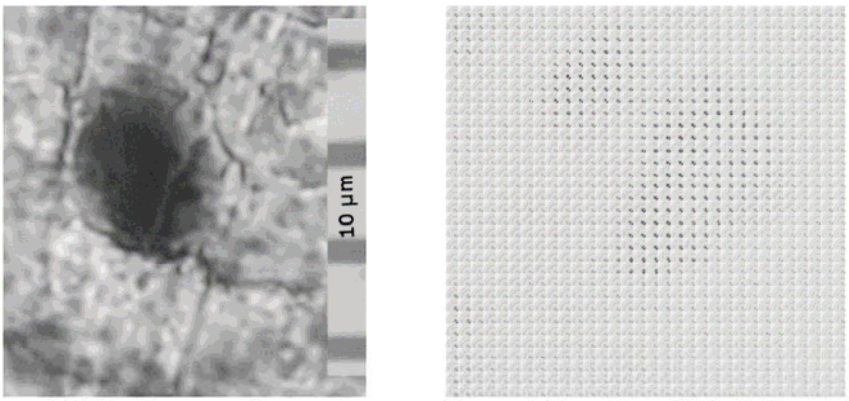

Figure 2: Light microscopy picture and corresponding scattering pattern (right). Each scattering pattern represents an area of 0.9x0.9µm². For better visibility only one quadrant of diffraction pattern is shown.

The inhomogeneous distribution of clay in the tested sample area can be seen on the plot shown in the center of Figure 3 (I_clay (001)). In principle, the scattered intensity concentrated in a certain region corresponds to the weight fraction of material. Therefore, the intensity can be used as a measure of clay distribution in the sample. The two parts of agglomerate are clearly visible, indicating that the concentration of nano-clay was not homogenous. In the SAXS intensity (I_SAXS, Figure 3 left) against position maps, the two parts of agglomerate are further visible. The overall scattered intensity scale for a sample volume, in contrast to the electron density is too sensitive for the concentrations of clay platelets. Interestingly, SAXS intensity distribution showed some bracelet-like maximum dispersion at left side of large agglomerate. This can also be seen in the intensity of correlation peak (I_correlation peak, Figure 3, right) vs. position map.

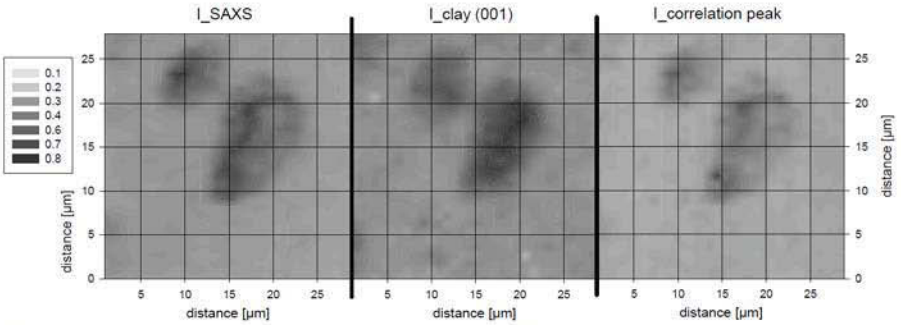

Figure 3: From left to right: Integrated SAXS intensity (I_SAXS), Intensity of clay (001) peak (I_clay (001) and intensity of gap correlation peak (I_correlation peak). For better visibility all maps were scaled to maximum intensity equal to one.

The degree of crystallinity, as shown in Figure 4 left, showed a minimum in the core of the agglomerate. The low crystalline regime covered both parts of the agglomerate. Areas with high crystallinity up to 54 wt% were found at the border of the scan area, where filler concentration was relatively low. A gap period, shown in the center of Figure 4, changed only slightly; the largest values were found in areas surrounding the large part of the agglomerate.

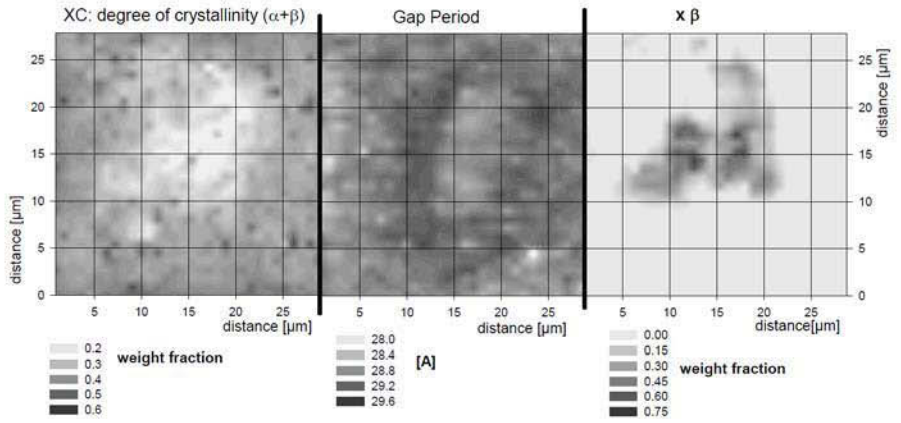

Figure 4: The distribution of degree of crystallinity, mean gap period and the fraction of βPP are shown (from left to right).

The phase composition of PP changed from pure α-PP to a high amount of β-PP in sample areas with high clay concentration,. β-PP was not only found directly near a large agglomerate, but also in an area with low concentration of clay (quadrant 5-10, 10-15). At the outermost borders of the scan area, no β-PP was found.

Discussion

Measurements on PP with X-Ray beams with high flux density lead to a degradation of material. We overcame this problem by choosing a relatively short integration time, which was half the time the material could resist. This integration time was clearly long enough for the determination of phase composition and Intensity of clay (100) peak. For SAXS data, this time was relatively short: the SAXS signals were relatively weak. In the SAXS pattern in Figure 1, different layer distances within one pattern can be assessed. Integration and data evaluation "integrates" over all distances, henceforth reveals mean values. Data quality did not allow for an adequate appraisal of the gap distance distribution in terms of largest-smallest distance in one measuring position. The mean gap period was changing only for about 0.2nm over the whole scanned area. Interestingly, the highest values were found in a ring around the "large" part of the agglomerate. This indicates that at transition from agglomerate to delaminated nano-composite, an area of strongly intercalated material existed. Exfoliated nanoparticles lead to high values of integrated SAXS intensity due to high electron density contrast. Stacked clay leads to a high intensity in the correlation peak (gap period). By combining these results, the present amount of exfoliated material can be assessed. This is visualized in the right graph of Figure 5, where the ratio between I _SAXS and I_correlation peak was plotted against position on sample. This ratio reached levels of 0.8 in areas outside the agglomerate, whereas inside the ratio was around 0.3 and below, indicating that especially on the left side of the probed area, most of the clay in volume was distributed randomly in a polymer matrix.

When concentration of clay platelets was compared to SAXS intensity, as displayed in the left graph of Figure 5, the inhomogeneous distribution of superstructure could be seen. The

dark areas indicate positions, where a relatively low amount of clay platelets formed by highly ordered intercalated stacks.

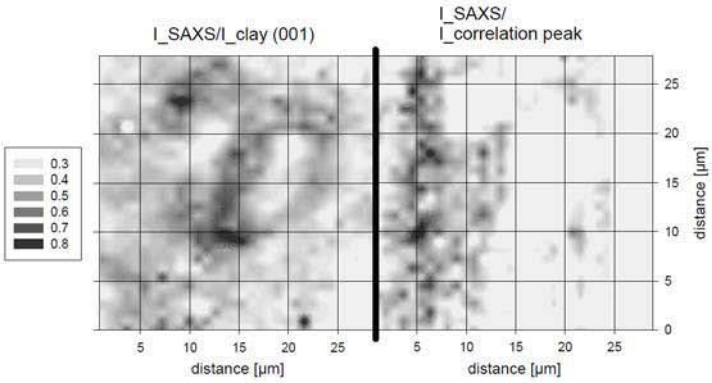

Figure 5: Scaled ratios I_SAXS/I_clay (001) and I_SAXS to I_correlation peak (left to right).

The degree of crystallinity varied strongly within the scanned area. Although being calculated as sum of the α and β phases, at positions with high amount of clay platelets, mass fraction of crystals was only around 20%. From this low amount of crystal material, the largest part contained the β-phase. The β-phase was only visible in a section of the sample, where a high concentration of clay platelets was located, and close to those areas. This lead to the conclusion, that the formation of β-phased material is supported by the presence of a high concentration of filler material. The relative uncertainty of this conclusion lies in the fact that sample thickness needs to be thicker than that of the agglomerate; therefore structures, which were either bigger or smaller than the agglomerate, could have influenced the results. We tried to determine this influence by scanning other agglomerates, which only demonstrated the same outcome: β-PP was only found at and near sample positions with high concentration of clay platelets.

Acknowledgments

This project was partly funded by the Austrian Competence Center Programme within the framework of K2-MPPE center in Leoben. The project was partly funded by Austrian

Nanoinitiative from FFG and FWF in the framework of the Placomp (FWF N901-NAN, FFG 822085) Project.

Literature

[1] Ray, S. S; Okamoto M. *Prog. Polym. Sci.* **2003**, *28*, 1539-1641.

[2] M. Alexandre and P. Dubois, *Materials Science and Engineering* **2000,** *28*, 1-63.

[3] S. Pavlidou, C. D. Papaspyrides, *Progress in Polymer Science* **2008**, *33*, 1119–1198.

[4] S. C. Tjong, *Materials Science and Engineering R* **2006**, *53*, 73-197.

[5] D.Y. Wang, C.A. Wilkie, *Polymer Degradation and Stability* **2003**, *80*, 171-182.

[6] L.A. Utracki, *Clay-Containing polymeric nanocomposites*, Rapra Technology Limited, 2004.

[7] A. Kiernowski, J.S. Gutmann, J. Piglowski, *Journal of Polymer Science: Part B: Polymer Physics* **2007**, 45, 2350-2367.

[8] S. Filippi, C. Marazzato, P. Magagnini, A. Famulari, P. Arosio, S.V. Meille, *European Polymer Journal* **2008**, 44, 987-1002.

[9] B. Yalcin, Z. Ergungor, Y. Konishi, M. Cakmak, C. Batur, *Polymer* **2008**, 49, 1635-1650.

[10] R. Masirek, E. Szkudlarek, E. Piorkowska, M. Slouf, J. Kratochvil, J. Baldrian, *Journal of Polymer Science: Part B: Polymer Physics* **2010**, 48, 469-478.

[11] V.V. Ginzburg, C. Singh, A.C. Balazs, *Macromolecules* **2000**, 33, 1089-1099.

[12] J. Karger-Kocsis, *Polypropylene - Structure, blends and composites*, Chapman & Hall, 1995.

[13] M. Feuchter, G.A. Maier, G. Pinter, M. Kracalik, S. Laske and G.R. Langecker, Annual Technical Conference - ANTEC, Conference Proceedings **2009**, 5, 2642-2646.

[14] S. Laske, M. Kracalik, M. Gschweitl, M. Feuchter, G. Maier, G. Pinter, R. Thomann, W. Friesenbichler, G. R. Langecker, *Journal of Applied Polymer Science* **2009,** *111*, 2253–2259.

[15] Labiche J.C. , Mathon O. , Pascarelli S. , Newton M.A. , Ferre G.G. , Curfs C. , Vaughan G., Homs A. , Fernandez Carreiras D, *Review of Scientific Instruments* **2007**, *78*. 091301.

[16] A. P. Hammersley, S. O. Svensson, M. Hanfland, A. N. Fitch, D. Hausermann, *High Pressure Research* **1996**, *14*, 235–248.

[17] E. Lezak and Z. Bartczak, *Fibres & Textile in eastern Europe* **2005,** *13 (5)*, 51-56.

[18] F. J. Balta-Calleja and C. G. Vonk, *X-ray scattering of synthetic polymers*, Elsevier, 1989.

4.3 Paper 5

M. Feuchter, G. Maier, G. Pinter, M. Kracalik, S. Laske, G. R. Langecker

Studies on the melting behavior of polypropylene nano-composites using X-ray diffraction and differential scanning calorimetry

Annual Technical Conference - ANTEC, Conference Proceedings 5 (2009), pp. 2642-2646

Studies on the melting behavior of polypropylene nano-composites using X-ray diffraction and differential scanning calorimetry

Michael Feuchter, University of Leoben and Polymer Competence Center Leoben, Austria
Günther A. Maier, Erich Schmid Institute and Department of Material Physics and Materials Center Leoben, Austria
Gerald Pinter, University of Leoben, Austria
Milan Kracalik, University of Leoben, Austria
Stephan Laske, University of Leoben, Austria
Günter R. Langecker, University of Leoben, Austria

Abstract

The structural details of polymeric composites produced by melt intercalation of polypropylene and layered silicates have been investigated at process-related temperatures. Various samples from different states of the production process have been investigated at temperatures ranging from 25 to 200°C by means of X-ray diffraction. These states included pure polypropylene, an unmodified (MMT) and an organically modified montmorrillonite (OMMT), a master batch (polypropylene filled with 20 wt% OMMT) and a dilute nano-composite (5 wt% OMMT). For the determination of the long period of polypropylene and of the interlayer distance of the silicate platelets, small angle X-ray scattering (SAXS) was used. To define the degree of crystallization and the crystal lattice, a wide angle X-ray diffraction (WAXD) was used. The structure of polymeric nano-composites was likewise confirmed by means of differential scanning calorimetry (DSC). By combining the results from both types of experiments, it was possible to assign energy-related parameters to structural details.

Introduction

In the last few years, polymer composites, especially with fillers in the nanometer range, have aroused more interest as it has become possible to produce nano-composites with outstanding mechanical, electrical and flame resistant properties. Especially polymer composites with layered silicates have developed into an area of high research interest [1].

Several strategies for the preparation of polymer-layered nano-composites have been developed. Among the different processes are in situ polymerization, polymer intercalation from solution and melt intercalation. Major efforts have also been put into the organic modification of the silicate platelets to change the nano-clay surface from hydrophilic to organophilic in order to strengthen the interaction between the filler and the polymer. The surface is mainly modified by ion exchange reactions with cationic surfactants like alkyl ammonium or alkyl phosphonium cations [2].

Basically three different states of nano-clay polymer composites are available: (1) layer-structured composites can be in the micro-composite state, in which the filler is in an agglomerated form with an interlayer spacing equivalent to that of neat nano-clay; (2) in the intercalated state, polymer chains are inclined between two silicate platelets and the interlayer distance becomes higher, while the layers are still stacked; (3) in the exfoliated state, single platelets are randomly distributed in the polymer without having any special correlation [3].

In this paper intercalated polypropylene nano-composites will be analyzed due to the interesting relationship between their structure properties. In addition, the intercalated structure is the first step towards reaching the exfoliation state by means of a melt intercalation. The main objective of this paper is to investigate the structure of polymeric composites produced by melt intercalation of polypropylene and layered montmorrillonite.

Experiment

Materials

The isotactic polypropylene (PP) homopolymer HC600TF (MFI 2.8 g/10 min; 230°C/2.16 kg) was provided by Borealis Inc., Linz, Austria. As a nano-filler an organically modified montmorrillonite with the commercial indication Nanofil 5, provided by Süd-Chemie Inc., Munich, Germany, was used. In order to combine the hydrophobic polymer and the hydrophilic nano-filler, a compatibilizer was needed. Therefore, the maleinic anhydride acid grafted polypropylene Scona TPPP 2112 FA, provided by Kometra Ltd., Schkopau, Germany, was used.

Sample preparation

For the compounding process, the intermeshing, co-rotating twin screw extruder Theyson TSK30/40D (Theyson Ltd., Vienna, Austria) with a string die was used. The feed rate was set at 20 kg/h, with a screw speed of 100 rpm for the master batch sample. First, a master

batch (MB) with 20 wt.% nano-filler and 20 wt.% compatibilizer was produced. This master batch was diluted down to 5 wt.% nano-clay content (G3) with pure PP. For the structural characterization, plates with a thickness of 2 mm were prepared by means of a hydraulic vacuum press machine (Collin 200 PV, Dr.Collin ltd., Ebersberg, Germany).

Sample analysis

Small angle X-ray measurements were performed using Bruker NanoStar (Bruker AXS, Karlsruhe, Germany). This system was equipped with a two-dimensional X-ray detector and a distance of 108 cm between the sample and the detector was chosen. Therefore, an angle ranging from 0.05 to 3.5° was adjusted for this configuration. A wavelength of 0.154 nm (CuKα) was used. The samples were measured in transmission and under vacuum. The samples were fixed on a temperature-controllable sample holder, where they were heated to 200°C, cooled down to room temperature and again heated to 200°C. The heating rate chosen was 1 K/min. The samples were fixed at mean variant measuring temperatures during the X-ray measurements (quasi-isotherm experiment). The measuring temperatures were 25, 50, 60, 70, 80, 95, 110, 130, 145, 150, 155, 160, 165, 170, 175, 180, 185, 190, 195 and 200°C for heating and cooling down. To avoid the influence of texture, all scattering measurements were performed on pressed plate samples. The background scattering was measured without a sample in the sample holder.

The gallery periods of the organically modified and the unmodified montmorrillonite were determined with powder samples. Therefore, the powder samples were fixed between two capton foils. These foils were also measured under heating influence and were taken as background scatter for these two samples [4].

To determine the long period of the polymer and the gallery period of the layered silicate platelets, scattering curves were corrected for background scatter. The Lorenz correction was performed by multiplying the scattered intensity I(q) by q^2, q being the magnitude of the scattering vector. The determination of peak positions – one position for the polymer and the second one for the silicate layers – was done by fitting with a Pseudo-Voigt function [4]. Detailed SAXS analyses for the determination of the crystalline thickness and the interlayer spacing were performed by applying a correlation function method according to Strobl and Schneider [5]. The gap distance of the nano-filler was determined by subtracting the platelet thickness from the measured interlayer distance. The platelet thickness was determined by applying the same correlation function method [5] used for the polymer.

Wide angle X-ray measurements were performed using the same equipment as for SAXS. Only the distance from the sample to the detector was changed to 10 cm. The accessible diffraction angle ranged from 1 to 23°2θ. The measurements were performed according to the SAXS procedure.

Wide-angle X-ray scattering was used to determine the degree of crystallinity. The crystallinity was calculated using equation 1, in which I_C is the sum of the scattered intensities of crystalline peaks and I_T is the total scattering intensity [4].

$$\alpha_{WAXS} = \frac{I_C}{I_T} * 100\% \qquad (1)$$

Differential scanning calorimetry measurements were performed using DSC822 (Mettler Toledo GmbH, Switzerland) in a temperature range from –50 to 250°C with a heating rate of 10 K/min in a nitrogen atmosphere. The crystallinity at a defined temperature was calculated using equation 2, in which ΔH_m is the melt enthalpy of the polymer from the given temperature up to 210°C and ΔH_m^0 is the melt enthalpy of 100% crystalline PP (ΔH_m^0=207 J/g) [6].

$$\alpha_{DSC} = \frac{\Delta H_m}{\Delta H_m^0} * 100\% \qquad (2)$$

Results

The characteristics of the temperature dependence of the degree of crystallinity determined by WAXD as shown in figure 1 correlated to the calculated degree of crystallinity determined by DSC, which is shown in figure 2.

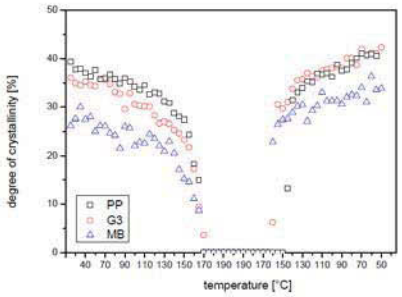

Figure 1. Temperature dependence of the degree of crystallinity determined by WAXD.

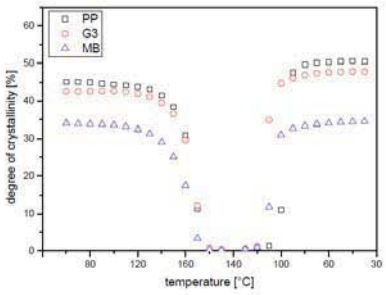

Figure 2. Temperature dependence of the degree of crystallinity determined by DSC.

At an elevated temperature, the long period was increased, as shown in figure 3, for all three different samples. It could be shown that in the beginning and during the heating all samples nearly had the same long period. When cooling them down first crystalline lamellas were formed at a temperature of 155°C with nearly the same size in all three samples. At a lower temperature, the long period of the PP reached a plateau at approximately 26 nm. Compared to the pure PP, the composites MB and G3 showed an additional increase in the long period at a lower temperature.

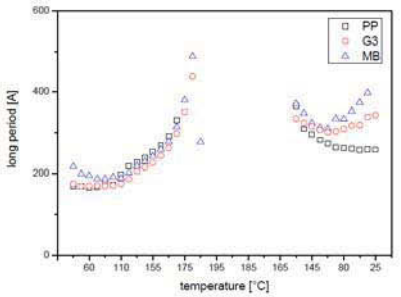

Figure 3. Temperature dependence of the long period.

Figure 4 illustrates the temperature dependence of the interlayer spacing of the nano-filler. The interlayer distance at unmodified montmorrillonite was hardly influenced by the temperature. Only in the beginning of the heating, a minimal decrease of the interlayer distance up to a temperature of approximately 110°C occurred. The interlayer distance at pure OMMT increased continuously with a rising temperature up to 200°C and decreased with falling temperature. At the end of the thermal process, the interlayer distance was lower than in the beginning.

The interlayer distance (gap distance) of the MB sample was hardly influenced up to 180°C, which was also the temperature at which the polymer composite was completely molten. After that temperature, the interlayer distance decreased up to 200°C and it was continuously decreasing when the sample was cooled down to 180°C. At this temperature, the interlayer distance was still decreasing with falling temperature, but the slope in the temperature-interlayer distance diagram was decreased. At the end of thermal process, the interlayer distance was as low as that of the pure OMMT.

The interlayer distance of the G3 samples increased up to 160°C as a function of temperature. During the heating from this point to 200°C and the cooling down to 115°C, the interlayer distance was hardly influenced. However, had the cooling process been continued to 25°C, the interlayer distance would have decreased to a value lower than that of the pure OMMT.

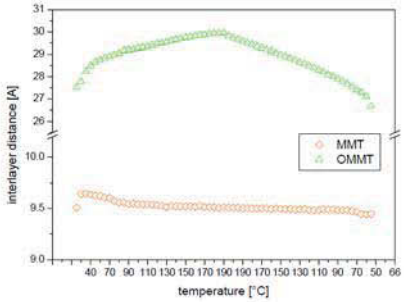

Figure 4. Temperature dependence of the interlayer spacing in modified (OMMT) and unmodified (MMT) montmorrillonite

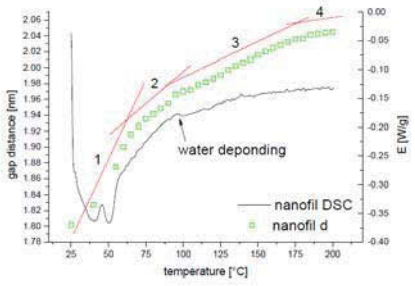

Figure 5: Comparison between the DSC curve and the gap distance (d) of Nanofil (first heating circle).

Figure 5 shows a comparison between the DSC and the gap distance of the OMMT. The DSC curve indicates some energy-releasing features between 25 and 75°C. Slightly above 100°C, the desorption "peak" of water can be seen. The GAP curve can be divided into four areas (marked as 1-4), of which all have a linear shape, but different slopes. At low temperatures (areas 1-2), the interlayer distance increased fast with temperature. A strong increase of the gap distance correlated to a high amount of energy consumption as shown in the DSC curve. The fluctuations in the DSC curve could not be seen in SAXS results. In area 2 between 60 and 100°C, the slope of the d-curve is a little bit lower than in area 1. The DSC curve also flatted. However, the DSC curve in this area did not only consist of information from Nanofil as there was also additional energy needed for the debonding of the water. After reaching the desorption temperature of water, the slope changes (areas 3-4) to a relatively small increase per temperature step. A gradual increase in the layer distance can be seen in this temperature range and the energy curve can be described with a logarithmic function.

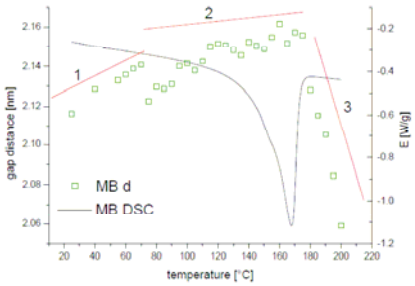

Figure 6: Comparison between the DSC (DSC) and the gap distance (d) of MB (first heating circle).

Figure 6 shows the temperature dependence gap distance and the DSC curve of the master batch sample. The GAP (d) curve can be divided into three areas (marked as 1-3), of which all have a linear shape, but different slopes. The gap distance changed about one percent in the first area and about two percent from the beginning of the measurements to the end of area 2. The main feature of the DSC curve was the polymer melting peak. In area 3, a strong decline of the gap distance occurred after the melting point had been reached.

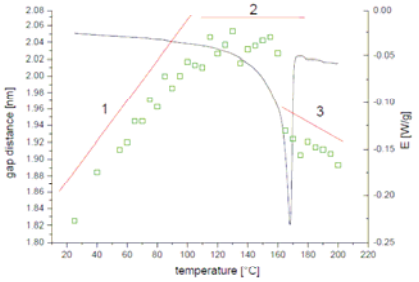

Figure 7: Comparison between the DSC and the gap distance (d) of G3 measured with SAXS.

The influence of the temperature on the gap distance in sample G3 and the corresponding DSC curve are shown in figure 7. The gap curve can be divided into three areas, which again have a linear shape, but different slopes. First, there is an increase in the gap spacing of about 15% from 1.82 to 2.06 nm. In the second region, no change of the gap spacing can be found. At the melting point, indicated by a strong minimum in the DSC curve, the gap distance strongly decreases to 1.88 nm (area 3). The DSC curve represents a polymer-dominated curve comparable to the MB sample.

Discussion

A high filler content let the degree of crystallinity decrease to lower values. With a lower concentration of the nano-filler, as in sample G3, the degree of crystallinity and, therefore, also the crystallizing process are comparable to pure PP.

The re-crystallization temperature of the composite melts was higher than in the case of pure polymer as the nano-particles might have acted as crystal nuclei. As for diluted polymer nano-composites, the degree of crystallinity was nearly the same as of pure PP. Similarly, the composite had a much higher long period. It could be shown that the long period increased with rising temperature. The mean crystalline thickness, determined with a correlation function method, showed similar characteristics as the long period. This could be explained by the melting of small crystals at a lower temperature due to which the average size of crystals became larger [6]. The divergence of the long period at lower temperatures may be caused by temper effects. Another possible cause of that effect is the nano-filler which may act as a nucleus for crystallization, resulting in a large number of small crystals.

The temperature had hardly any effect on the interlayer distance of unmodified montmorrillonite. Only in the beginning of the heating the interlayer distance

increased slightly, most probably due to the desorption of water [7].

The pure organically modified nano-filler (OMMT) showed an increase in the interlayer spacing under heating conditions. Alkyl chains located on the surface of the OMMT oscillated and stretched more and more and thus used more space which resulted in an increase in the interlayer distance. This is important for the application of OMMT since the large distance between clay and clay at higher temperatures allows for an easier separation of platelets and exfoliation in a polymer. The DSC curve of OMMT showed a melt-like behavior at low temperatures between 25 and 75°C. The peaks can be explained by a melting process of the alkyl chains grafted on the surface of the filler. The two peaks can be interpreted as two different sizes of alkyl chains. In this temperature region, the increase in the gap distance was high with about eight percent from 1.8 to 1.92 nm, most probably caused by the quasi-melting and stretching of the alkyl chains. In area 2, adsorbed water was desorbed between 75 and 110°C which alleviated the alkyl chains to stretch and oscillate. In area 3, the gap between two single platelets slowly increased between 110 and 170°C as a function of temperature. The DSC curve also changed from oscillating at low temperatures to a logarithmic shape. In this temperature range, the stretching and oscillating of the small chains were the main features. In the last region (area 4), the DSC curve reached a plateau while the gap distance still increased with rising temperature. After cooling down to room temperature (see figure 4), the interlayer distance in OMMT was smaller than in the beginning of the temperature-controlled X-ray diffraction experiment which may have been caused by the release and destruction of some of the alkyl chains on the platelet surface at a high temperature (see figure 5) [7].

In the composite, a different behavior was found for the nano-filler. The DSC curves of MB and G3 were dominated by the polymer and none of the mentioned effects of pure nano-filler were visible. The increase in the gap distance in area 1 and 2 was caused by the higher mobility (stretching and oscillating) of the polymer chains which were inclined between two platelets. The high amount of filler in the master batch (MB) sample built up a stable inner structure, similar to a card house, which was hardly influenced by the polymer chain mobility, while the influence on the gap distance was much more pronounced in the G3 sample.

At a higher temperature, the polymer melted and the interlayer spacing decreased, which may have been caused by the high polymer melt weight.

Conclusion

In this paper the structure of polymeric composites produced by the melt intercalation of polypropylene and layered silicates have been investigated. Therefore, an unmodified montmorrillonite, a modified montmorrillonite, a master batch and a dilute polymeric nano-composite have been measured with WAXS, SAXS and DSC under heating and cooling conditions.

The degree of crystallinity determined by WAXD and by DSC had the same characteristics in the heating and cooling process as expected. The melting and crystallization temperature depending on the filler content determined by WAXD could be confirmed by DSC measurements. Likewise the temperature dependence of the long period under heating conditions determined by SAXS was expected due to DSC literature [6]. The interlayer distance as a function of temperature depended on the filler content. It could be shown that the gap distance (determined by SAXS) of both filled materials (MB and G3) rapidly decreased at the melting temperature (determined by DSC).

At process-related temperatures, the gap distance in the pure organically modified clay was significantly larger than at room temperature and, therefore, the attracting forces between clay platelets were reduced, which helps dissipating nano-filler in the polymeric matrix.

Acknowledgement

The research work of this paper was performed in the scope of the Research Project Cluster NanoComp ("Performance Optimization of Polymer NanoComposites"), coordinated by the Polymer Competence Center Leoben GmbH. Funding by the Federal Ministry of Traffic, Innovation and Technology and the Austrian Research Promotion Agency within the AUSTRIAN NANO-Initiative is gratefully acknowledged.

References

1. S. S. Ray and M. Okamoto, Prog. Polym. Sci., 28, 1539 (2003).
2. M. Alexandre and P. Dubois, Materials Science and Engineering, 28, 1 (2000).
3. S. C. Tjong, Materials Science and Engineering R, 53, 73 (2006).
4. F. J. Balta-Calleja and C. G. Vonk, *X-ray scattering of synthetic polymers*, Elsevier (1989).
5. G. R. Strobl and M. Scheider, Journal of polymer science: Polymer physics edition, 18, 1343 (1980)
6. G. W. Ehrenstein, G. Riedel and P. Trawiel, *Praxis der Thermischen Analyse von Kunststoffen*, Carl Hanser Verlag (2003).
7. M. Gelfer, C. Burger, A. Fadeev, I. Sics, B. Chu, B. S. Hsiao, A. Heintz, K. Kojo, S.-L. Hsu, M. Si and M. Rafailovich, Langmuir, 20, 3746 (2004).

Key Words: Polypropylene, silicate layers, temperature dependence of X-ray scattering, WAXS, SAXS.

5 Micromechanics of clay polypropylene nanocomposites

This chapter details the structure-property relationships of polymeric nanocomposites at a sub micron resolution. Mechanical properties correlated to material structure are of high interest to the scientific community. Deformation of material strongly depends on the material's structure (Grellmann and Seidler, 2005). The two main deformation mechanisms, observable in polymers, are crazing and shear-yielding (Strobl, 2007). In case of a classical filler being present, the deformation mechanism is mostly controlled by debonding, accompanied by void formation and growth (Dubnikova et al., 1997). While the influence of classical fillers are widely studied, there is still a lack of understanding the influence of nanostructured (layered silicates) fillers (which deformation mechanism predominates and how a filler with such dimensions influences them). Therefore, three papers presented in this chapter discuss the differences between micromechanics of the matrix polymer and the corresponding polymeric nanocomposites (layered silicates).

5.1 Major results

Paper 6 presents the introduction to this chapter and concerns a qualitative analysis of deformation mechanisms of the produced polymeric nanocomposites. It became evident, that virgin polypropylene and two differently produced polymeric nanocomposites demonstrate different fracture behaviour. While pure polypropylene showed a rearrangement of crystal phases, the filled samples broke due to hampered rearrangement and formation of micro cavities. The determination of strains in different parts of the sample (crystalline, amorphous and inorganic parts) allowed for a description of basic deformation and fracture mechanisms.

Paper 7 focuses on the micro mechanics behaviour of polymeric nanocomposites at a crack tip. This initial point for deformation delivered information on the deformation mechanism. Thereupon, the orientations and micro elongations near a crack tip were investigated. The parameters were determined via samples, which were exposed to external load. For comparison purposes, virgin polypropylene and one nanocomposite were measured. It was revealed that polypropylene and the silicate-reinforced material possessed different orientation zones. Awareness of the form of the oriented zone and the height of orientation helped to adequately explain the different deformation mechanism. A very thin

zone with a high degree of orientation (nanocomposite) was related to brittle failure; meanwhile, a very broad zone with a relatively low degree of orientation (polypropylene) caused a ductile material behaviour.

The last Paper in this part (Paper 8) details microstress (stresses of the crystallographic planes) determination of the virgin polymer as well as the clay-filled polymer with the use of in-situ X-ray measurements. For this purpose, it was necessary to determine X-ray specific elastic constants. Determination of the X-ray specific elastic constant has been widely studied in metals, ceramics and polymers (Nielsen and Martin, 1985; Daniel et al., 2010). It is often used to analyze the internal stress in ceramics and metals (Fitzpatrick and Lodini, 2003*;* Almer and Stock, 2005). These investigations are hardly applied on polymeric materials, due to the fact that with polymeric material, the X-ray specific constants change. Molecular mass distribution, strong temperature dependency and aging are the most common reasons wherefore the constants can fluctuate. Nonetheless, the determination of X-ray specific constants was carried out in paper 8. The strains of the crystallographic planes were correlated to the applied stress. For this purpose it was necessary to know the exact amount of applied stress in the measured area; therefore, special test specimens were prepared. Thereby, it was possible to establish X-ray specific elastic constants for every crystallographic plane. These were applied to in-situ X-ray measurements on rectangular samples, where the applied stress was unknown. With the use of the ascertained X-ray specific constant, it was possible to detect the applied stress in rather inaccessible sites. It was proven, that the suggested approach works if there are no lamellar fragmentation and no rearrangement of the crystallographic planes.

5.2 References

Almer, J.D., Stock, S.R. (2005). Journal of Structural Biology, **152**, 14.

Daniel, R., Martinschitz, K.J., Keckes, J., Mitterer, C. (2010). Acta Materialia, **58**, 2621.

Dubnikova, I.L., Muravin, D.K., Oshmyan, V.G. (1997). Polym. Eng. Sci. **37**, 1301.

Fitzpatrick, M.E., Lodini, A. (2003). "Analysis of Residual Stress by Diffraction using Neutron and Synchrotron Radiation", Taylor & Francis, London.

Grellmann, W., Seidler, S. (2005). "Kunststoffprüfung", Carl Hanser Verlag, München.

Nielsen, O.H., Martin, R.M. (1985). Physical Review B, **32**, 3792.

Strobl, G. (2007). "The Physics of Polymers", 3rd edition, Springer-Verlag, Berlin.

5.3 Paper 6

M. Feuchter, G. Maier, G. Pinter, M. Kracalik, S. Laske, G. R. Langecker

Determination of Hierarchical Strains in Intercalated clay-Polypropylene Nanocomposites

Materials Research Society Symposium Proceedings (2008), 1146, pp. 183-190

Determination of Hierarchical Strains in Intercalated clay-Polypropylene Nanocomposites

Michael Feuchter[1,2], Günther A. Maier[3,4], Gerald Pinter[1], Milan Kracalik[5], Stephan Laske[5] and Günter .R. Langecker[5]
[1] Institute of Materials Science and Testing of Plastics, University of Leoben, Franz-Josef Str. 18, 8700 Leoben, Austria
[2] Polymer Competence Center Leoben GmbH, Roseggerstrasse 12, 8700 Leoben, Austria
[3] Erich Schmid Institute and Department of Material Physics, Universtiy of Leoben, Jahnstrasse 12, 8700 Leoben, Austria
[4] Materials Center Leoben Forschung GmbH., Roseggerstrasse 12, 8700 Leoben, Austria
[5] Institute of Plastics Processing, University of Leoben, Franz-Josef Str. 18, 8700 Leoben, Austria

ABSTRACT

When external loads were applied on a polymer-nanocomposites (PNC) the internal strains are distributed in the matrix and the filler. Depending on the distribution of filler and type of polymer various kinds of strain distributions can be addressed. In a semi-crystalline polymer intercalated composite system strains are dissipated in amorphous and crystalline phase and in stacked filler. Within the stacks, strains are dissipated between clay platelets and the polymeric interlayer. We used in-situ simultaneous synchrotron SAXS and WAXD during deformation of polymer and composites for characterization of strain. The technique allows for simultaneous determination of strains in crystalline and amorphous domains of polymer as well as of clay crystals and interlayer. The assessed dimensions are spanned between 30 nm and 0.4 nm and cover therefore nearly two orders of magnitude.

With these experiments, we were able to determine influence of filler on system and primary fracture mechanism in the polypropylene intercalated nano-clay system.

INTRODUCTION

Polymer composites, especially with fillers in the nanometers range, are attracting much interest by both scientific and industrial communities. Nanocomposites with outstanding mechanical, electrical and flame resistant properties can be produced. There are several types of nanofillers existing; they differ in form (e.g. spherical, plate like and tube like form) and in their properties. Especially polymer composites with layered silicates have been an area of high research interest [1].

Several strategies for polymer-layered nanocomposites preparation have been developed. These different processing routes are in situ polymerization, polymer intercalation from solution and melt intercalation. Large efforts have also gone into organic modification of the silicate platelets to change nanoclay surface from hydrophilic to organophilic to make strengthen interaction between filler and polymer. Surface modification is mainly performed by ion exchange reactions with cationic surfactants like alkylammonium or alkyl phosphonium cations [2].

Basically three different interactions between the polymer and the layers are available. First there are agglomerates of the silicate platelets which have dimensions in the μm range.

There are no or less interactions between polymer and filler existing. The second state is the intercalated one, where polymer chains are inclined between two silicate platelets. Interlayer distance becomes higher, but the layers are still stacked. The third state is the exfoliated state, where single platelets are randomly distributed in the polymer. These single platelets have no special correlation between each other [3].

In-situ synchrotron SAXS and WAXD combinations are mainly used to investigate structure property relations in various materials, for example in polymers e.g. [4, 5] and biological composites e.g. [6,7]

EXPERIMENT

Materials

The isotactic polypropylene (PP) homopolymer HC600TF (MFI 2.8 g/10 min; 230°C/2.16 kg) was supplied by Borealis Inc., Linz, Austria. As nanofiller a organic modified montmorrillonite with commercial indication Nanofil 5 supplied by Süd-Chemie Inc., Munich, Germany was used. To combine the hydrophobic polymer and the hydrophilic nanofiller a compatibilizer is needed. Therefore a maleinic anhydride acid grafted polypropylene, which was supplied by Kometra Ltd., Schkopau, Germany and named Scona TPPP 2112 FA, was used [8].

Preparation of nanocomposites

For the compounding process, an intermeshing, co-rotating twin screw extruder Theyson TSK30/40D (Theyson Ltd., Vienna, Austria) with a string die was used. The feed rate was set at 20 kg/h, with a screw speed of 100 rpm at the masterbatch sample. First a masterbatch with 20 wt.% nanofiller and 20 wt.% compatibilizer was produced. This masterbatch was dilute with pure PP down to 5 wt.% nanoclay content. To get a better distribution of nanoclay this diluting process was performed with different rotation speeds of the twin screw extruder [8].

In this work tested polymeric nanocomposites were processed by using one special (high shear) screw geometry G3 and two different rotation speeds (100 and 200 min^{-1}).

Samples

For structural characterization during tensile testing, plates with a thickness of 1 mm were prepared using the hydraulic vacuum press machine (Collin 200 PV, Dr.Collin ltd., Ebersberg, Germany). The rectangular samples (50x10 mm^2) for tensile testing were cutted out of these plates. For better localization of the macroscopic crack pass, samples were performed with a 1 mm deep crack located at both sides on the middle of the sample length.

Synchrotron experiments

The experiments were executed at µ-spot beamline at BESSY (Berliner Elektronenspeicherring-Gesellschaft für Synchrotronstrahlung m.b.H., Berlin, Germany). This system was equipped with a two dimensional X-ray detector (Mar Mosaique, Mar Research, Germany).

In situ tensile tests were performed with a computer controlled tensile testing apparatus (Anton Paar, Graz, Austria). A sample to detector distance of 430 mm was chosen and a wavelength of 0.0827 nm was used for the experiments. The samples were measured in transmission during a tensile test and the size of the last beam definition pinhole had a diameter of 30 µm. In that way it was possibly to measure small angle x-ray scattering (SAXS) and wide angle x-ray diffraction (WAXD) at one in-situ tensile test experiment. The setup of experiment is sketched in Figure 1. The shown scattering pattern was typical for undeformed material. The zoom region shows the small angle scattering area on detector.

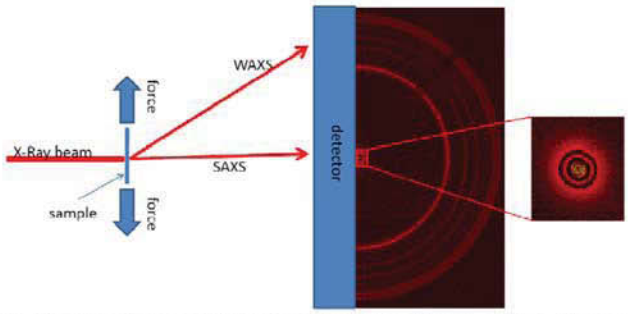

Figure 1. Sketch of synchrotron experiment and typical scattering pattern. The small pattern on the right side is a zoom in the SAXS signal.

For determination of morphological parameters, diffraction patterns I(q,ψ) were averaged in arcs with respect to ψ=-15 to 15 (parallel to drawing direction) using Fit2D software. The drawing direction was defined as ψ = 0 and ψ denotes the azimuth angle. The modulus of scattering vector q is defined as $q = (4\pi^*\sin\theta)/\lambda$ where λ is the wavelength of the used radiation and θ is the half of the scattering angle 2θ. For data evaluation, all scattering curves were corrected for background scatter.

DATA EVALUATION

Small angle x-ray scattering (SAXS)

To determine long period of the polymer and gallery period of the layered silicate platelets scattering curves I(q) were multiplied by q^2 (the so called Lorenz correction). The long period can be understood as a sum of thickness of amorphous interlayer and thickness of lamellae crystal. The gallery peak arises from regular arrangement of clay platelets and the size derived from position of peak is the sum of thickness of one clay platelet (0.95nm) and of the polymeric interlayer. The determination of peak positions was done by fitting data with a Pseudo Voigt function [2,9].

Wide Angle X-ray Diffraction (WAXD)

Crystal structure and lattice parameters were determined by wide angle x-ray diffraction pattern, scattering curves were corrected for background scatter. Lattice spacing was calculated by using Bragg's law. Positions of peaks were determined by fitting data using Pseudo-Voigt function.

The calculation of the micro strain was done with equation 1, where d_0 is the mean value of the first 3 lattice spacing (long period, interlayer distance) values and d is the concrete lattice spacing (long period, interlayer distance).

$$\varepsilon_{Micro} = \frac{d - d_0}{d_0} * 100\% \qquad (1)$$

Tensile tests

In-situ tensile testing experiments were performed using a tensile testing machine and the testing velocity was set to 1 mm/min, which is a strain rate of 4.54%/min. Calculating of applied strain was done with using equation 2, where l_0 is the length between the two chuck jaws and Δl is the change of way during tensile test.

$$\varepsilon_{applied} = \frac{\Delta l}{l_0} * 100\% \qquad (2)$$

RESULTS

The diffraction pattern of an undeformed specimen is shown in Figure 2. The pattern can be separated in two areas: SAXS region from 0 to 2.5 deg 2θ and WAXD region from 2.5 to 13 deg 2θ. The miller indeces from polymer were taken from [10]. For evaluation of strains the crystalline (110) reflection, the gallery peak and the long period were chosen.

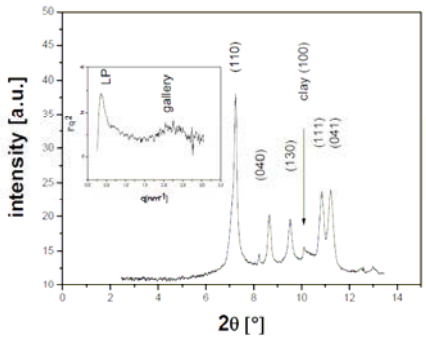

Figure 2. Representative WAXD (large graph) and SAXS (small graph) scattering curves from intercalated composite.

Polymer

The results of three different samples, namely pure polypropylene (PP) and the two polymeric nanocomposites are shown in figures 3 and 4. The two composites had different intercalation properties. All shown results were analyzed in tensile direction.

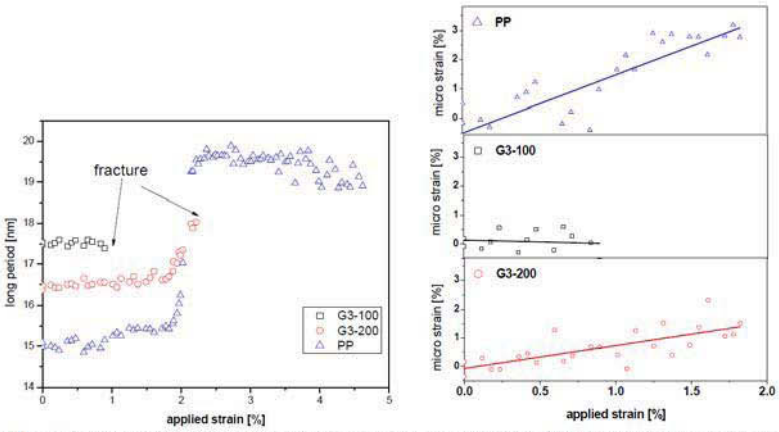

Figure 3. Results from SAXS analysis of polymer part of material. On left side the values for long period are plotted against applied strain. On the right side, microscopic strain in long period was plotted against applied strain in the elastic region.

Long period was strongly affected by the filler. In native material (PP) the initial LP was 15 nm, in G3-200 sample 16.5 and 17.5 nm for G3-100 respectively. At applied strains higher than 1.8%, in samples G3-200 and PP morphological changes occurred, leading to a strong increase of LP. Fracture strain in pure PP was very high and decreased in composites materials. In sample G3-200 plastically deformation occurred prior fracture while G3-100 showed brittle fracture behavior. The strains in elastic regime were also different for samples under investigation. While in pure PP strains in long period were large, even above the applied strain, strains calculated from LP in other samples were lower than applied strain. It needs to be mentioned, that amorphous and crystalline phase can behave different from each other, due to the fact that amorphous material is softer that crystalline. In sample G3-100 no change in LP occurred, the strains in amorphous phase seemed to be very low. The dependence of microscopic strain in crystalline as calculated from position of (110) reflection as a function of applied strain is shown in Figure 3.

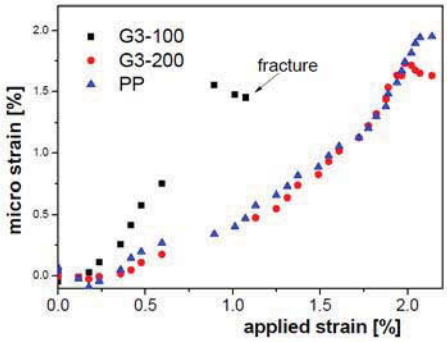

Figure 4. Microscopic strain of (110)-plane as a function of applied strain.

The sample G3-100 showed a higher increase of micro strain than the applied strain, whereas PP and G3-200 represented a more moderate slope in strain/strain behavior. All samples demonstrated a slightly decrease of micro strain before they broke. In addition PP and G3-200 showed a similar behavior with three different linear segments during the increasing of strain/strain relation; on the other hand G3-100 had only one linear segment at this section.

Clay

In Figure 5 the interlayer distance (left hand) and the microscopic strain in the gap (right) between clay platelets was plotted as a function of applied strain.

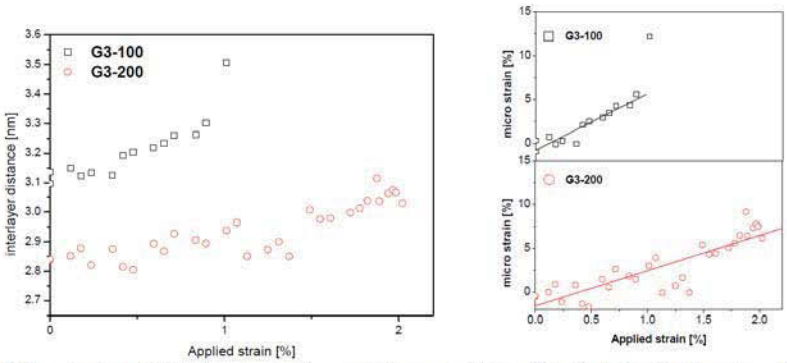

Figure 5. Results from SAXS analysis of composite part of material. On left side the values for interlayer distance are plotted against applied strain. On the right side, microscopic strain in interlayer was plotted against applied strain in the elastic region.

The initial interlayer distances were 3.1 nm and 2.8 nm for G3-100 and G3-200 samples, respectively. The microscopic / applied strain behavior could be fitted by linear regression in both cases, but the slopes were very different. The slope for material G3-100 was nearly two times higher than in samples produced from G3-200 material. Interestingly, fracture occurred in both samples when a micro-strain of appr. 10% was reached.

DISCUSSION

Micro and applied fracture strains in polymer were strongly influenced by the filler. In case of the neat polymer large strains were found in the LP evaluation, while in crystals strains were smaller than applied one. At a strain of 2% long period increased dramatically in G3-200 and pure PP samples, but this was much more pronounced in the pure polymer. In these two materials, the increase of long period was caused by morphological changes. The polymer crystals were fragmented and rearranged, as could be deduced in scattering patterns recorded at larger strains. In these patterns an additional oriented scattering signal perpendicular to tensile axis occurred, indicating the formation of fibrils. Interestingly, the long period in sample G3-100 was not affected changed during experiment, while in crystalline phase a maximal strain of about 1.5% at an elongation of 0.8% was found. This indicates, that amorphous phase consisted either of stretched polymer chains or the mobility of amorphous material was suppressed by the filler. The crystalline region of materials G3-200 and pure PP showed a similar behavior on applied strain. Only at applied strains of about 1.8% a difference occurred. While PP still showed an increase, the strain in composite decreased prior fracture. The maximum value reached in composite G3-200 was nearly the same as in G3-100 and in the range of 1.5%.

Also for the strain dependence of interlayer distance a comparable maxima between composite materials was found: Fracture occurred at strains of about 10+-3%. This was most probably caused by delamination of clay, which caused defect formations and led to brittle fracture. This fact could be supported by an increase in overalls scattering intensity in the SAXS regime, indicating the formation of cavities.

The micro strain between the silicate platelets was found to be much higher than in the polymer surrounding the platelets, indicating that the layers between platelets were rather soft. Due to the low concentration, the overall contribution to material extension was quite low.

CONCLUSIONS

Polymeric nanocomposites featured other deformation and fracture mechanism than virgin polymer. While pure polypropylene was showing rearrangement of crystal phases , polymeric nanocomposites broke due to hampered rearrangement and formation micro cavities. The determination of strains in different parts of sample (crystalline, amorphous and inorganic parts) allowed for description of basic deformation and fracture mechanisms. It could be shown that fracture in intercalated clay – PP nano-composites can be addressed to microscopic features in the size range between 30 and 0.3 nm.

ACKNOWLEDGMENTS

The research work of this paper was performed within the Research Project Cluster NanoComp ("Performance Optimization of Polymer NanoComposites"), coordinated by the

Polymer Competence Center Leoben GmbH. Funding by the Federal Ministry of Traffic, Innovation and Technology and the Austrian Research Promotion Agency within the AUSTRIAN NANO-Initiative is gratefully acknowledged.

The help during synchrotron experiments at y-spot beamline (BESSY, Berlin, Germany) by Dr. Ivo Zizak and Prof. Dr. Oskar Paris is grateful acknowledged.

This work was supported by the European Community - Research Infrastructure Action under the FP6 "Structuring the European Research Area" Programme (through the Integrated Infrastructure Initiative" Integrating Activity on Synchroton and Free Electron Laser Science - Contract R II 3-CT-2004-506008).

REFERENCES

1. S.S. Ray and M. Okamoto, Prog. Polym. Sci., 28, 1539 (2003).
2. M. Alexandre and P. Dubois, Materials Science and Engineering, 28, 1 (2000).
3. S.C. Tjong, Materials Science and Engineering R, 53, 73 (2006).
4. Gupta, H.S., Seto, J., Wagermaier, W., Zaslansky, P., Boesecke, P., Fratzl, P. Proceedings of the National Academy of Sciences of the United States of America 103 (47), pp. 17741-17746.
5. Kawakami, D., Burger, C., Ran, S., Avila-Orta, C., Sics, I., Chu, B., Chiao, S.-M., (...), Kikutani, T.; *Macromolecules* 41 (8), pp. 2859-2867 (2008).
6. Günther A. Maier, Gernot M. Wallner, Reinhold W. Lang, Jozef Keckes, Heinz Amenitsch and Peter Fratzl, J. Appl, Cryst., 40, 564-567 (2007).
7. Martinschitz, K.J., Boesecke, P., Garvey, C.J., Gindl, W., Keckes, J. Journal of Materials Science 43 (1), pp. 350-356 (2008).
8. M. Feuchter, G.A. Maier, G. Pinter, M. Kracalik, S. Laske and G.R. Langecker, ANTEC techn.paper 2009, submitted
9. F.J. Balta-Calleja and C.G. Vonk, X-ray scattering of synthetic polymers, Elsevier (1989).
10. E. Lezak and Z. Bartczak, Fibres & Textile in eastern Europe, 13, (2005).

5.4 Paper 7

M. Feuchter, G. Maier, I. Zizak, G. Pinter, M. Kracalik, S. Laske, G. R. Langecker

Characterization of the orientation parameters around crack tips in unfilled and nanofilled polypropylene using in-situ synchrotron small and wide angle scanning scattering techniques

Macromolecular Symposia (2010), 296, 1, pp. 189-196

Characterization of the orientation parameters around crack tips in unfilled and nanofilled polypropylene using in-situ synchrotron small and wide angle scanning scattering techniques

Michael Feuchter,[1,2] Günther Maier,[3,4] Ivo Zizak,[5] Gerald Pinter,[1] Milan Kracalik,[6] Stephan Laske,[6] Günter Rüdiger Langecker[6]*

[1] Institute of Materials Science and Testing of Plastics, University of Leoben, Franz Josef Strasse 18, 8700 Leoben, Austria; e-mail: Michael.Feuchter@mu-leoben.at

[2] Polymer Competence Center Leoben GmbH, Roseggerstrasse 12, 8700 Leoben, Austria

[3] Erich Schmid Institute and Department of Material Physics, Jahnstrasse 12, 8700 Leoben, Austria

[4] Materials Center Leoben Forschung GmbH., Roseggerstrasse 12, 8700 Leoben, Austria

[5] Berliner Elektronenspeicherring-Gesellschaft für Synchrotronstrahlung m.b.H., Albert-Einstein-Straße 15, 12489 Berlin, Germany

[6] Institute of Plastics Processing, University of Leoben, Franz Josef Strasse 18, 8700 Leoben, Austria

Summary: The fracturing behavior of polymers and polymeric composites is of great interest in the scientific and application community. Especially in the case of silicate-layered nanocomposites the influence of fillers on the fracturing behavior is still fairly unclear. Fractures of semicrystalline polymers are accompanied by various processes of which shearing and cavitations are the most common ones. Nanocomposite deformation due to the delamination of fillers seems to be the most practical way leading to fractures with relatively low strains. With the method of scanning small angle X-ray scattering (SAXS) and wide angle X-ray diffraction (WAXD) it is possible to combine information on the structural details with the position on the sample, with the actual position resolution of the investigation being defined by the size of the X-ray beam used to scan the sample. By means of the application of synchrotron radiation it is nowadays possible to adjust the actual beam size to the dimensions of the region of interest, which is why it is an adequate tool for studying the deformation region near a crack tip.

In a native polypropylene sample, the fracturing process was accompanied by shear yielding as well as lamellae fragmentation and reorienting. In the highly deformed material near the crack tip fibrillated material could be found. However, in the polymeric nanocomposites (PNC) shearing, lamellae fragmentation, and fibrillation were hindered by the filler due to which the material did not have so much freedom to dissipate energy and fractures occurred much earlier. In this paper the comparison of a PNC and its native

polymer is to provide an overview of the different deformation mechanism and the structural details around the crack tip.
Keywords: crack tip; orientation; X-ray; synchrotron radiation; nanocomposites

Introduction

Polymeric nanocomposites, especially with the filler montmorrillonite, have become of predominant interest to the scientific and application community in the last years [1-4] as the fracturing behavior of polymeric nanocomposites and especially the changes caused by the presence of nanofillers are still rather unclear. For this reason in-situ synchrotron small and wide angle scattering techniques during tensile testing used to be employed to characterize fracturing processes under dynamical conditions [5-9]. Another possibility to study fracturing behavior of polymers and their nanocomposites by using synchrotron radiation is scanning around a loaded crack tip and thereby interpreting the texture [10-14]. With this method it is possible to determine the microstructural characteristics around defects and crack tips. Nanoclay fillers can be distributed in the polymer in three different ways: first there are agglomerates of the silicate platelets with overall dimensions in the µm range and no or less interactions between the polymer and the filler. The second state is the intercalated one, in which polymer chains are inclined between two silicate platelets. The interlayer distance increases, but the layers are still stacked. The third state is the exfoliated state with single platelets being randomly distributed in the polymer without any special correlation between each other [1].

There are different methods to produce polymer nanocomposites [2]. In this study melt compounding has been applied in order to produce intercalated silicate polypropylene nanocomposites since their intercalated structure is of special interest due to its melt compounding process. On the one hand it is always possible that in this process the degree of exfoliation can be less than a hundred percent and that some stacks of intercalated clay can be found in the composite. On the other hand the intercalated structure is a "natural" structure (e.g. bone [15-16]) and thus the desired one for (e.g. [17]) for various applications.

Experiment

Materials

The isotactic polypropylene (PP) homopolymer HC600TF (MFI 2.8 g/10 min; 230°C/2.16

kg) has been provided by Borealis Inc., Linz, Austria. As a nanofiller an organically modified montmorrillonite with the commercial indication Nanofil 5, provided by Süd-Chemie Inc., Munich, Germany, has been used. In order to combine the hydrophobic polymer and the hydrophilic nanofiller, a compatibilizer was needed. In this case, the maleinic anhydride acid grafted polypropylene Scona TPPP 2112 FA, provided by Kometra Ltd., Schkopau, Germany, has been chosen.

Sample preparation

For the compounding process, an intermeshing, co-rotating twin screw extruder Theyson TSK30/40D (Theyson Ltd., Vienna, Austria) with a string die was used. The feed rate was set at 20 kg/h with a screw speed of 150 rpm in the masterbatch sample. First a masterbatch with 20 wt. % nanofiller and 20 wt. % compatibilizer was produced which then was diluted with pure PP down to 5 wt. % nanoclay content. [18-19]

For the structural characterization around crack tips, samples had to prepared by carrying out the following steps: first the granulated materials were pressed to plates with a thickness of 1 mm using a hydraulic vacuum press machine (Collin 200 PV, Dr. Collin Ltd., Ebersberg, Germany). Then rectangular pieces (50 x 10 mm^2) were cut out of these plates. For the localization of the crack tip and the scanning regions the samples were equipped with a 1 mm deep notch. To do so, the same tool was used as for the production of the charpy test samples. This notch was made on both sides at the middle of the sample's length. In figure 1 the dimensions of a specimen are indicated.

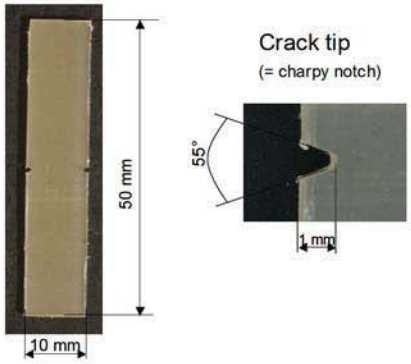

Figure1: Illustration of a double notched scanning specimen. On the right side the crack tip is illustrated.

Scanning SAXS/WAXS

The synchrotron experiments were performed by means of a µ-spot beam line at the BESSY (Berliner Elektronenspeicherring-Gesellschaft für Synchrotronstrahlung m.b.H., Berlin, Germany). This system was equipped with a two-dimensional X-ray detector (Mar Mosaique, Mar Research, Germany). The applied forces were created with the help of a computer controlled tensile testing apparatus (Anton Paar, Graz, Austria). The distance from the sample to the detector was 430 mm, and the wavelength for the experiments was 0.0827 nm. The samples were measured in transmission with the size of the last beam definition pinhole having a diameter of 30 µm. Thus, it was possible to measure small angle x-ray scattering (SAXS) and wide angle x-ray diffraction (WAXD) simultaneously.

Mechanical testing

Figure 2 shows a typical force displacement curve for the selected polypropylene. The samples were stressed with the maximal load, and the scanning experiment was started. The force lost during the scanning experiment due to creep was less than 10 %.

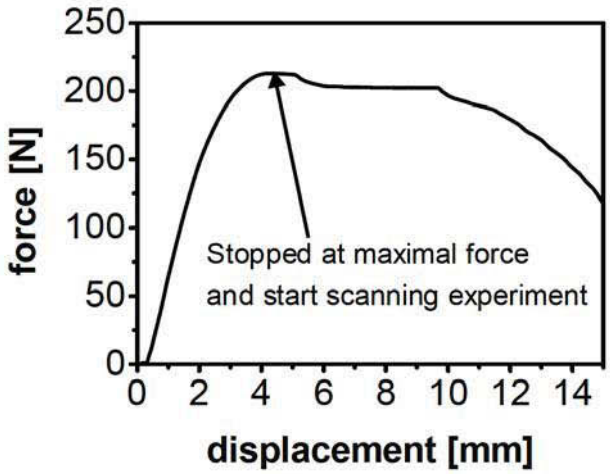

Figure 2: A typical force displacement curve of polypropylene. The scanning experiment was started at the maximum reached force at which the tensile test machine stopped as well.

Data evaluation

For the determination of the orientation (= texture) parameters, two-dimensional SAXS

data were averaged in azimuthal direction using the Fit2D software [20]. In order to evaluate the data, all scattering curves were corrected for background scatter. Figure 3 shows a typical diffraction pattern recorded near the crack tip. The exact determination of the orientation parameters, such as the direction of the orientation and its degree, of the diffraction pattern in figure 3 is illustrated in figure 4. The degree of orientation α was calculated by using equation 1, in which I_p and I_u represent the areas as defined in the diagram on the left in figure 4. The position of the peaks in the azimuthal intensity distribution (as shown in the diagram on the right side in figure 4) provided information on the direction of the orientation, and were located by fitting data with a Gaussian function. The WAXD signal, providing information on the crystallographic structure and texture, was only used to gather qualitative information on structural details.

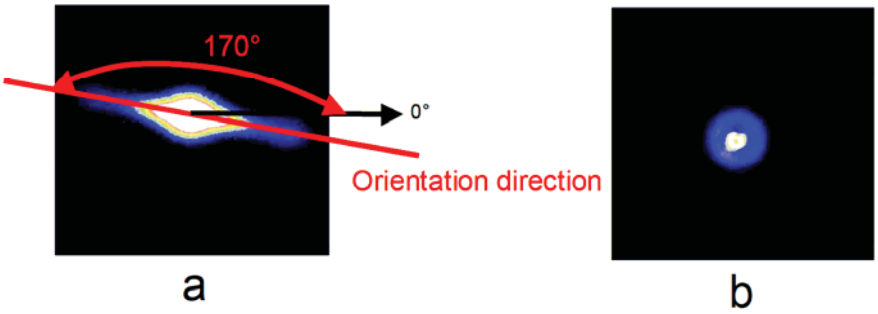

Figure 3: SAXS diffraction patterns of a high oriented (a) and an isotropic location (b).

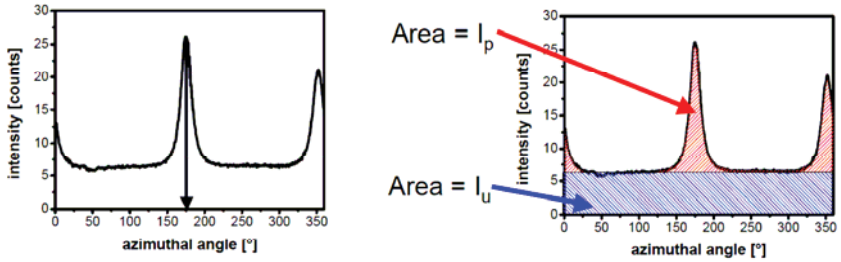

Figure 4: Determination of orientation parameters. The diagram on the left shows the determination of the orientation direction, while the diagram on the right illustrates the analysis of the degree of the orientation

$$\alpha = \frac{I_p}{I_p + I_u} * 100\% \qquad (1)$$

Results

For the X-ray scanning experiment special regions of interest were selected. The regions should be near the crack tip in order to find out more about the mechanism at work during the deformation process. The selected regions of interest are illustrated in figure 5.

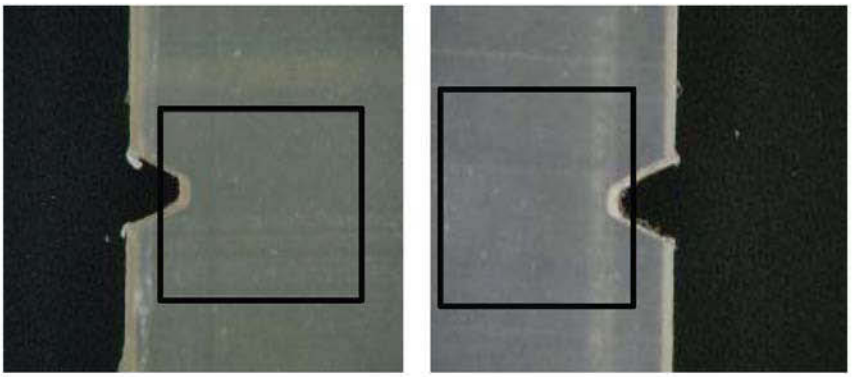

Figure 5: Regions of interest for the scanning experiment. On the left side the polymeric nanocomposite can be seen. In the picture on the right side the polypropylene is illustrated.

Figure 6 and 7 show two-dimensional SAXS and WAXS data. Every visible point or ring demonstrates a single measurement, which means that there are more than 900 diffraction patterns illustrated in each figure. The crack tip could be identified by the black zone in which there was no material. In these two figures the difference between polypropylene and its polymeric nanocomposite can already be recognized. For the quantification of the varieties in the deformation process the orientation parameters can be drawn on.

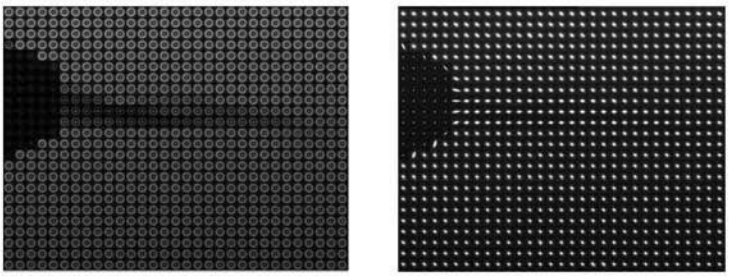

Figure 6: WAXS data (diagram on the left) and SAXS data (diagram on the right) for PNC.

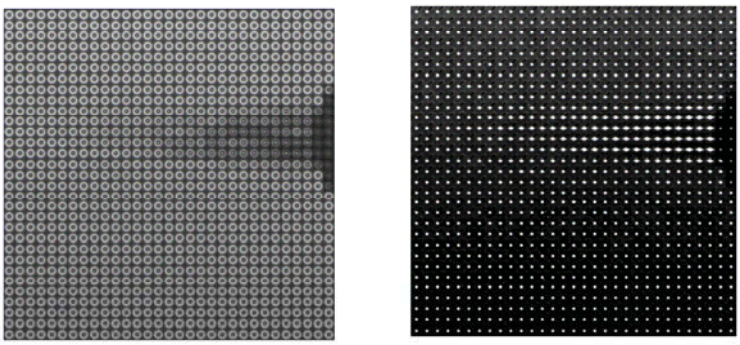

Figure 7: WAXS data (diagram on the left) and SAXS data (diagram on the right) for polypropylene.

Near the crack tips, regions with high oriented material could be found in both materials. In virgin polypropylene, microfibrils had been formed as indicated by fiber-like SAXS and WAXD pattern as shown in figure 8. The corresponding WAXS data from the same measuring point is illustrated on the left side in this figure. Next to the crack tip, the originally isotropic structure changed to a fiber-like structure, where the 110 plane was found to be orthogonal to the fibril direction. The left side in figure 9 illustrates two-dimensional WAXS data from the nanocomposite. Scattering experiments indicated that the changes in the texture were not as pronounced as in pure PP. The corresponding SAXS data pointed to the formation of microfibrils in the polymeric component. Stacks of intercalated clay has been reoriented in the same direction as the polymeric fibrils.

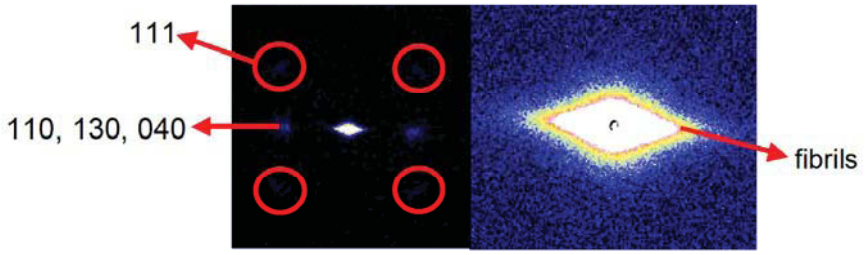

Figure 8: High oriented WAXS (on the left) and SAXS diffraction pattern of polypropylene.

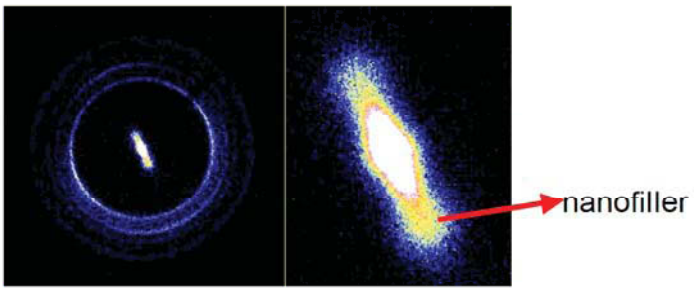

Figure 9: High oriented WAXS (on the left) and SAXS diffraction pattern of PNC.

The degree of orientation around the crack tip, as calculated on the basis of the SAXS data, is illustrated in figure 10. Figure 10a shows the polymeric nanocomposite, while in figure 10b the orientation of the virgin polypropylene can be seen. The main difference between these two materials could be determined in the characteristics of the oriented zone. In polymeric nanocomposites there was a very thin but high oriented region almost over the entire measuring region, while in virgin polymer a broader and shorter zone could be found.

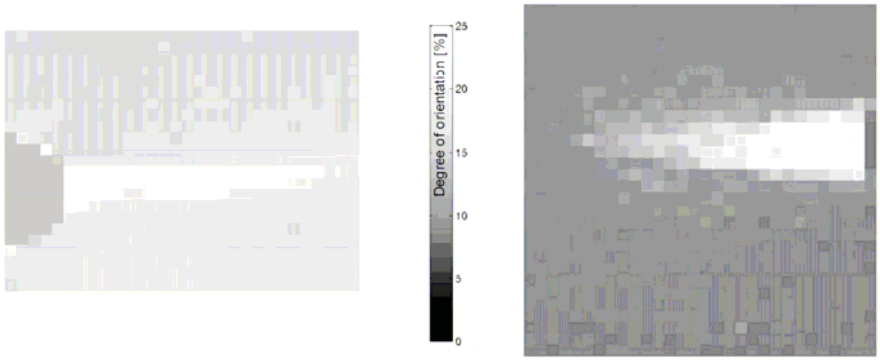

Figure 10: Degree of orientation. In figure 10a a scan of the polymeric nanocomposite is shown, and in figure 10b a scan of the polypropylene can be seen.

The direction of the microfibrils and of the stacks of intercalated clay around the crack tip are shown in figures 11a and b. It can be seen that the direction of the high oriented fibrils

changed around the tip. The intercalated filler likewise more or less followed the orientation of polymer which implies that stacks of filler rotated to follow the main shear stress direction equal to the polymer. This effect may have been caused by stress distribution around a defect. However, the same characteristics, yet more pronounced, were found in polypropylene as well.

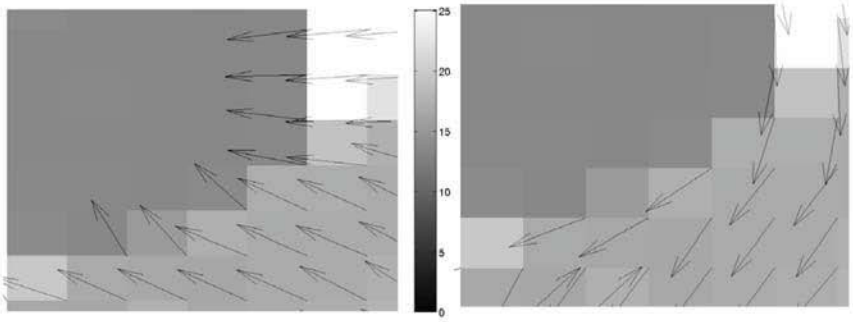

Figure 11: Direction of the stacked nanofiller (a) and the generated microfibrils (b) around the crack tip.

Discussion

Around the crack tips the originally isotropic material changed to an oriented, fiber-like structure. These fibrils follow the main shear stress directions in the polymer which is an effect that can especially be seen in the SAXS pattern. The orientation and the degree of the orientation of the microfibrils clearly indicate the effects in the material. In nanocomposites the stacked nanofiller is perpendicularly oriented to the microfibrils which indicates that stacks are arranged around the formed fibrils. Due to the high aspect ratio of the stacked nanoclay (10-20 layers per stack), the highest free surface of the stacks would be on the top (and the bottom) of the thereby formed cylinder. These stacks would be arranged in such a way that the free surface could interact with the free surface of the microfibrils.

In pure PP samples, the WAXD pattern also indicates the formation of a fiber-like orientation next to the crack tip. However, this phenomenon could not be observed in polymeric nanocomposites. Deformation processes are therefore different in PP and clay-PP composites. In pure PP shearing, lamellae rotation, and the complete reorientation of the crystalline lattice are possible, while the nanofiller reduces the freedom. As shear

bands, originating from highly deformed areas, could not develop, smaller plastic zones and stress concentration in nanocomposites were the result. This can be seen in figure 10, in which the orientation parameters of both types of samples are shown. Therefore, fractures occur at significantly lower strains compared to pure PP.

Conclusion

The fracture properties of polypropylene or its nanocomposite strongly depend on the degrees of freedom in the material to react to external forces. The formation of plastic zones, accompanied by a reorientation of the crystalline lattice, and of microfibrils can be imaged by scanning SAXS and WAXS. An orientation parameter to quantify the dimensions and the structure of plastic zones has been used. The pure polymer featured a very broad orientation zone allowing the material to yield. Therefore, the dominant material behavior was ductile. However, the nanocomposite has shown different formations of the high oriented region (= plastic zone). The rather thin, high oriented plastic zone with ran from one crack tip to the opposite ones. In contrast, no strong reorientation of the crystalline lattice has occurred in the PP sample as one of the main stress relaxation mechanisms of the polymer has been hindered by the filler. Since the stress concentrated in the polymer part of the composite, the plastic zone formed between the two notches and the material showed a dominant brittle material behavior.

Acknowledgments

The research work of this paper was performed within the Research Project Cluster NanoComp ("Performance Optimization of Polymer NanoComposites"), coordinated by the Polymer Competence Center Leoben GmbH. Funding by the Federal Ministry of Traffic, Innovation and Technology and the Austrian Research Promotion Agency within the AUSTRIAN NANO-Initiative is gratefully acknowledged. The help during the synchrotron experiments at the μ-spot beam line (BESSY, Berlin, Germany) by Dr. Ivo Zizak and Prof. Dr. Oskar Paris is highly appreciated. This work was supported by the European Community – Research Infrastructure Action under the FP6 "Structuring the European Research Area" Program (through the Integrated Infrastructure Initiative "Integrating Activity on Synchroton and Free Electron Laser Science" – Contract R II 3-CT-2004-506008).

[1] S. S. Ray and M. Okamoto, Prog. Polym. Sci. **2003**, 28, 1539.

[2] M. Alexandre and P. Dubois, Materials Science and Engineering **2000**, 28, 1.
[3] S. C. Tjong, Materials Science and Engineering R **2006**, 53, 73.
[4] S. Pavlidou, C. D. Papaspyrides, Progress in Polymer Science **2008**, 33, 1119–1198.
[5] N. Stribeck, U. Nöchel, S. S. Funari, T. Schubert, A. Timmann, Macromol. Chem. Phys. **2008**, 209, 1992–2002.
[6] M. C. Garcia Gutierrez, J. Karger-Kocsis, C. Riekel, Chemical Physics Letters **2004**, 398, 6–10.
[7] C. Lorenz-Haas, P. Müller-Buschbaum, T. Ittner, J. Kraus, B. Mahltig, S. Cunis, G. V. Krosigk, R. Gehrke, C. Creton and M. Stamm, Phys. Chem. Chem. Phys. **2003**, 5, 1235–1241.
[8] C. Lorenz-Haas, P. Müller-Buschbaum, O. Wunnicke, C. Cassignol, M. Burghammer, C. Riekel, M. Stamm, Langmuir **2003**, 19, 3056–3061.
[9] R. J. Davies, N. E. Zafeiropoulos, K. Schneider, S. V. Roth, M. Burghammer, C. Riekel, J. C. Kotek, M. Stamm, Colloid Polym Sci **2004**, 282, 854–866.
[10] G. A. Maier, G. Wallner, R. W. Lang, P. Fratzl, Macromolecules, **2005**, 38, 6099–6105.
[11] G. A. Maier, G. M. Wallner, R. W. Lang, J. Keckes, H. Amenitsch, P. Fratzl, J. Appl. Cryst. **2007**, 40, 564–567.
[12] N. E. Zafeiropoulos, R. J. Davies, S. V. Roth, M. Burghammer, K. Schneider, C. Riekel, M. Stamm, Macromol. Rapid Commun. **2005**, 26, 1547–1551.
[13] A. Boger, B. Heise, C. Troll, O. Marti, B. Rieger, European Polymer Journal **2007**, 43, 3573–3586.
[14] F. Heidelbach, C. Riekel, H.-R. Wenk, J. of Appl. Crys. **1999**, 32, 841–849.
[15] P. Fratzl, R. Weinkamer, Progress in Materials Science **2007**, 52, 1263–1334.
[16] P. Fratzl, H. S. Gupta, O. Paris, A. Valenta, P. Roschger, K. Klaushofer, Progr Colloid Polym Sci **2005**, 130, 33–39.
[17] P. Podsiadlo, A. K. Kaushik, E. M. Arruda, A. M. Waas, B. S. Shim, J. Xu, H. Nandivada, B. G. Pumplin, J. Lahann, A. Ramamoorthy, N. A. Kotov1, SCIENCE, 318, 80–83.
[18] S. Laske, M. Kracalik, M. Gschweitl, M. Feuchter, G. Maier, G. Pinter, R. Thomann, W. Friesenbichler, G. R. Langecker, Journal of Applied Polymer Science **2009**, 111, 2253–2259.
[19] S. Laske, M. Kracalik, M. Gschweitl, M. Feuchter, G. Maier, G. Pinter, R. Thomann, W. Friesenbichler, G. R. Langecker, Journal of Applied Polymer Science **2009**, in press.
[20] A. P. Hammersley, S. O. Svensson, M. Hanfland, A. N. Fitch, D. Hausermann, High Pressure Research 1996, 14, 235–248.

5.5 Paper 8

M. Feuchter, G. Maier, I. Zizak, M. Kracalik, S. Laske, G. Pinter

Analysation and application of crystalline elastic constants in polypropylene and its nanocomposite

Journal of Applied Polymer Science, *to be submitted*

Analysation and application of crystalline elastic constants in polypropylene and its nanocomposite

Michael Feuchter[1,2], Günther Maier[3,4], Ivo Zizak[5], Milan Kracalik[6], Stephan Laske[6], Gerald Pinter[1]

[1] *Chair of Materials Science and Testing of Polymers, University of Leoben, Franz-Josef Str. 18, 8700 Leoben, Austria*
e-mail: Michael.Feuchter@mu-leoben.at
[2] *Polymer Competence Center Leoben GmbH, Roseggerstrasse 12, 8700 Leoben, Austria*
[3] *Erich Schmid Institute and Department of Material Physics, Jahnstrasse 12, 8700 Leoben, Austria*
[4] *Materials Center Leoben Forschung GmbH., Roseggerstrasse 12, 8700 Leoben, Austria*
[5] *Berliner Elektronenspeicherring-Gesellschaft für Synchrotronstrahlung m.b.H., Germany*
[6] *Chair of Polymer Processing, University of Leoben, Franz-Josef Str. 18, 8700 Leoben, Austria*

Abstract

Fracture behavior of polymers and polymeric composites is of high interest in scientific community, especially in regard to industrial applications. Especially, stress levels in inaccessible locations are still rather difficult to analyse accurately. In the scope of this work, trials were conducted to correlate strains in crystallographic planes with the stress level of a sample. Therefore, a calibrated cuboid samples were necessary to determine x-ray specific elastic constants. To perform simultaneous SAXS/WAXD, scanning experiments with a beamsize of 30 µm the capabilities of µ-spot beamline at BESSY (BESSY, Berlin, Germany) were completed. Application measurements were performed on notched samples and the determined strains were combined with the elastic constants to calculate the stress levels in the difficult non-accessible sites. For comparison, x-ray measurements and – in order to determine the applied stress levels- an optical deformation analysis system were carried out as well.

Introduction

In polymer-layered silicate nanocomposites, the size of the crystalline layer in the polymer and the dimensions of the filler are similar. Montmorillonite is one a material, where the dimensions for usage range in the nanometer range. Organic modification of the silicate platelets to change nanoclay surface from hydrophilic to organophilic is necessary to strengthen the interaction between filler and polymer. Surface modification of the montmorillonite is mainly performed by ion exchange reactions with cationic surfactants like alkylammonium or alkyl phosphonium cations [1,2]. Several strategies for polymer-layered nanocomposites preparation have been developed in the past. These different processing routes are in situ polymerization, polymer intercalation from solution and melt intercalation. Basically three different interactions between the polymer and the layers are possible. The polymer and the filler have to run through these three stages in the melt compounding process route, which was employed for this work.
First, there are agglomerates of the silicate platelets, which exhibit dimensions in the µm range. There are no or very few interactions between polymer and filler existing. The second stage is the intercalation, where polymer chains are inclined between two silicate platelets. Interlayer distance expands, but the layers are still stacked. The third stage is the exfoliation, where single platelets are randomly distributed in the polymer. These single platelets posses no special correlation between each other [3].
In-situ synchrotron small angle x-ray scattering (SAXS) and wide angle X-ray diffraction (WAXD) combinations are primarily used to investigate structure property relations in various materials, for example in polymers e.g. [4,5] and biological composites e.g. [6].

Determination of an x-ray specific elastic constant has been widely studied in metals, ceramics and polymers e.g. [7]. In this manner it has found widespread utilization to analyze the internal stress of the materials.[8]
In this paper, intercalated polypropylene nanocomposites will be examined due to the rather interesting relationship between their structural properties. Moreover, the intercalated structure is the first step in achieving the exfoliation stage by means of melt intercalation. The main objective of this paper is to investigate a method to detect stress levels in crystallographic planes in polypropylene and its layered silicate nanocomposite.

Experiment

Materials

The isotactic polypropylene (PP) homopolymer HC600TF (MFI 2.8 g/10 min; 230°C/2.16 kg) was provided by Borealis Inc., Linz, Austria. As a nano-filler an organically modified montmorrillonite with the commercial indication Nanofil 5, provided by Süd-Chemie Inc., Munich, Germany, was selected. In order to combine the hydrophobic polymer and the hydrophilic nanofiller, a compatibilizer was required. Therefore, the maleinic anhydride acid grafted polypropylene Scona TPPP 2112 FA, provided by Kometra Ltd., Schkopau, Germany, was used.

Sample preparation

Preparation of nanocomposites

For the compounding process, an intermeshing, co-rotating twin-screw extruder Theyson TSK30/40D (Theyson Ltd., Vienna, Austria) with a string die was used. The feed rate was set at 20 kg/h, with a screw speed of 150 rpm for the masterbatch sample. First, a masterbatch with 20 wt. % nanofiller and 20 wt. % compatibilizer was produced. This was diluted with pure PP down to 5 wt. % nanoclay content. To get a better distribution of the nanoclay, this dilution process was performed with varying rotation speeds by the twin-screw extruder. Only samples, which were produced at a screw speed of 150 rpm (G3-150), were selected for the determination of the elastic constants.

Tensile test specimen preparation

For structural characterization during tensile testing, plates with a thickness of 1 mm were prepared using the hydraulic vacuum press machine (Collin 200 PV, Dr.Collin ltd., Ebersberg, Germany). Rectangular samples (50x10 mm2) for tensile testing were extracted out of these plates. These samples served to ascertain the elastic constants. For improved localization of the macroscopic crack pass, some of the rectangular samples were modified with a 1 mm deep crack, located at both sides on the middle of the sample length. These notched samples were used for the application measurements.

Sample analysis

The synchotron experiments were performed at μ-spot beamline at BESSY (Berliner Elektronenspeicherring-Gesellschaft für Synchrotronstrahlung m.b.H., Berlin, Germany). This system was equipped with a two dimensional X-ray detector (Mar Mosaique, Mar Research, Germany). In situ tensile tests were realized with a computer controlled tensile testing apparatus (Anton Paar, Graz, Austria). A sample detector distance of 430 mm and a wavelength of 0.0827 nm were used for the experiments. The samples were measured in transmission during a tensile test and the size of the last beam definition pinhole had a diameter of 30 μm. Thereby, it was possibly to measure small angle x-ray scattering (SAXS) and wide angle x-ray diffraction during one in-situ tensile test experiment.
For the determination of morphological parameters, diffraction patterns $I(q,\psi)$ were averaged in arcs using Fit2D software. [9] The drawing direction was defined as $\psi = 0$, where ψ denotes the azimuth angle. The modulus of the scattering vector q is defined as $q = (4\pi*\sin\theta)/\lambda$, where λ is the wavelength of the used radiation and θ is half of the scattering

angle 2θ. For data evaluation, all scattering curves were aligned to compensate for background scatter.

Data evaluation

Small angle x-ray scattering

To certify the long period of the polymer and gallery period of the layered silicate platelets, scattering curves I(q) were multiplied by q^2 (the so-called "Lorenz correction"). The long period can be understood as the sum of the thicknesses of the amorphous interlayer and of the lamellae crystal. The gallery peak arises from the regular arrangement of clay platelets, and the size, derived from the position of the peak, is the sum of the thicknesses of one clay platelet (0.95nm) and of the polymeric interlayer. The estimation of the peak positions was conducted by implementing the Pseudo Voigt function. [10]

Wide Angle X-ray Diffraction

The Crystal structure and lattice parameters were determined via wide-angle x-ray diffraction pattern; scattering curves were aligned to comply for background scatter. Lattice spacing was calculated by using Bragg's law. Positions of peaks were again established via the usage of the Pseudo-Voigt function.

The calculation of the micro strain was done with Equation 1, where d_0 is the mean value of the first 3 lattice spacing (long period, interlayer distance) values and d is the concrete lattice spacing (long period, interlayer distance).

$$\varepsilon_{Micro} = \frac{d - d_0}{d_0} * 100\% \quad (1)$$

Tensile tests

In-situ tensile testing experiments were performed using a tensile testing machine, where the testing velocity was set to 0.1 and 1 mm/min, which indicates a strain rate of 0.45 and 4.5 %/min.

A full-field strain analysis system based on digital image correlation was used for the determination of the exact, applied elongation in longitudinal and transverse direction. Evaluation of the strains was carried out with ARAMIS 3D, an optical deformation analysis system developed by GOM (Gesellschaft für optische Messtechnik mbH; Braunschweig, D). [11] Calculation of applied strain was accomplished by using Equation 2, where l_0 is the start length and Δl is the change of way during a tensile test. For the application measurements, the region for strain measurement was chosen between the two prepared cracks and in order to allocate the elastic constants, the region in the middle of the samples were used for examining the strains.

$$\varepsilon_{applied} = \frac{\Delta l}{l_0} * 100\% \quad (2)$$

The applied stress was calculated by using Equation 3, where F is the applied force (signal from the tensile testing machine) and A is the smallest cross sectional area of the sample before starting the tensile tests.

$$\sigma_{applied} = \frac{F}{A} \quad (3)$$

Determination of elastic constants and Poisson's ratio

The resulting applied stress from the tensile testing machine was plotted against the micro strains for every crystallographic plane, the long period of the polymer and gallery period of the layered silicate platelet. For the assessment of the elastic constants, a linear fit between 0.05 and 0.25 % micro strain was created in applied stress over micro strain diagram. The slope of this linear fit can be understood as constant for the elastic deformation process. [12]

The materials further showed a lateral contraction, perpendicular to the drawing direction. A Poisson's ratio ν can be defined by using Equation 4, where ε_{trans} is the microscopic strain perpendicular to the drawing direction (ψ=90°) and ε_{axial} is the microscopic strain in the drawing direction (ψ=0°). The region from 0.05 to 0.25 % micro strain would be utilized for the determination of the Poisson's ratio.

$$\nu = -\frac{\varepsilon_{trans}}{\varepsilon_{axial}} \tag{4}$$

Application of elastic constants

With the aid of elastic constants it should be possible to determine microscopic stress in an otherwise inaccessible regions. Therefore x-ray measurements of the high stress region were performed on notched samples. The observed micro strain was multiplied with the elastic constants for every crystallographic plane, to calculate the micro stress.

Results

Figure 1 shows a typical diffraction pattern of a non-deformed polypropylene nanocomposite. The small window in the left upper corner represents the Lorenz-corrected small angle x-ray scattering data. In this region, the diffraction angle region is 0 to 2.5 deg 2Θ For the large graph, whereas WAXD is presented, the diffraction angle region is set from 2.5 to 13 deg 2Θ. The miller indeces from polymer were taken from literature [13].

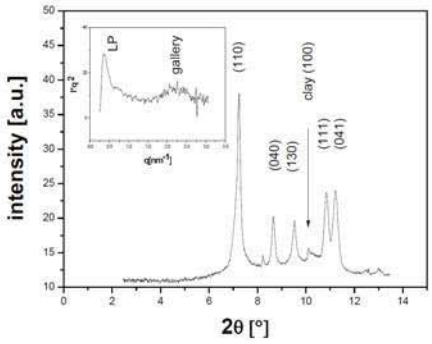

Figure 1 Representative WAXD (large graph) and SAXS (small graph) scattering curves for intercalated polypropylene nanocomposite.

Macroscopic data

Estimation of macroscopic data was performed by using a full-field strain analysis system. Table 1 represents the results of the macroscopic stress-strain analysis for both tensile test velocities.

Table 1 Macroscopic data for PP and G3-150

Sample	Tensile Test Speed 1.0 mm/min		Tensile Test Speed 0.1 mm/min	
	Young's Modulus [MPa]	Poisson's ratio	Young's Modulus [MPa]	Poisson's ratio
PP	1100	0.49	1250	0.43
G3-150	1890	0.38	1440	0.36

Determination of elastic constant

The left diagrams in Figure 2 show the correlation between micro strain and applied strain for the crystallographic planes (110), (040) and (041) of PP (top left diagram) and G3-150 (central picture on the left side). Additionally, the results from the SAXS measurements like long period and gallery height are also plotted in Figure 2. The correlation of micro strain and applied stress is illustrated on the right side of this chart as well. According to literature, there is a linear relation of a positive slope of applied stress to micro strain at crystallographic planes, however the results from SAXS measurements exhibited no or very little linear relation in the strain-stress curves. Nevertheless, the polymeric nanocomposite possessed a higher stress-strain slope than the virgin polymer, which was resulting in a higher elastic constant. Every crystallographic plane had a different slope in the stress-strain diagrams, leading to different elastic constants.

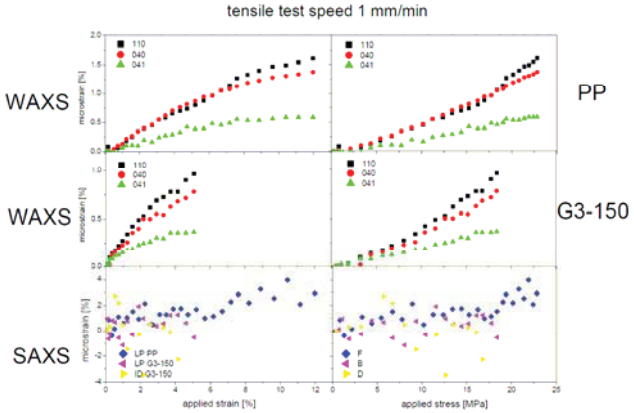

Figure 2 Micro strain plotted against applied strain and applied stress for tensile test speed of 1 mm/min for the polypropylene and its intercalated nanocomposite.

Figure 3 presents the same diagrams as Figure 2, the difference being the tensile test velocity. While Figure 2 displays the results of the faster tensile tests with a speed of 1 mm/min are pictured, Figure 3 contains the results from the tests performed with a velocity of 0.1 mm/min. The lower speed test includes more data points , due to increased measuring time allotted to the in-situ tensile test experiments.

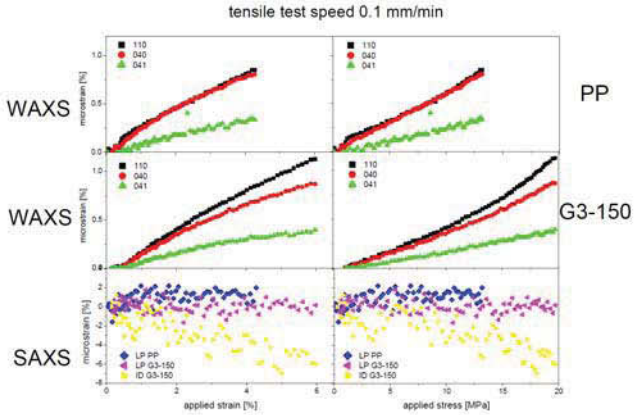

Figure 3 Micro strain plotted against applied strain and applied stress for tensile test speed of 1 mm/min for the polypropylene and its intercalated nanocomposite.

The slopes of the applied stress-micro strain curves in the region of interest (from 0.05 to 0.25 % strain) were the same during the fast and the slow experiments, therefore the elastic constants were the same too. This fact is visible in Figure 4, where the elastic constants for every crystallographic planes are illustrated. The mean value of three measurements and their standard deviation are pictured in this diagram and it's shown that the constants are nearly independent from the tensile test velocity.

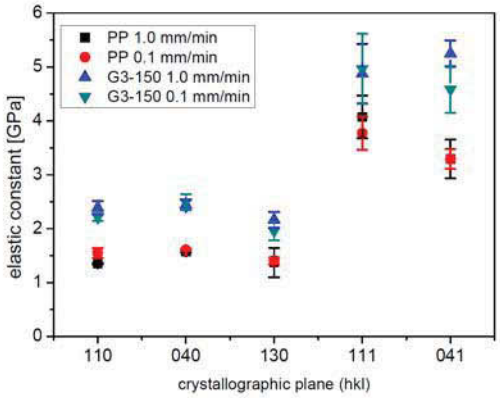

Figure 4 Elastic constants parallel to drawing direction (ψ=0°) for polypropylene and its nanocomposite.

The summarized results are listed in Table 2 and 3. The crystallographic planes (111) and (041), which possessed a l-component, showed higher amounts elastic constants than the other ones. Furthermore, Poisson's ratio was higher for these crystallographic planes.

Table 2 Results of elastic constants and the x-ray specific Poisson's ratio for tensile test velocity of 1.0 mm/min

Crystallographic Plane	G3-150	G3-150 ν	PP	PP ν
110	2390	0.30	1351	0.35
040	2437	0.29	1575	0.21
130	2163	0.42	1373	0.34
111	4876	0.29	4075	0.55
041	5246	0.28	3294	0.29

Table 3 Results of elastic constants and the x-ray specific Poisson's ratio for tensile test velocity of 0.1 mm/min

Crystallographic Plane	G3-150	G3-150 ν	PP	PP ν
110	2219	0.32	1550	0.34
040	2492	0.29	1605	0.26
130	1961	0.36	1406	0.34
111	4965	0.24	3774	0.51
041	4583	0.27	3291	0.41

Application of elastic constants

Elastic constants were estimated on notched samples. It is suggested that the same elastic constant is used for the crystallographic planes. In Figure 5, applied strain is plotted against micro stress at different tensile test speeds. To compare these curves with macroscopic properties, the applied stress is shown as well.

The applied stress-applied strain curves of the initial PP (illustrated in the lower two diagrams in Figure 5) exhibit stress-strain curves typical for engineering purposes. The maximum reached stress was at 35 MPa for the faster experiment, while 28 MPa represented the maximum level reached for the slower experiments. Nearly the same variation occurred for polymeric nanocomposite.

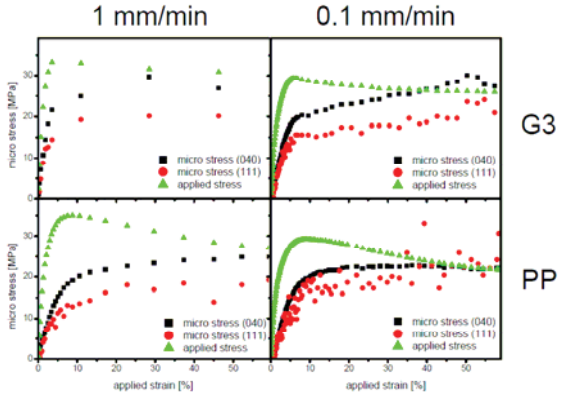

Figure 5 Estimated micro stress and applied stress for PP and G3. Left diagrams present the results for tensile test velocity of 1 millimetre per minute and the right ones for 0.1 mm/min.

The micro stress, acting in crystallographic planes (040) and (111) at PP as illustrated here, reached a plateau at higher strain levels. The maximum stress level will be attained at double the applied strain rate than normal for the applied stress curve. Polymeric nanocomposite demonstrate a rather different behaviour than the original polymer. Alterations in the slopes of the stress-strain curves were nearly at the same strain levels. The curves present a second

linear increase in the higher strain regions and at 50 % applied strain a decrease at the slower measurements. This decrease seems to exist conjointly for the faster experiment at 30 % applied strain rate.

Discussion

Comparison of the elastic constants determined by x-ray scattering and the macroscopic properties showed, that the crystallographic planes presented higher values than the whole (macroscopic Young's Modulus) material. The polypropylene and the polymeric nanocomposite possessed a degree of crystallinity of approximately 50 %. Moreover, the amorphous content of the material could absorb only little forces at the beginning of a tensile experiment; hence, the crystalline regions of the materials have to be stiffer to achieve the macroscopic Young's Modulus.

The crystallographic planes with a l-component reveal higher elastic constants. The explanation of this phenomenon is the crystallographic arrangement of the polymeric crystal. Polypropylene folded chains build up the crystal structure [14]. Furthermore, the l-direction seemed to be the direction along the chains and therefore the elastic constants were higher. Perpendicular to the chain-direction only weak secondary bonds existed, which ceased earlier than the covalent C-C bonds along the chain.

Long period of polymer and interlayer distance of the silicate platelets presented no or little microscopic strain in the linear elastic region. Therefore it could not be established whether there were any elastic constants for these two quantities. However, both showed a high micro strain due to increased applied strain. [15] It was further evident that for the linear elastic region, the determined elastic constants were equal for the fast and the slow experiment. Therefore the measured x-ray-specific properties were seen as a constant under these two measuring conditions.

The application of the elastic constants for the notched samples assumes that the elastic constants are accountable for the whole area. This work suggests that, if there were no lamellar fragmentation and rearrangement in the crystallographic planes, the discussed approach would be rather effective in industrial implementation.

The micro stress and the applied stress present the same curve progression: a linear increase at the beginning, a distinct stress maximum and a slightly decrease (or increase) at the end of the tensile test. Due to more time for relaxation at lower tensile test rates, there were higher maximal stress levels during the faster experiment in comparison. The second linear increase in the higher strain regions for polymeric nanocomposite seemed to be induced from the interference from the filler. After the ensuing decrease, delamination of filler and polymer occurred and finally the sample broke. The initial polypropylene showed rearrangement of crystallography planes and lamellar fragmentation at higher applied strain levels (>60 %), therefore the curves were cut off at increased strains levels.

Conclusion

The analysation and application of elastic constants would work in polymeric materials like initial polypropylene and layered silicate nanocomposites. Using the presented approach, it was possible to determine the stress levels in inaccessible sites, one of them the inside of an indentation.

Acknowledgements

The research work of this paper was performed within the Research Project Cluster NanoComp ("Performance Optimization of Polymer NanoComposites"), coordinated by the Polymer Competence Center Leoben GmbH. Funding by the Federal Ministry of Traffic, Innovation and Technology and the Austrian Research Promotion Agency within the AUSTRIAN NANO-Initiative is gratefully acknowledged. The help during synchrotron experiments at y-spot beamline (BESSY, Berlin, Germany) by Dr. Ivo Zizak and Prof. Dr.

Oskar Paris is grateful acknowledged. This work was supported by the European Community - Research Infrastructure Action under the FP6 "Structuring the European Research Area" Programme (through the Integrated Infrastructure Initiative" Integrating Activity on Synchroton and Free Electron Laser Science - Contract R II 3-CT-2004-506008).

References

[1] Ray S S and Okamoto M 2003 Prog. Polym. Sci **28** 1539-1641.
[2] Alexandre M and Dubois P 2000 Materials Science and Engineering **28**, 1-63.
[3] Pavlidou S and Papaspyrides C D 2008 Progress in Polymer Science **33** 1119–1198.
[4] Varga J 2002 Journal of Macromolecular Science - Physics **41** 1131-1171.
[5] Utracki L A 2004 Clay-Containing polymeric nanocomposites, Rapra Technology Limited,.
[6] Fratzl P, Gupta H S, Paris O, Valenta A, Roschger P and Klaushofer K 2005 Progress in Colloid and Polymer Science **130** 33-39.
[7] Nielsen O H and Martin R M 1985 Physical Review B **32** 3792-3805.
[8] Kirchlechner C, Martinschitz K J, Daniel R, Klaus M, Genzel C, Mitterer C and Keckes J 2010 Thin Film Solids **518** 2090-2096.
[9] Hammersley A P, Svensson S O, Hanfland M, Fitch A N and Hausermann D 1996 High Pressure Research **14** 235–248.
[10] Balta-Calleja F J and Vonk C G, 1989 X-ray scattering of synthetic polymers, Elsevier.
[11] Jerabek M, Major Z and Lang 2010 R W Polymer Testing **29** 407-416.
[12] Tscharnuter D, Jerabek M, Major Z and Lang R W 2011 Mechanics of Time-Dependent Materials, **15**, 15-28.
[13] Lezak E and Bartczak Z 2005 Fibres & Textile in eastern Europe **13** 51-56.
[14] Karger-Kocsics J 1995 Polypropylene - Structure, blends and composites, Chapmann & Hall, London.
[15] Feuchter M, Maier G, Pinter G, Kracalik M, Laske S and Langecker G R 2008 Materials Research Society Symposium Proceedings **1146** 183-190.

6 Macromechanics of clay polypropylene nanocomposites

Correlation of macroscopic properties with the structural details of a material is a great objective for a research work. This chapter intends to connect the topics of structural parameters of clay-containing polypropylene nanocomposites to micro- and macro-mechanical properties. This is accomplished by structural investigations (X-ray scattering techniques) on the one hand, and by mechanical investigations (thermomechanical, tensile and puncture tests) on the other hand. The structural results (degree of exfoliation) are correlated with thermomechanical (mobility of polymer chains) and macro-mechanical (stiffness) results. In the case of a macro-mechanical test, there is a further distinction between slow (tensile tests) and fast (puncture tests) kind of stressing.

6.1 Major results

Paper 9 investigates the structural parameters as well as the micro- and macro-mechanical properties and establishes correlations between structural and mechanical properties. It illustrates that the degree of exfoliation depends on the process conditions (inserted shear energy) during the production route melt compounding. Another highlight is how the exfoliation process works, being a result of the mentioned production process. The exfoliation mechanism functions via the destruction of individual silicate stacks, without primarily forming intercalated stacks. This is shown with two different types of polypropylene and thereby proving that tuneable nanocomposites can be produced via a semi-industrial process route. The mobility of the polypropylene alters according to the arrangement of the clay. This results in a shifting of glass transition (represents the mobility of the amorphous content) and α-relaxation (represents the mobility of the crystalline content) temperatures. The higher the degree of exfoliation, the more the mobility of the polymer chains was hindered, causing both temperatures to rise. Furthermore, macroscopic mechanical properties were determined by puncture and tensile tests. In the presence of intercalated stacks, the stiffness of the composite increases, while the elongation at break decreases. This happens as the stiffly layered package act as strengtheners on the one side, while still operating as a defect. Thus, the degree of exfoliation influences the mechanical properties. Highly intercalated clay polypropylene nanocomposites exhibit a high stiffness and a low elongation at break; however, for

composites with a high degree of exfoliation, the mechanical properties exhibit a lower stiffness and a higher strain at break.

6.2 Paper 9

M. Feuchter, G. Pinter, G. Maier, A. Witschnigg, M. Kracalik, S. Laske

Investigations on molecular mobility in melt intercalated polypropylene-silicate nanocomposites and the effects on mechanical properties

Journal of Applied Polymer Science, *submitted*

Investigations concerning molecular mobility in melt intercalated polypropylene-silicate nanocomposites and the effects on mechanical properties

Michael Feuchter[1,2], Gerald Pinter[1], Günther Maier[3,4], Andreas Witschnigg[5], Milan Kracalik[5], Stephan Laske[5]

[1] *Chair of Materials Science and Testing of Polymers, University of Leoben, Franz-Josef Str. 18, 8700 Leoben, Austria*
e-mail: Michael.Feuchter@mu-leoben.at
[2] *Polymer Competence Center Leoben GmbH, Roseggerstrasse 12, 8700 Leoben, Austria*
[3] *Erich Schmid Institute and Department of Material Physics, Jahnstrasse 12, 8700 Leoben, Austria*
[4] *Materials Center Leoben Forschung GmbH., Roseggerstrasse 12, 8700 Leoben, Austria*
[5] *Chair of Polymer Processing, University of Leoben, Franz-Josef Str. 18, 8700 Leoben, Austria*

Abstract

The relationships of polymeric nanocomposites regarding structural properties, especially those in combination with the filler montmorrillonite, have become of interest to the scientific community in the recent years. In this work, structural properties of a silicate layered reinforced polypropylene and the influence of the well characterized morphological structure on mechanical and thermomechanical properties are presented. For characterization of the morphological structure, small angle x-ray scattering was used. Mechanical properties were determined via a standard tensile test, an instrumented impact test and thermomechanical tests. Varying quantities of applied shear energy concluded in various structural details. The produced structures of the polymeric nanocomposites (PNC) altered the mobility of the polymer chains and thus the mechanical properties. Abiding to this procedure allowed to allocate important structure-property relationships. Furthermore it was proven that the production of PNC - via route melt intercalation – can be induced for two different polypropylenes on a semi-industrial scale.

Introduction

Organic-inorganic nanometer composites are demanding increasing amounts of interest among the scientific community and industry in the last years. Especially structural details and their relationship to the mechanical, rheological, optical and permeation properties of the nanocomposites are of outermost importance [1]. The most commonly used filler is the smectite clay mineral montmorrillonite, generally ranging in nanometric dimensions. Organic modification of the silicate platelets to change the nanoclay surface from hydrophilic to organophilic is necessary to strengthen interaction between filler and polymer. Surface modification of montmorrillonite is mainly performed by ion exchange reactions with cationic surfactants like alkylammonium or alkyl phosphonium cations [2]. Several strategies for a most efficient preparation of polymer-layered nanocomposites have been developed in the past. These different processing routes are in situ polymerization, polymer intercalation from solution and melt intercalation [2 - 4]. Basically, three different interactions between the polymer and the layers are possible. The polymer and the filler have to run through these three stages in the melt intercalation process route, which is used in this work [2, 4].
First, there are agglomerates of the silicate platelets, ranging in micrometers. There are no or few interactions between polymer and filler existing. The second state is the intercalated one, where polymer chains are inclined between two silicate platelets. Interlayer distance increases, but the layers are still stacked. The third state is the exfoliated state, where single platelets are randomly distributed in the polymer. These single platelets posses no interactions between each other [5, 6]. Commonly, a

certain amount of tactoids (silicate agglomerates) persists in polymer nanocomposites, prepared by melt mixing [1, 2].
In this work the production route melt intercalation will be applied to commercial organic modified montmorrillonite and polypropylene (PP). Further experiments aim to discern a correlation between structural details and mechanical properties of layered silicate reinforced polypropylene.

Experiment

Materials and sample preparation

As polymer matrices, a polypropylene with a melt mass flow rate of $MFR_{230°C,\ 2.16\ kg}$ = 2.8 g/10 min (PP1) and a pipe grade polypropylene (PP2) with a lower MFR ($MFR_{230°C,\ 2.16\ kg}$ = 0.3 g/10 min) were used; both materials were provided by Borealis Inc., Linz, Austria. The commercial nanofiller, a layered silicate intercalated with dimethyl distearyl ammonium chloride with the indication Nanofil 5 provided by Süd-Chemie Inc., Munich, Germany was used. For the combination of the hydrophobic polymer and the hydrophilic nanofiller, a compatibilizer was needed. Therefore a PP, grafted with maleic acid anhydride (PP–MA, Scona TPPP 2112 FA, Kometra/D, Schkopan, Germany), was used.
For the compounding process, an intermeshing co-rotating twin screw extruder (Theysohn TSK30/40D, Korneuburg, Austria) with a string die was utilized. First, a masterbatch with 20 wt. % nanofiller and 20 wt. % compatibilizer was produced. This masterbatch was diluted with pure PP down to 5 wt. % nanoclay content and the feed rate was set at 20 kg/h [7, 8]. The inserted shear energy may influence the dilution process of the silicate stacks, hence the screw speed was varied between 100 and 300 rotations per minute (rpm).
The produced mixtures were named PP1-XXX or PP2-XXX, where XXX represents the rotation speed of the twin screw extruder. For the structural and thermomechanical characterization, plates with a thickness of 1 mm were prepared by means of a hydraulic vacuum press machine (Collin 200 PV, Dr. Collin Ltd., Ebersberg, Germany). The impact penetration test was carried out on plates with a thickness of 4 mm, which were prepared by using the above mentioned press machine. The tensile tests were carried out on injection-moulded multi-purpose test specimens.

Sample analysis and data evaluation

Small angle x-ray scattering (SAXS) measurements were performed using a Bruker NanoStar (Bruker AXS, Karlsruhe, Germany). Angles ranging from 0.05 to 3.5 ° were required for the characterization of the structural properties. To reach those scattering angles, a wavelength of 0.154 nm (CuKα) and a sample to detector distance of 108 cm was adjusted. The system was equipped with a two dimensional x-ray detector. To determine the long period of the polymer and the interlayer distance of the layered silicate platelets, scattering curves were corrected by elimination of background scattering. The Lorenz correction was performed by multiplying the scattered intensity I(q) by q^2 (q being the magnitude of the scattering vector) [9]. The determination of the peak position and the peak profile was done via concurrence to the Pseudo-Voigt function [9]. As results of this matching process, the peaks - one for the polymer and one for the silicate layers - could be described through the position, the width and the area of the peak.
A universal tensile testing machine (Type: Z010, Zwick Ltd and Co. KG, Ulm, Germany) was used to carry out the tensile tests according to ISO 527-1. All tests were carried out under standardised conditions (23 °C and 50 r.H.). The data was evaluated by using the testXpert II software (ZWICK, Ulm, Germany). The tensile tests were performed using standardised test specimens and were carried out 10 times for each mixture to get a significant average value. The test velocity for measuring the Young's Modulus was set to 1 millimeter per minute; however the determination of the tensile strength and the strain at break, the test speed was increased to 50 millimeters per minute.
A droptower impact system (type: Instron CEAST 9350, Ceast Spa, Turin, Italy) was used to perform the instrumented impact penetration tests according to ISO 6603-2. All tests were carried out at a temperature of -10 °C. The impact tests were performed using 4 mm thick pressed plates (60x60 mm2) and carried out 8 times for each mixture to achieve an average value. The test velocity was set to 4.43 meter per second and the impact test weight was set to 15.045 kilogram to get a legal puncture. For interpretation of the results, some new definitions had to be appropriated. A distortion ratio was defined as a ratio between the deformation at maximum force and the deformation at half of the maximum force (see also Equation 1). This definition could give information about the failure

mechanism (ductile or brittle) and is helpful for discussing the force-deformation curves. The slope at the beginning of the force-deformation curves could be interpreted as stiffness of the material. The slopes were determined by linear regression of the force-deformation curves in the deformation range from 0 to 1 mm deformation. For comparison of the different mixtures it was necessary to reduce the results on sample thickness (see Equation 2). The mentioned procedure can be seen in Figure 1.

$$\text{distortion ratio} = \frac{\text{distortion at } F_{max}}{\text{distortion at } \frac{F_{max}}{2}} = \frac{d_1}{d_2} \qquad \text{(equation 1)}$$

$$\text{normalised stiffness} = \frac{\text{slope at the beginning}}{\text{sample thickness}} \qquad \text{(equation 2)}$$

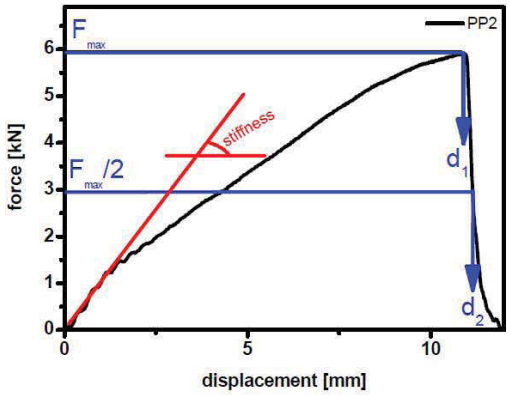

Figure 1: Determination and definitions of the instrumented puncture test.

To characterize the thermomechanical properties dynamic-mechanical analysis in tensile mode was performed by using a DMA 861e (Mettler Toledo, Schwerzenbach, Switzerland). The samples were applied with a sinusoidal load with a strain amplitude of 15 µm and a force amplitude of 15 N, an offset of 110 % and a frequency of 1 Hz. The scans were run at a temperature range from –30 to 160 °C, the heating rate was set to 2 K/min. Deducing from these measurements, storage modulus (E'), loss modulus (E'') and loss factor (tan δ) curves were generated as a function of sample temperature. The glass transition temperature was detected by determining the maximum loss factor tan δ [10]. The determination of the midpoint temperature of the α-relaxation was done by constructing three tangents: one before (tangent 1), one after (tangent 2) and one intersecting both tangent 1 and 2 (tangent 3). The midpoint between the two intersection points was defined as the desired temperature [10]. The procedure is pictured in Figure 2. The mentioned temperatures represent the mobility of the polymer chains. The glass transition temperature indicates the mobility of the amorphous content and the α-relaxation is characterized by the crystalline content of the semi-crystalline PP.

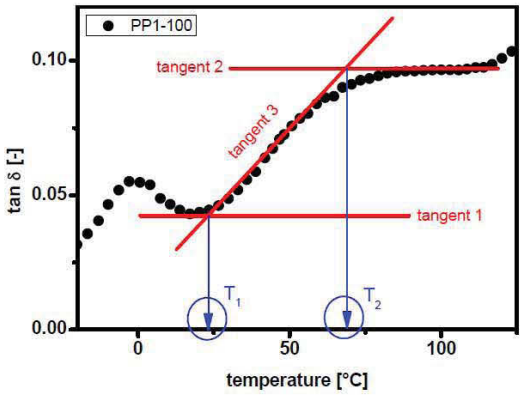

Figure 2: Definition and determination of the midpoint temperature of the α-relaxation.

Results and Discussion

The peak position of the silicate stacks delivers information in regard to the mean interlayer distance, which is defined as the distance between two single platelets plus the thickness of one layer. Additionally, the stack size could be evaluated via the usage of the Scherrer equation [11]. In this equation, the stack size is a function of the peak width. Finally, the peak area represents the quantity of scattering elements inside the scattered volume - the more elements, which are able to scatter, the higher the peak area [12, 13].

The small angle x-ray scattering curves are illustrated as a function of screw speed in figure 3 (for the formulations with PP1), which shows two different peaks. The long period scattering peak - which can be observed in the low q-region (approximately at 0.05 A^{-1}) - represents the lamellar structure of the polymer. The peak, representing the silicate layered stacks, can be found at higher q-values (approximately at 0.22 A^{-1}). Moreover, it's possible to demonstrate that the peak positions were nearly the same for all mixtures. Therefore no alterations in interlayer distance (and long period) were observed for the various mixtures. However, the peak position slightly changed, compared to the virgin filler, therefore the stacks were intercalated. Furthermore the peak width remained unaffected by the process.

In the case of layered silicate reinforced polymer, the knowledge that the structure of the PNC is the intercalated one, and peak position and width persist aid to interpret the height of the peak area as the quantity of agglomerates, thus as a consequence of the degree of exfoliation. However, the peak area changed for the different mixtures, while at PP1-100, a high peak area was observed. The area decreased with increasing screw speed, and in the case of decreasing area, the number of layered stacks is decreasing as well. The explanation for these effects could for once indicate that depending on applied shear energy, several stacks were exfoliated simultaneously. However, the amount of residual layered stacks is dependent on the screw rotational speed. At low rotational speed, the residual stack amount was high and the quantity was decreasing with increasing rotational speed. Nevertheless, there were still layered stacks present in the highest sheared mixture PP1-300. Further research work was deemed necessary to correlate this effect, until a fully exfoliated state could be achieved. The problem presented itself in the inability to effectively control the temperature inside the extruder at higher rotational speed.

All these mentioned effects were observed in the second series with PP2 as base polymer as well. In figure 4, the peak area (as a function of screw speed for both different basic PP) is illustrated. For direct comparison, the values were standardised for the peak area of the first formulation of every series (PP1-100 or PP2-100). It was then shown, that the degree of exfoliation increases with increasing rotational speed for both base polymers. This served to display that the process route would work for different base polymers.

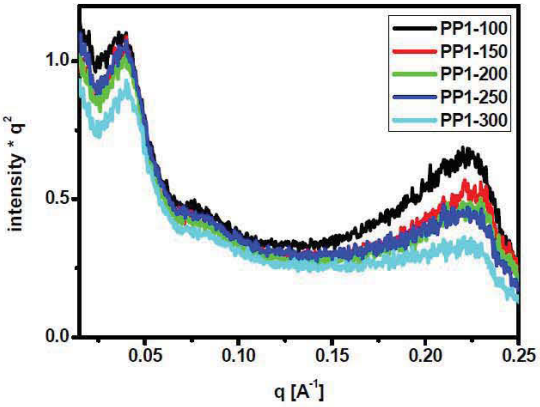

Figure 3: Small angle x-ray scattering curves for different produced mixtures of PP1.

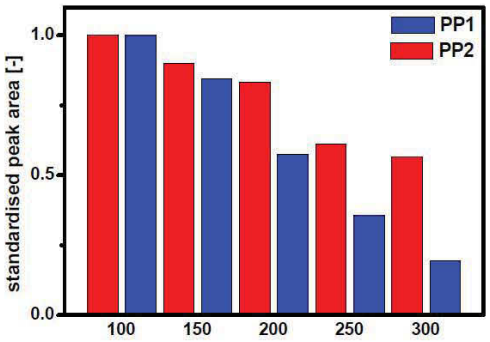

Figure 4: Standardised peak area for all related mixtures. The standards for the various used PP were the mixtures PP1-100 or PP2-100.

The mechanical properties of the investigated PPs were evaluated based on tensile tests and droptower tests. In Figure 5, the different stress-strain curves are illustrated for the unfilled PP1 and the filled mixtures. The mixtures present different deformation characteristics. While PP1-100 was breaking after necking, the elongation at break increased with increasing rotational speed.

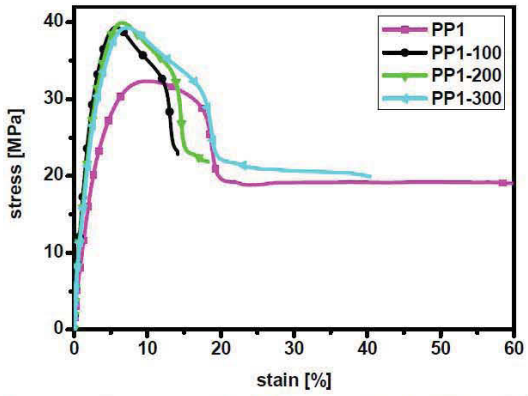

Figure 5: Representative stress-strain curves for different produced mixtures of PP1.

In Figure 6, results of Young's Modulus and elongation at break are compared for the filled PP1 formulations. It is asserted that the Young's Modulus is hardly affected by a screw rotation from 100 to 250 rpm. However, at higher rotation speed (300 rpm) the Young's Modulus decreases. The elongation showed opposite characteristics. The breaking strain rose from 16% at rotation speed of 100 up to 52% at rotation speed of 300. The highest strain at break was detected at the highest rotational speed, at PP1-300 the size of the elongation at break was detected almost as high as at the virgin PP1. No difference was detected in strength, when comparing the filled formulations. The results were further undermined with the formulations of PP2. In addition, the results of the tensile experiments are listed in Table 1.

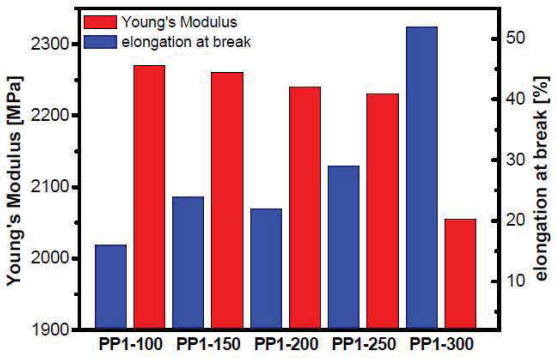

Figure 6: Mechanical properties as a function of the inserted shear energy.

The results of the tensile experiments were explained via structural properties [14]. The different degrees of exfoliation were caused by the varying amounts of stacks in the polymer nanocomposite. On the one hand, the stiff stacks increase the Young's Modulus, but on the other hand, they act as defects, stress concentrations (where cracks can initiate premature failure) and a strong influence on the strain at break [15]. This effect was shown dramatically at the elongation at break, where the highest sheared mixture possessed nearly the same level as the virgin PP1, which stands in contrast to the lowest sheared mixture, where the elongation at break dramatically decreased. For comparison, the Young's Moduli of the mixtures with different base polymer are shown in Figure 7. There, the

structural influence could be seen for both polymers, serving as an another proof that the production route worked for both base polymer [16].

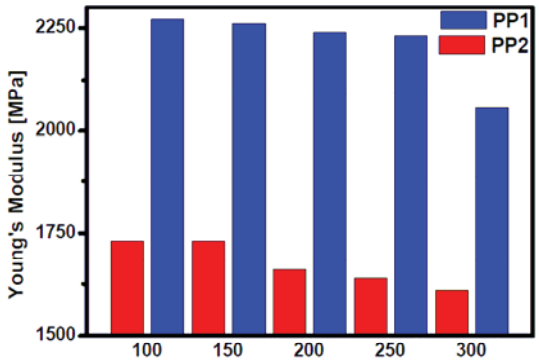

Figure 7: The Young's Modulus as a function of the inserted shear energy for both base polymer.

The results of the instrumented puncture tests are shown for the mixtures with PP2 as base polymer. In Figure 8, the standardised peak area – as a standard, the area of PP2-100 was selected - and the standardised distortion ratio - as a standard the distortion ratio from the mixture PP2-300 was selected – were illustrated as a function of the screw speed. The distortion ratio gives information about the failure mechanism. In the case of a brittle failure, the values of the distortion ratio are around zero. In case of ductile failure the ratio will raise to one. The distortion ratio was increasing with increasing screw speed, therefore the ductility was increasing as well. Furthermore displayed in Figure 8, the peak area is presented and therefore it can be shown that with increasing degree of exfoliation, the ductile failure mechanism becomes more and more dominant. It is thus safely assume that the layered stacks act as defect and stress concentration. Therefore, these defects can lead to premature failure and posses a strong influence on deformation mechanism, as was shown in the results of the tensile experiment.

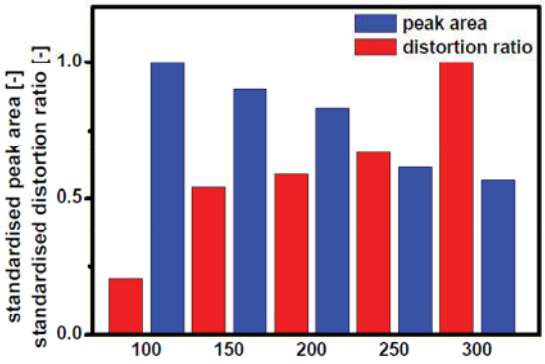

Figure 8: Standardised peak area and distortion ratio as a function of the inserted shear energy for the formulation with PP2 as base polymer.

The Young's Modulus as result of the tensile test and the normalised stiffness as result of the impact penetration test are illustrated in Figure 9. It indicates that both mechanical properties were decreasing

with increasing rotational speed. This effect might be due to structural details. The presence of stiff agglomerates might affect the ability to increase the stiffness of the global mechanical properties. Figure 9 further shows that the agglomerated filler increased the uniaxial (Young's Modulus) and the biaxial (normalised stiffness) stiffness of the polymer mixtures.

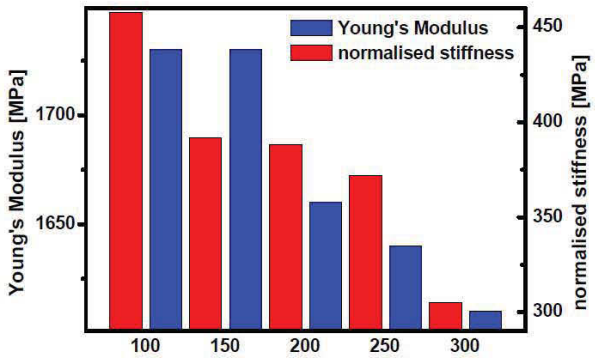

Figure 9: Young's Modulus and normalised stiffness as function of the inserted shear energy for the formulation with PP2 as base polymer.

Figure 10 presents the loss modulus as a function of temperature for all five silicate reinforced PP1-mixtures. Displayed here is the correlation between the midpoint temperatures of the so-called α-relaxation increasing with increasing rotation speed. The α-relaxation is representing inter- and intra-crystalline movement of the polymer chains and can be seen in Figure 10 in the temperature range from 50 to 100 °C.
The glass transition temperature in the temperature range around 0 °C is illustrated in Figure 10 as well. This temperature rose from 0 °C at the formulation PP1-100 up to 12°C at a screw speed of 300 rpm. In order to compare the mixtures, the natural PP1 was measured as well. The glass transition temperature of PP was detected at 8 °C; the α-relaxation midpoint temperature was determined at 67 °C. This effect can be found in other works, relating to experimentations with PP as well [17]. The results for all determined mixtures and the PP1 are shown in Table 1.

Table 1: Summarized results of tensile and thermomechanical experiments

Sample	Young's Modulus	Tensile strength	Strain at break	Midpoint temperature α-relaxation	Glass transition temperature	Normalised stiffness	Distortion ratio
	MPa	MPa	%	°C	°C	N/(mm*mm)	--
PP1	1360	32.4	60	67	8	--	--
PP1-100	2220	39.5	16	45	0	--	--
PP1-150	2190	39.7	24	55	2	--	--
PP1-200	2220	39.5	22	49	2	--	--
PP1-250	2200	39.1	29	63	7	--	--
PP1-300	2010	38.9	52	74	12	--	--
PP2	1640	30.6	--	--	--	314	0.07
PP2-100	1730	31.6	--	--	--	458	0.10
PP2-150	1730	32.3	--	--	--	392	0.27
PP2-200	1660	31.7	--	--	--	388	0.29
PP2-250	1640	31.4	--	--	--	372	0.33
PP2-300	1610	31.0	--	--	--	305	0.49

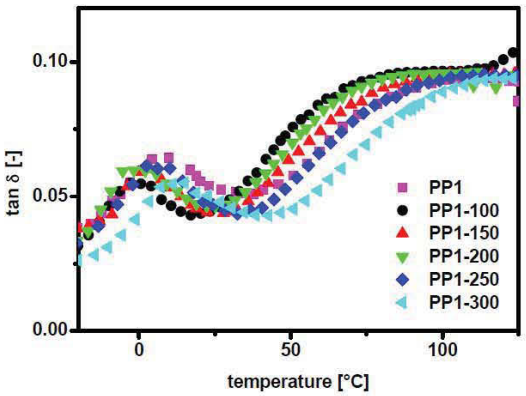

Figure 10: Loss factor tan δ as a function of the sample temperature for the produced formulations.

The glass transition temperature and the midpoint temperature of the α-relaxation are representing the mobility of polymer chains; if these temperatures are increasing then the mobility is obstructed [10].
For the temperature differences between the virgin PP1 and the mixtures, two possible explanations exist: for once, a high amount of shear energy was inserted in the polymer due to the processing route. This broke the chemical bonds of the polymer and the molecular weight was reduced. Therefore, the structural details were changed as well and thus the polymer was aged by thermal and mechanical degradation [18]. This aging phenomena could be effect the interesting temperatures [10]. On the other hand, the filler was not dried and so water could have entered the polymeric nanocomposites during the process route. This water then possibly acted as a flexibiliser and reduced the mentioned temperatures [10]. Thereby, the interesting temperatures of the virgin polymer were lowered dramatically, while the nanofiller increased the temperatures again.
With the knowledge that the quantity of agglomerates is decreasing with increasing rotational speed, the shift of the interesting temperatures to higher temperatures could be explained. Whether the quantity of agglomerates is decreasing, the quantity of single platelets in the composite is still increasing. In case of the glass transition temperature, the mobility of chains is depending on the

amount of free accessible space. As for the identical filler content, the presence of single silicate layers (exfoliated state) reduced the free space. This is in opposition to the presence of layered stacks (intercalated state), where the filler is concentrated on a small part of the material. The explanation in the case of α-relaxation could be that at the presence of more single layer (degree of exfoliation) helps the distance between the filler to decrease. Henceforth, the crystalline regions cannot grow due to the absence (or less stacks) of silicate particles [19]. The crystalline regions were getting smaller and, therefore less possibilities for intermolecular motions in that regions were existing. For this precise reason, the midpoint temperature were increasing with increasing degree of exfoliation.

Conclusion

During the course of this work it was shown, that the structural details of polymeric nanocomposites pose as a strong influence on the mechanical properties. The different inserted shear energy (generated by variation of rotation speed) altered the filler distribution. The shear energy, a function of the screw speed, influenced the degree of exfoliation. It could be shown that the exfoliation process worked over destroying individual silicate stacks simultaneously. The dependency of the morphological structure on the inserted shear energy was shown for two different PPs. Hence, the presented work helped to establish that the production of exfoliated silicate polypropylene nanocomposites by melt intercalation in a semi-industrial dimension does work.
Additionally, the differences of intercalated and exfoliated PNCs were displayed. The degree of exfoliation exhibited a strong dependency on mechanical properties. The stiff filler could increase the stiffness (Young's Modulus and the normalised stiffness) in agglomerated form; however, the agglomerates could further act as defects and stress concentrations, where initiated cracks lead to premature failure and pose as a strong influence on the deformation mechanism. Furthermore, the silicate layers influence the mobility of the polymer. Both temperatures - one representing the mobility of the amorphous content (glass transition temperature) and the second representing the crystalline content (α-relaxation) - demonstrated a strong dependence on the degree of exfoliation. The higher the degree of exfoliation, the more the mobility of the polymer chains was hindered.
Consequently, it was possible to produce silicate reinforced polymeric nanocomposites with adjustable mechanical and morphological properties.

Acknowledgements

The research part of this analysis was performed within the Research Project Cluster NanoComp ("Performance Optimization of Polymer NanoComposites"), coordinated by the Polymer Competence Center Leoben GmbH. Funding was provided by the Federal Ministry of Traffic, Innovation and Technology and the Austrian Research Promotion Agency within the AUSTRIAN NANO-Initiative and is hereby very gratefully acknowledged. Additionally I am indebted Alexander Lovas, who performed the thermo-mechanical measurements.

Literature

[1] Ray S. S, Okamoto M. *Prog. Polym. Sci.* **2003**, *28*, 1539-1641.
[2] Alexandre M. , Dubois P., *Materials Science and Engineering* **2000,** *28*, 1-63.
[3] Pavlidou S., Papaspyrides C. D. *Progress in Polymer Science* **2008**, *33*, 1119–1198.
[4] Ke Y.C., Stroeve P. *Polymer-Layered Silicate and Silica Nanocomposites,* Elsevier B.V., **2005**.
[5] Tjong S. C. *Materials Science and Engineering R* **2006**, *53*, 73-197.
[6] Utracki L.A., *Clay-Containing polymeric nanocomposites*, Rapra Technology Limited, **2004**.
[7] Feuchter M., Maier G.A., Pinter G., Kracalik M., Laske S., Langecker G.R., *Annual Technical Conference - ANTEC, Conference Proceedings* **2009**, 5, 2642-2646.
[8] Laske S., Kracalik M., Gschweitl M., Feuchter M., Maier G., Pinter G., Thomann R., Friesenbichler W., Langecker G. R., *Journal of Applied Polymer Science* **2009,** *111*, 2253–2259.
[9] Balta-Calleja F. J.,Vonk C. G. *X-ray scattering of synthetic polymers*, Elsevier, **1989**.

[10] Ehrenstein G. W., Riedel G., Trawiel P. *Praxis der Thermischen Analyse von Kunststoffen*, Carl Hanser Verlag **2003**.
[11] Guinier A. *X-Ray Diffraction in Crystals, Imperfect Crystals, and Amorphous Bodies*, W.H. Freeman and Company **1963**
[12] Alexander L.E. *X-Ray Diffraction Methods in Polymer Science*, John Wiley & Sons, **1969.**
[13] Guinier A., Fournet G. *Small-Angle Scattering of X-Rays*, John Wiley, New York, **1955.**
[14] Chan C.M., Wu J., Li J.X., Cheung Y.K. *Polymer* **2002**, 43, 2981-2992.
[15] Svoboda P., Zeng C., Wang H., Lee L.J., Tomasko D.L. *Journal of Applied Polymer Science* **2002**, 85, 1562-1570.
[16] Dayma N., Satapathy B.K. *Materials and Design* **2010**, 31, 4693-4703.
[17] Liu X., Wu Q. *Polymer* **2001**, 42, 10013-10019.
[18] Kumar A.P., Depan D., Tomer N.S., Singh R.P. *Progress in Polymer Science* **2009**, 34, 479-515
[19] Nam P.H., Maiti P., Okamoto M., Kotaka T., Hasegawa N., Usuki A. *Polymer* **2001**, 42, 9633-9640.

7 Summary and outlook

7.1 Summary of major results

The objectives of this work were to find a new, fast method for the determination of distribution quality and analyze structure-property relationships with the help of micro- and macromechanics. Following expertise was gained during the scope of this work.

In chapter 3, a new method to demonstrate the distribution quality of clay-reinforced polypropylene was presented. Near infrared spectroscopy allowed determining the structural (and mechanical) properties during the process. For this reason, structural (and mechanical) properties had to be correlated with the observed near infrared spectra. Structural details were investigated using simple X-ray scattering techniques. With the use of the chemometric model, it was possible to correlate the infrared spectra with structural (and mechanical) properties. Subsequently, a fast method for quality control of the production parameter was implemented in the process.

The structure of a clay polypropylene nanocomposites was investigated in greater detail in chapter 4. The structure around an agglomerate was investigated, using a small X-ray beam. Different structure formations of polypropylene (α- and β-form) around a layered silicate stack were observed. The different superstructures of the silicate layers were noted as well. Agglomerated layers of clay were surrounded by a highly intercalated clay structure, which in turn was surrounded by an exfoliated polypropylene-clay bulk. Structural details of clay polypropylene nanocomposites under process related temperatures were also considered in chapter 4. It was shown that: the gap distance of the organic modified montmorillonite increased at process related temperatures (easier to intercalate), a super structure (card house) was found in the high filled sample and the differences in structure between low and high filled samples at process related temperatures were pointed out. These findings should help to optimize the production process.

In chapter 5, the micromechanisms of deformation in virgin and clay filled PP were investigated. The chapter starts with a qualitative analysis of deformation mechanism. Due to the difference in virgin and clay-reinforced polypropylene, further investigations were performed. Orientation determination at and around a crack tip under external load delivered information on the deformation mechanism. A very thin zone with high degree of

orientation was found in clay polypropylene nanocomposites and was related to brittle failure. A broad zone with low degree of orientation was related to a ductile failure mechanism in virgin polypropylene. Additionally, a method to correlate micro-strains (strains in crystallographic planes) with applied strains is presented. This was obtained via the determination of X-ray specific elastic constants. These constants can be applied for stress determination in selective and inaccessible regions. The suggested approach functioned efficiently unless the crystallographic planes of the polymer (and nanocomposite) are not rearranged due to applied stress.

The correlation of structural and (macro) mechanical properties was illustrated in chapter 6. There, the exfoliation process with the adaptation of the production route melt compounding is illustrated in great detail. It is evident that tuneable clay nanocomposites (with different types of virgin polypropylene) can be produced over a semi-industrial process route. Furthermore, macroscopic mechanical properties can be correlated as follows: highly intercalated clay polypropylene nanocomposites exhibit a high stiffness and a low elongation at break; nevertheless, for composites with a high degree of exfoliation, the mechanical properties change to a lower stiffness and a higher strain at break. Henceforth, a structure-property relationship was found and interpreted via the means of sophisticated methods.

7.2 Outlook

In addition to the above mentioned findings, resulting from the conducted scientific study, further demand for future research work has become apparent.

Establishing appropriate routines for a standard analysis of clay polymeric nanocomposites was not possible due to the highly complex optimization of the developed Matlab code, which in turn was based on Vaia 2003 (see chapter 2.2). With the approach mentioned here, it is possible to gather more structural information, therefore posing as a next step forward to broaden the currently existing perception of clay-containing polymeric nanocomposites.

Further investigations on structural details seem to be necessary to fully understand the structure of clay polypropylene nanocomposites. β-polypropylene formation and the location of β-polypropylene are quite unclear. Three-dimensional X-ray measurements of such layered stack pose as a possibility to clarify the formation of β-polypropylene. Other

methods like infrared spectroscopy can provide additional information on β-formation. The influence of the found β-polypropylene on mechanical properties should be investigated as well. In paper 5, the increase of the long period during cooling is quite mysterious. Meanwhile, the formation of smectic phases near the layered stacks can be explained as a mesomorphic state, where the molecules are oriented in layers. Consequently, if the composite is able to build smectic phases, the influence on mechanical and structural properties should be determined. The production of highly oriented and layered polymer segments (smectic phases) can increase the mechanical properties dramatically.

The wide field of fracture mechanics may give some further explanations, concerning the deformation mechanism of clay-containing polypropylene nanocomposites. Fatigue crack growth tests can be utilized as a "nanomicroscope" (during one cycle, crack length changes in the nanometer range) and can help understand deformation mechanism and the influence of layered silicates on mechanical behaviour.

The issue “long-term mechanical behaviour of clay-reinforced polypropylene” was not considered during this thesis. Further investigations on this field of work are still ongoing.